AD-A181 055 PHOTON-ENHANCED ELECTRON ATTACHMENT PROCESSES IN DISCHARGE-OPENING SWITCHES(U) SRI INTERNATIONAL MENLO PARK CA M J ROSSI ET AL. FEB 87 ARO-19934.5-PH 1/2

UNCLASSIFIED DAAG29-83-K-0113 F/G 7/4 NL

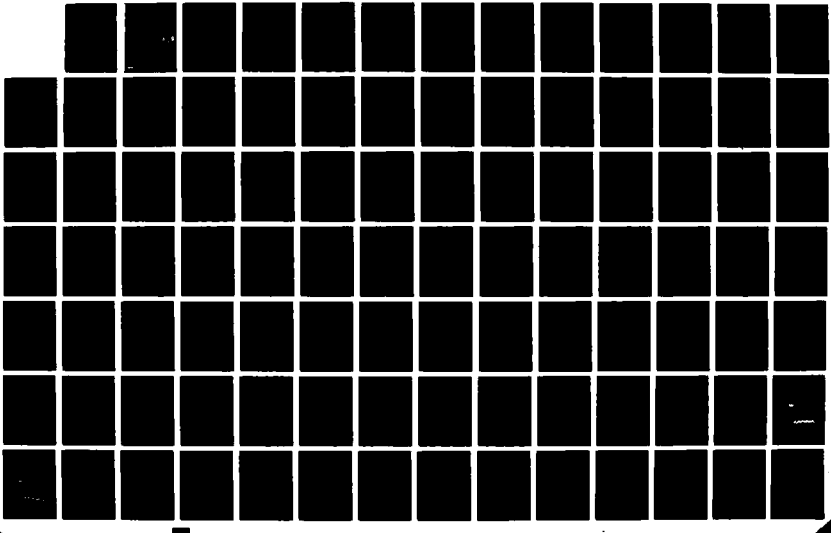

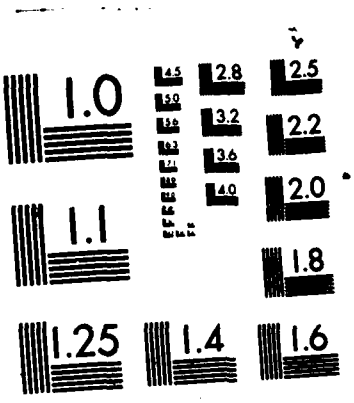

PHOTON-ENHANCED ELECTRON ATTACHMENT PROCESSES IN DISCHARGE-OPENING SWITCHES

February 1987

Final Report
Covering period from 15 August 1983 through ~~15 August 1986~~ 30 JUNE 1987

By: M. J. Rossi, H. Helm, and D. C. Lorents

Prepared for:

U.S. ARMY RESEARCH OFFICE
P.O. Box 12211
Research Triangle Park, NC 27709

Attention: Dr. R. Gunther and Dr. D. Skatrud

Contract No. DAAG29-83-K-0113

SRI Project PYU-6261

Approved for public release; distribution unlimited.

SRI International
333 Ravenswood Avenue
Menlo Park, California 94025-3493
(415) 326-6200
TWX: 910-373-2046
Telex: 334486

Unclassified
SECURITY CLASSIFICATION OF THIS PAGE

AD-A181 055

REPORT DOCUMENTATION PAGE

1a. REPORT SECURITY CLASSIFICATION	1b. RESTRICTIVE MARKINGS
2a. SECURITY CLASSIFICATION AUTHORITY	3 DISTRIBUTION / AVAILABILITY OF REPORT
2b. DECLASSIFICATION / DOWNGRADING SCHEDULE	
4 PERFORMING ORGANIZATION REPORT NUMBER(S)	5. MONITORING ORGANIZATION REPORT NUMBER(S) ARO 19934.5-PH
6a. NAME OF PERFORMING ORGANIZATION SRI International 6b. OFFICE SYMBOL (If applicable)	7a. NAME OF MONITORING ORGANIZATION
6c. ADDRESS (City, State, and ZIP Code) 333 Ravenswood Avenue Menlo Park, CA 94025	7b. ADDRESS (City, State, and ZIP Code)
8a. NAME OF FUNDING / SPONSORING ORGANIZATION U.S. Army Research Office 8b OFFICE SYMBOL (If applicable)	9 PROCUREMENT INSTRUMENT IDENTIFICATION NUMBER DAAG29-83-K-0113
8c. ADDRESS (City, State, and ZIP Code) P.O. Box 12211 Research Triangle Park, NC 27709	10 SOURCE OF FUNDING NUMBERS PROGRAM ELEMENT NO. / PROJECT NO 6261 / TASK NO / WORK UNIT ACCESSION NO

11 TITLE (Include Security Classification)

PHOTON-ENHANCED ELECTRON ATTACHMENT PROCESSES IN DISCHARGE-OPENING SWITCHES

12. PERSONAL AUTHOR(S)
Michel J. Rossi, Hanspeter Helm, and Donald C. Lorents

13a TYPE OF REPORT	13b. TIME COVERED	14. DATE OF REPORT (Year, Month, Day)	15 PAGE COUNT
Final Report	FROM 8/15/83 TO 6/30/87	1987 February	

16. SUPPLEMENTARY NOTATION The view, opinions, and/or findings contained in this report are those of the author(s) and should not be construed as an official Department of the Army position, policy, or decision, unless so designated by other documentation.

17 COSATI CODES			18 SUBJECT TERMS (Continue on reverse if necessary and identify by block number)
FIELD	GROUP	SUB-GROUP	

19 ABSTRACT (Continue on reverse if necessary and identify by block number)

Electron attachment data for dissociative electron attachment are reported for several species in the ground electronic state as well as after laser excitation. The experimental apparatus used consisted in a Gruenberg type drift cell fitted with windows for cathode illumination and laser excitation of a volume oriented parallel to the electrodes forming the gap. The time dependent electron swarm population was monitored as a transient voltage as a function of various swarm parameters and laser irradiation conditions.

20 DISTRIBUTION / AVAILABILITY OF ABSTRACT	21 ABSTRACT SECURITY CLASSIFICATION	
☐ UNCLASSIFIED/UNLIMITED ☐ SAME AS RPT ☐ DTIC USERS		
22a NAME OF RESPONSIBLE INDIVIDUAL	22b TELEPHONE (Include Area Code)	22c OFFICE SYMBOL

DD FORM 1473, 84 MAR — 83 APR edition may be used until exhausted. All other editions are obsolete.

SECURITY CLASSIFICATION OF THIS PAGE
Unclassified

The attachment coefficient of HCl in helium was measured, and a low energy attachment process in addition to the known dissociative attachment process at 1.5 Td (1 Td = 10^{-17} V cm^2) was observed. The photoenhanced attachment coefficients for vinylchloride (C_2H_3Cl) and trifluoroethylene (C_2F_3H) were measured for 193 nm laser illumination at a few mJ/cm^2 and were compared to the ground state attachment behaviour. The photoenhanced attachment effect amounts to 3 - 5 orders of magnitude with respect to the ground state quantities and depends only weakly on the reduced electric field strength (E/N) up to several Td. A complication arises in our experiments in that multiphoton ionization of the above compounds are a facile process under our conditions. The absolute ionization yields of C_2H_3Cl and C_2F_3H were measured using a time-of-flight mass spectrometer in an ancillary experiment. The attachment experiments were conducted in such a way as to minimize the effect of the positive charge carriers on the transient voltage either by working at low laser fluence conditions or illuminating a volume adjacent to the cathode.

The ground state attachment coefficient for p-benzoquinone ($C_6H_4O_2$) and its tetrachloroderivative ($C_6Cl_4O_2$) were measured in helium at 373K as well as under laser irradiation conditions (308 and 350 nm respectively). No photoenhancement effect could be detected in helium for the above two quinones. However, experiments in molecular nitrogen as a buffer gas revealed the existence of a large photoenhancement effect for p-benzoquinone in nitrogen when the gas mixture was excited by a few mJ/cm^2 at 308 nm.

CONTENTS

ILLUSTRATIONS

Section 1

INTRODUCTION AND SUMMARY OF ACHIEVEMENTS

The goal during this contract period (15 August 1983 through 15 August 1986) was to demonstrate the possibility of externally controlling the attachment properties of gas mixtures using laser light. The basic idea of such schemes is to select gases (and mixtures of gases) that in their nascent state show little or no affinity to thermal electrons, but that can be converted into strongly attaching species following laser irradiation. We have demonstrated the feasibility of such a concept using several cases, namely, vinylchloride (VCl) and trifluoroethylene (TFE), on the one hand, and benzoquinone and its tetrachloroderivative on the other hand. For low-energy electrons, the photoenhancement of the attachment coefficient was determined to be several orders of magnitude.

Most of the experiments were conducted in a high-purity drift tube apparatus, which was built and tested during the first six months of the contract period. Then we performed the initial demonstration experiments that unambiguously showed the effect of photon-induced attachment in VCl and TFE. However, we realized the importance of UV-multiphoton ionization processes of VCl and TFE even at fluences as low as a few mJ/cm^2 for the measurement of attachment coefficients by the Gruenberg method. This realization led to an investigation that culminated in the determination of quantitative UV-multiphoton ionization cross sections for VCl and TFE at 193 nm so that the importance of this mode of charge generation could be assessed with respect to the photoelectric generation of the swarm electrons by direct UV-irradiation of the cathode. Our results on VCl led us to investigate the influence of 193-nm laser radiation on a VCl-containing hollow cathode discharge, as an example to achieve optical control on dc glow discharges.

The results of each effort are summarized below and discussed in detail in the following sections. Papers that have appeared in scientific journals or that have been submitted for publication are appended.

Attachment in HCl/He Mixtures

We performed attachment experiments in HCl/He mixtures to address the question of electron attachment to ground-state HCl in dilute and highly concentrated mixtures with helium buffer gas. The general phenomenon of dissociative attachment for high-energy electrons is supported by these measurements. Our results also show that, as expected, in concentrated mixtures the HCl content significantly influences the energy distribution in the electron swarm. We modeled this situation using a Boltzmann code and are able to describe the reduced electric field strength (E/N) dependence and concentration dependence of the attachment coefficient in a quantitative way. At low values of E/N, an electron attaching species other than HCl is observed. This species is probably an HCl aggregate molecule.

Multiphoton Fragmentation and Ionization in VCl and TFE

Both gases chosen for the photoenhanced attachment work, VCl and TFE, show at modest laser fluence the possibility of multiple photon absorption leading to fragmentation and ionization in the gas phase. We measured absolute cross sections for multiphoton ionization of both species using a time-of-flight mass spectrometer, determined the neutral and ion fragmentation patterns, and investigated effects of the pulse width and intensity on the ionization cross sections. The results are discussed in more detail in Appendices A and B.

Photoenhanced Electron Attachment in VCl and TFE

We measured the electron-attachment coefficient for both gases as a function of E/N both for the unexcited and laser excited case. For both gases the attachment coefficient for thermal energy electrons is very low when they are in their ground state, and VCl displays a dissociative attachment channel for high-energy electrons (mean energy ~ 1 eV). With modest laser illumination, both gases are efficiently photodissociated and form fragments with high attachment coefficients. At 0.1 Td (1 Td = 10^{-17} V•cm^2) three orders-of-

magnitude enhancement in the attachment coefficient is observed. Based on the fragmentation/photoionization results discussed above, the effect is attributed to the formation of vibrationally excited HCl and HF species and possibly other previously not well-characterized molecules that are formed in photodissociation of VCl and TFE at 193 nm. Experiments were also conducted to determine the lifetime of the attaching species by time-delaying the electron swarm with respect to the photodissociation laser. More detailed results are presented in Appendix C.

Laser Switching of DC Discharge

We observed that in a discharge gap operated at voltages below breakdown, a DC-glow discharge can be initiated by laser illumination. This effect appears to be independent of the type of gas used and is probably associated with the generation of electrons from surfaces by the photoelectric effect. Avalanching of these electrons will then initiate the DC discharge. In mixtures of VCl with helium, however, we observed that such a discharge can also be extinguished by illumination with the laser. We attribute this effect to the generation of electron-attaching species following photodissociation of the VCl gas. These experiments appear to be a first demonstration of our concept of using controlled photon-induced electron attachment to externally control a low pressure discharge.

Photoenhanced Attachment of Electronically Excited Metastable Triplet States of p-Benzoquinone (BQ) and Chloranil (CA)

Excitation of BQ by 308-nm and CA by 350-nm laser radiation affords a high yield of the lowest excited triplet states whose lifetimes range from microseconds to milliseconds. Electron attachment to the respective ground states was measured as a baseline for comparison with any enhancement of the electron attachment due to the presence of the triplet state. We found that the ground-state attachment behavior of BQ and CA differed drastically from each other. No photoenhancement on UV-laser illumination was observed in He even when the degree of excitation reached 20%. However, a large photoenhancement effect was found for BQ at 308 nm in N_2.

Section 2

ATTACHMENT EXPERIMENTS IN DILUTE HCl/He MIXTURES

To provide benchmark experiments with which the attachment behavior of highly vibrationally excited HCl could be compared, we measured the attachment coefficient, η, of cold, ground state HCl. Our results are presented in Figure 2-1, which shows the electric field strength (E/N) dependence of the attachment coefficient at various dilutions of HCl in He. At high HCl concentrations, the maximum value of η as well as the peak position is a function of both the absolute partial pressure of HCl as well as the dilution factor. At low concentrations of HCl (less than 0.05 Torr), the value of N was independent of HCl pressure. This implies that the E/N dependence of the electron energy distribution in the swarm is only determined by collisions with the buffer gas. Because the attachment curves are independent for concentrations $\leq$ 100 ppm of HCl in He, we can compare these results with the swarm data of Christophorou et al. [CC68]. These authors used N_2 as a buffer gas. Our data show the maximum to be at 1.55 Td with an attachment rate constant of 2.4×10^{-10} cm^3 s^{-1}, whereas Christophorou et al. report a value of 1.4×10^{-10} cm^3 s^{-1} with no clear maximum over their range of E/N values.

The interesting portion of the data, however, is the attachment at very low values for E/N, which is controversial, but potentially significant from an applications point of view (high power rare-gas halide excimer lasers). This behavior was reported previously by Christophorou et al. [CC68] and others, but it is not known which molecular process is responsible for this thermal electron-energy attachment. This process, if it is due at all to the presence of HCl and not to an impurity in the gas, mmust be a nondissociative attachment process perhaps involving an aggregate. Aggregates were also invoked in the electron-attachment studies of Armstrong and Nagra [AN75], who suggested the dimeric species of HCl and HBr as the electron attachers at low-electron energies. The experimental work described so far has essentially been discontinued in view of the more pertinent subjects described below.

Using a Boltzmann code and the accepted literature data for the respective elastic and inelastic cross sections of electrons in He and HCl, we calculated the dependence of the attachment coefficient on E/N for the various concentrations shown in Figure 2-1. These results show quantitative agreement with our experimental curves for $E/N \geq 0.5$ Td.

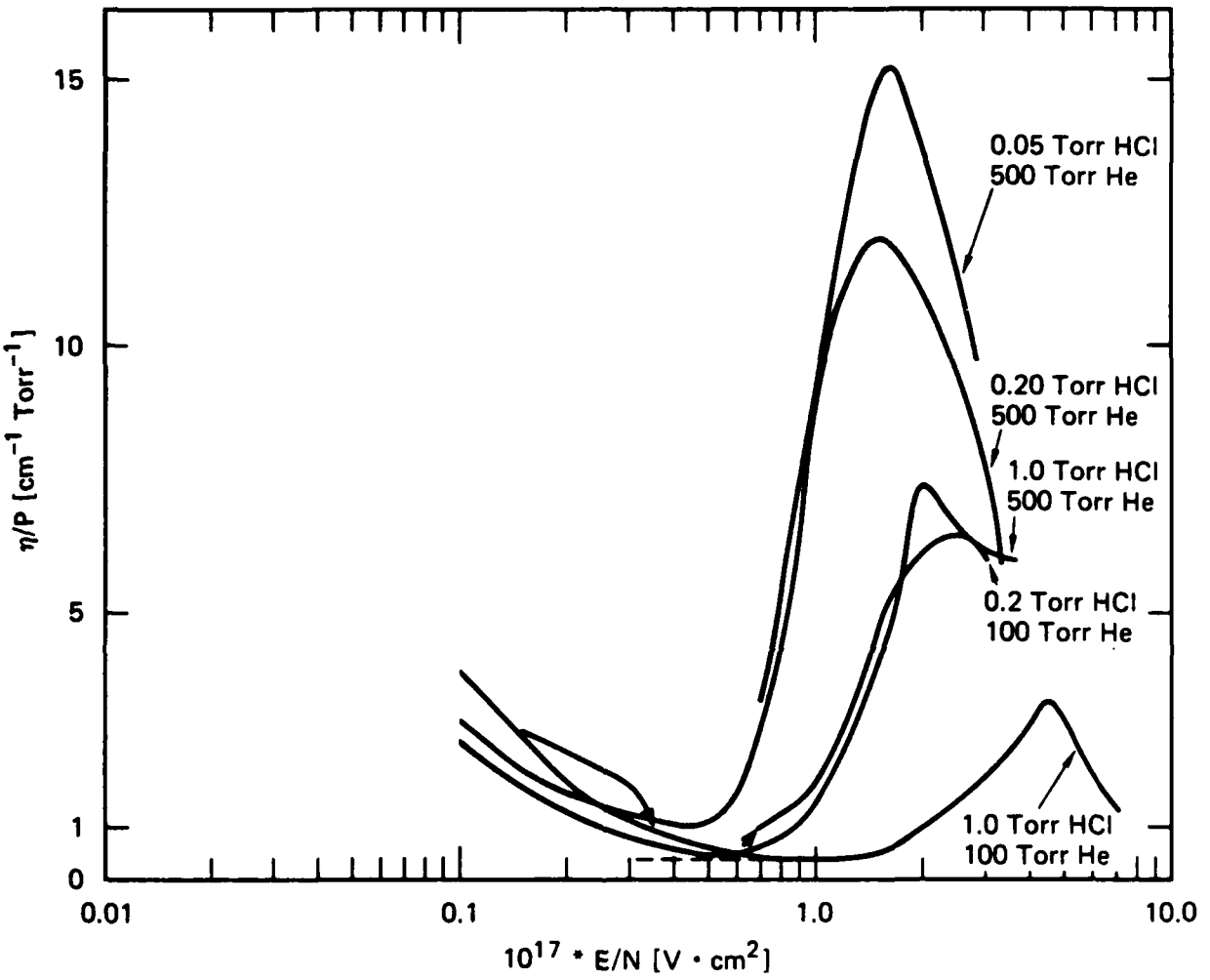

FIGURE 2-1 DISSOCIATIVE ELECTRON ATTACHMENT IN HCl/He AT 300 K AS A FUNCTION OF THE REDUCED ELECTRIC FIELD E/N

The data points for 0.02 Torr HCl in 500 Torr He coincide with the curve taken for 0.05 Torr HCl in 500 Torr He.

Section 3

PHOTOENHANCED ELECTRON ATTACHMENT IN VINYLCHLORIDE AND TRIFLUOROETHYLENE AT 193 nm

Background

Electron attachment processes in atoms and molecules are among the fundamental electron-molecule interactions, and an impressive array of experimental and theoretical data have been gathered over the years [CH84a]. Much less is known, however, about the dependence of attachment cross sections and attachment rate constants of excited or transient species on the degree of internal excitation. One of the most common methods of exciting atomic and molecular species is to increase their temperature in thermal equilibrium. In spite of the paucity of data of this kind, the significance of temperature studies in determining true onsets for the appearance of specific product ions and the deduction of thermochemical data from those data has been demonstrated for a few molecular species.

One of the earliest examples of a temperature-dependent attachment cross section σ_{DA} was in the dissociative attachment of O_2, which had been shown to have an increased peak value with increasing temperature [FB63] and a decrease in the energetic position of the resonance maximum. From a comparison of the experimental variation of σ_{DA} with temperature with theoretical predictions, O'Malley [OM67] concluded that the effect was due entirely to vibrational excitation of O_2. Another well-studied case was H_2 and D_2, in which a strong effect of rotational and vibrational excitation on dissociative electron attachment was predicted [CP67] and, in fact, found [AW78] although the role of rotational excitation was less important than vibrational excitation. For HCl, DCl and HF a large increase of σ_{DA} with increasing temperature was observed [AW81]. Interesting structure in σ_{DA} in the low electron energy region was interpreted, and an enhancement of σ_{DA} by a factor of 40 and 20 upon one quantum vibrational excitation from $v'' = 0$ to $v' = 1$ was measured for HCl and HF, respectively. Bardsley and Wadehra [BW83] calculated a peak cross section of $\sim 10^{-17}$ cm^2 at 0.8 eV electron energy for $v'' = 0$ in HCl, whereas for $v' = 3$ the cross section peaked near zero energy and had a value of $\sim 10^{-14}$ cm^2.

The situation with respect to assessment of temperature-dependent cross sections for electron attachment is more sketchy for polyatomics, such as N_2O [CH79] and SF_6 [CC79], where two peaks for the attachment cross section are observed, but the effect of temperature is less pronounced than in the diatomic molecules. However, the identities of two attaching states were confirmed from those temperature studies with the lower of the two showing a dramatic temperature enhancement. Finally, Christophorou et al. [CJ74] and McCorkle et al. [MS82] measured electron attachment rate constants for 1,1-dichloroethane over the temperature range of 323 to 473 K and found a modest increase with increasing temperature. The attachment cross section $\sigma_{DA}(\epsilon,T)$ was resolved into two vibrational components, one originating from $v'' = 0$ and a second one originating from $v'' = 1$. The temperature dependence of the electron attachment of C_3F_8 revealed the simultaneous occurrence of dissociative as well as nondissociative attachment processes that could be identified according to their differing temperature dependence [SC85a].

In other instances the study of the temperature-dependent attachment coefficient led to unusual conjectures about the attaching species. In C_6F_6, there seem to be two molecular species with widely differing electron-attaching properties. The ground state of C_6F_6 seems to have a large cross section for electron capture, whereas an excited state occurring preferentially at higher temperatures has an attachment cross section many orders of magnitude lower than the corresponding ground state [SC85b; CH85]. Another curious feature of molecular systems studied at high buffer gas pressures and revealed by temperature-dependent electron swarm studies is the existence of van der Waal's complexes between NO_2^- and inert gas molecules such as Ar and N_2 [SH86]. It is clear from this discussion that some information on thermally excited molecular systems exists, but in few cases has the attacher been excited directly in a non thermal way. Our work tries to fill this gap by examining the attachment behavior of excited molecular systems far from equilibrium.

The motivation for the present study is the prospect of controlling diffuse discharges by the photolytic generation of electron attachers using a laser. The sequence of events is roughly as follows: simultaneous with or slightly preceding the trailing edge of the electron-beam pulse that maintains

the diffuse discharge, a short but intense UV laser pulse generates a given density of electron attachers that accelerate the plasma decay. The concept here is to use an energetic laser pulse to convert an appropriate precursor into an electron-attaching molecule whose attaching properties are different from those of the precursor. The precursor is chosen to yield vibrationally or electronically excited products whose attachment behavior for low-energy electrons is vastly different from either the ground state of the precursor or its daughter species that potentially might be formed as a result of the interaction of the precursor to the diffuse plasma.

Thus, our experiment involved generating a nonequilibrium population of attaching species in high-lying vibrational states by photodissociation at 193 nm of vinylchloride (VCl, C_2H_3Cl) to yield HCl and of trifluoroethylene (TFE, C_2F_3H) to obtain HF. The attaching properties of this population of excited states were then probed by an electron swarm whose transmission was measured in a drift tube. Therefore, the "philosophy" of our approach is equivalent to injecting an attaching species at a given time that the experimenter can choose.

The electron-attaching properties of the VCl precursor were recently studied [SC86; DA85; MC84], whereas the electron attachment of TFE has not been examined.

Experimental Details

Our measurements on the photoenhanced electron attachment were performed in a Gruenberg-type drift tube apparatus [Gr69]. This method of obtaining electron attachment rates is based on the analysis of the transient wave form induced by the movement of charged particles in the parallel plate discharge gap. A schematic diagram of our drift cell apparatus is shown in Figure 3-1. The essence of the method is as follows: at time t = 0 a swarm of electrons is released at the cathode by the photoelectric effect using either a short-pulse flash-lamp or a laser-pulse directly irradiating the cathode surface. Under the influence of the electric field E established by the electrodes, an

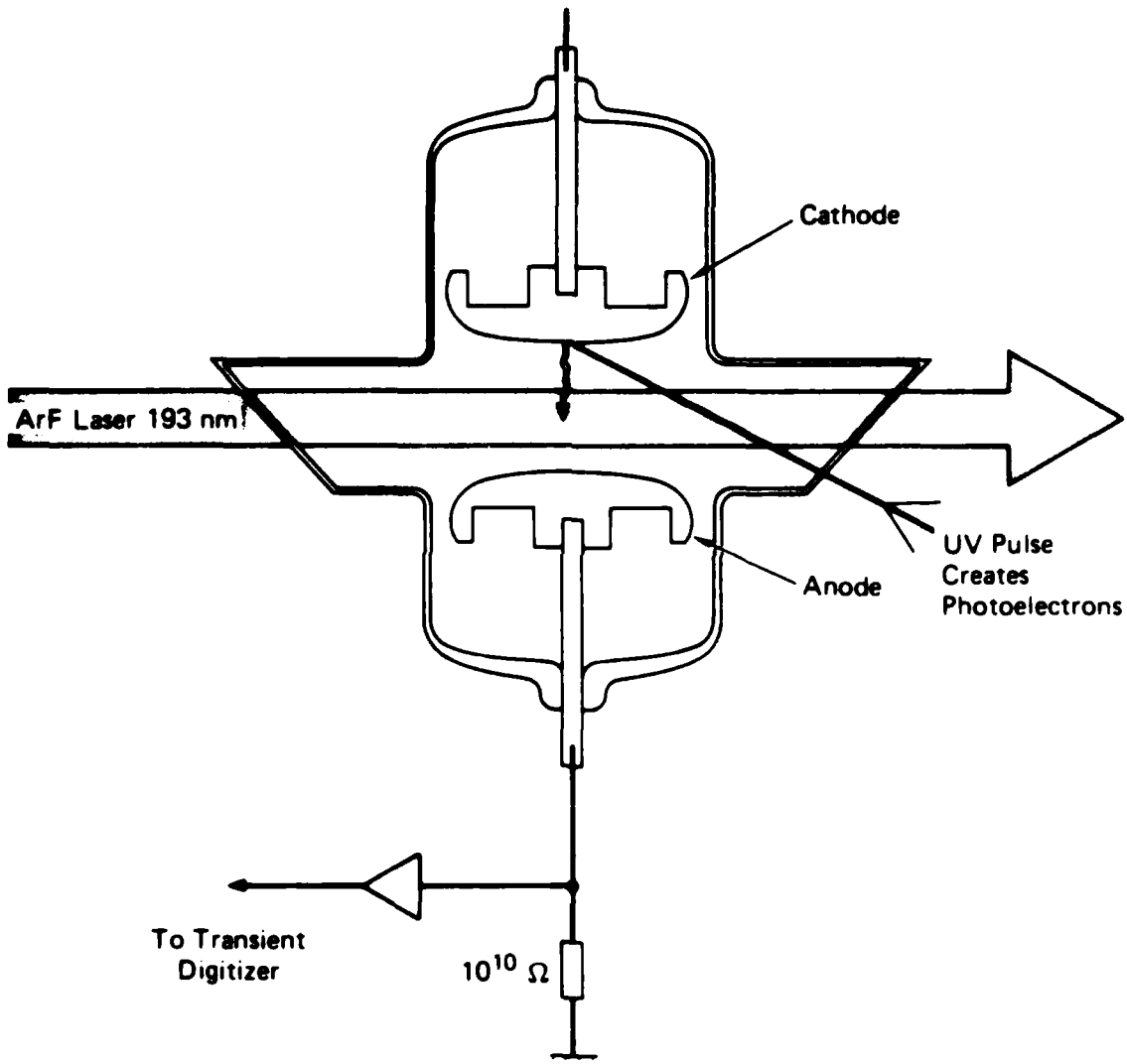

FIGURE 3-1 DRIFT CELL FOR PHOTOENHANCED ATTACHMENT EXPERIMENTS

The electrode diameter is 5 cm, the gap is 1.51 cm, and the electron swarm generating light-flash or laser beam enters the cell through a window parallel to the paper plane

electron swarm drifts to the anode creating slowly moving negative ions in the gap as attachment occurs. If N_0 electrons are released from the cathode at t = 0, the anode potential V_e at time t_e, the electron drift time, is given by

$$V_e = (N_0 e/C)\eta d(1 - e^{\eta d}) \qquad (3\text{-}1)$$

Equation (3-1) holds if the transient current is integrated with an anode circuit time constant that is large compared with the drift time of the slowly moving negative ions. In other words, all ions must have been discharged at the respective electrodes before the accumulated charge on the anode can flow to ground. In equation (3-1) e is the electronic charge, C the gap capacitance, η the attachment coefficient (number of attachments events per centimeter drift distance), and d the gap distance. For our drift tube the RC time constant was measured as 150 ms.

After a sufficiently long time the negative ions formed in the gap by electron attachment drift to the anode, raising its potential further to

$$V_0 = N_0 e/C \qquad (3\text{-}2)$$

which corresponds to the situation in which all the charge ($Q = N_0 e$) initially generated at the cathode has been collected at the anode (that is, no recombination has been assumed during the drift time of the electrons). Experimentally, a plateau in the anode potential is observed for times $t > t_n$, where t_n is the drift time of the anions. This voltage then decays with the RC time constant mentioned above. Because of the large difference of the drift times of electrons and negative ions, usually two orders of magnitude, a break in the transient voltage occurs at $t = t_e$. From the transient waveforms, the ratio V_0/V_e can be determined with considerable accuracy and is used to evaluate the attachment coefficient η:

$$V_0/V_e = \eta d/[(1 - \exp(-\eta d)] \qquad (3\text{-}3)$$

The dynamic range of our measurements is about 400 since V_e can be measured to about 5% accuracy relative to V_0. Equation (3-3) is valid as long as the sum of the duration of the light flash used to generate the electron swarm and the electron drift time, t_e, is short with respect to t_n, the anion drift time.

In the drift cell shown in Figure 3-1 the discharge gap is formed by two aluminum electrodes machined to a Rogowski-type profile separated by 1.51 cm. The cathode was illuminated by an EG&G FX 200-U high pressure xenon flash-lamp in oblique incidence using a light pulse that lasted about 150 ns and had a low intensity tail of up to 1 μs. Each pulse contained typically 7×10^{13} photons/pulse at the average wavelength of 300 nm, ejecting 10^6 to 10^7 photoelectrons from a 1-cm^2 cathode area defined by external apertures. When the excimer laser was used to excite the gas mixture, photoelectrons were also generated by scattered light from the windows and the gas mixture. The yield was up to three orders of magnitude larger than those generated by the flash-lamp even though the laser beam illuminated the gap parallel to the electrode surface and was passing through three apertures before it entered the electron drift region. The laser apertures were 0.64 cm high by 2.05 cm long, so the electrons drifted through a slab 0.64 cm thick, which was illuminated by the excimer laser (Lambda Physik EMG 101). The relative importance of the scattered light contribution to photoelectron generation is discussed more extensively in the Experimental Results subsection. Consequently, the flash-lamp could not be used to generate the electron swarm when the gas was excited by the laser. Therefore, on the photoelectric effect brought about by the scattered photons to generate the electron swarm probing the excited volume.

During this work we found that reference experiments were needed to confirm the homogeneous nature of the attachment process. One such experiment consisted of using a portion of the volume-exciting 193-nm laser light entering the Brewster window to generate photoelectrons by directly irradiating the cathode through the side window. Figure 3-2 is a schematic view of this experimental arrangement in which a beamsplitter (uncoated quartz window) is used to direct 8% of the 193-nm laser light onto the cathode. However, the arrangement shown in Figure 3-2 does not provide a means for probing the

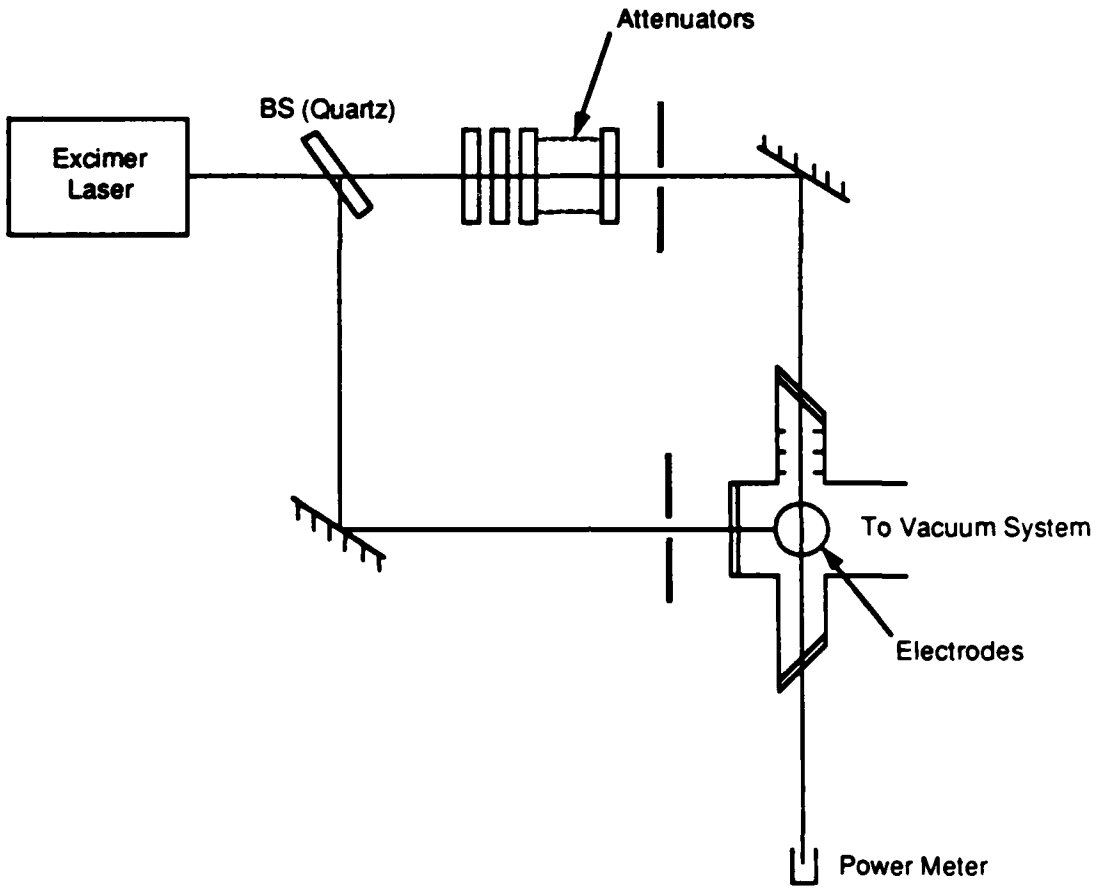

JA-M-330543-81A

FIGURE 3-2 ARRANGEMENT FOR PHOTOENHANCED ELECTRON ATTACHMENT EXPERIMENTS USING THE SAME LASER TO GENERATE PHOTOELECTRONS AND EXCITED ATTACHERS IN THE ELECTRODE GAP.

attachment behavior of the excited gas at various time delays after the excitation. This information was obtained by replacing the split-off portion of the 193-nm light (see Figure 3-2) by an additional excimer laser that could be triggered at a given time delay before or after the 193-nm volume exciting laser.

We chose to irradiate the cathode with 248-nm laser light because neither VCl nor TFE absorb at that wavelength. The timing between both laser pulses was controlled by an analog delay generator (ORTEC416A), and the 248-nm laser power impinging onto the cathode was chosen such that the signal corresponding to total charge generated exceeded the one generated by scattered 193-nm photons by at least an order of magnitude. This setup limited the 193-nm laser power that we could use for volume excitation, but we later found that laser powers in excess of 2 mJ/cm^2 gave rise to multiphoton ionization that precluded the use of high 193-nm laser powers (see Appendix B).

The capacitance of the discharge gap was measured to be 7 ± 2 pF. The decay time constant of the anode potential with R = 10^{10} Ω (Figure 3-1) was measured as 0.165 s, indicating a total capacitance of 16 pF. We attribute the added capacitance of the circuit to the input capacitance of the operational amplifier (NS LH0032 CG ultrafast FET Op amp) used to feed the signal into the transient recorder. We used either a BIOMATION 805 or a TRANSIAC 2001 waveform recorder, and the recorded data were processed by either a digital storage oscilloscope (EG&G PAR 4202) or a laboratory minicomputer (DEC LSI/1102). The pulse repetition rate was essentially given by the above RC time constant and was chosen as 1 Hz. Typically 50 to 100 transient waveforms were recorded and accumulated before being analyzed using equation (3-3) or another procedure discussed later.

The purity of the buffer gases was critical in some experiments. Helium of 99.999% purity was used for the drift velocity measurements to check the performance of the apparatus. When helium was used as buffer gas in photoenhanced attachment experiments, it had to be purified with Ti sponge heated to 950°C and passed through a liquid nitrogen trap. Without these precautions, "pure" helium showed considerable ion formation due to an unidentified impurity when the gas was irradiated with a laser pulse of 5 mJ at

193 nm. Trifluoroethylene (TFE, C_2F_3H) was purchased from PCR, Inc., and was used without further purification, whereas vinylchloride (C_2H_3Cl) was bought from Matheson as a 2.05% mixture in He (analysis by GC). The pressure of the various gases were measured by a series of capacitance manometers (MKS Baratron). All the experiments described in this section were performed with a static gas fill that was replaced after about 200 laser shots.

We tested the drift tube apparatus by measuring the electron drift velocities in He at values of E/N between 8×10^{-3} and 2×10^{-1} Td (10^{17} V•cm^2) at room temperature. Agreement with literature data [HC74] was within 5% in the pressure range studied (100 to 700 Torr He). Also, attachment in pure O_2 was measured at 25 and 88 Torr and compared with the data obtained by Gruenberg for the same pressures [Gr69]. Overall agreement was found with the Gruenberg data. However, at 25 Torr our attachment coefficients η/P are higher by 10%-20% in the low E/N region (0.2 to 2.3 Td), and at 88 Torr our η/P data were lower by 10-20% in the wings of the attachment curve (high and low E/N values, respectively). Despite this yet unexplained discrepancy in the O_2 attachment data, we believe that reliable data can be obtained in our drift tube apparatus.

Experimental Results

Attachment in Unexcited Mixtures

To establish a basis for comparing the attachment behavior of the excited with the unexcited "ground state" sample, we first measured the attachment coefficient of VCl and TFE in helium. Figure 3-3 shows results for η/P of VCl as a function of E/N at different concentrations, and at a constant buffer gas pressure of 500 Torr He and 300 K. A weak dependence on concentration is observed and is most pronounced in the steeply rising portion of the attachment curve at ~ 0.8 Td. The curve drawn through the data in Figure 3-3 merely represents a guide to the eye.

At the concentrations used in our experiment attachment was not detectable below 0.5 cm^{-1} Torr^{-1}. Tests at E/N values less than 0.1 Td revealed no

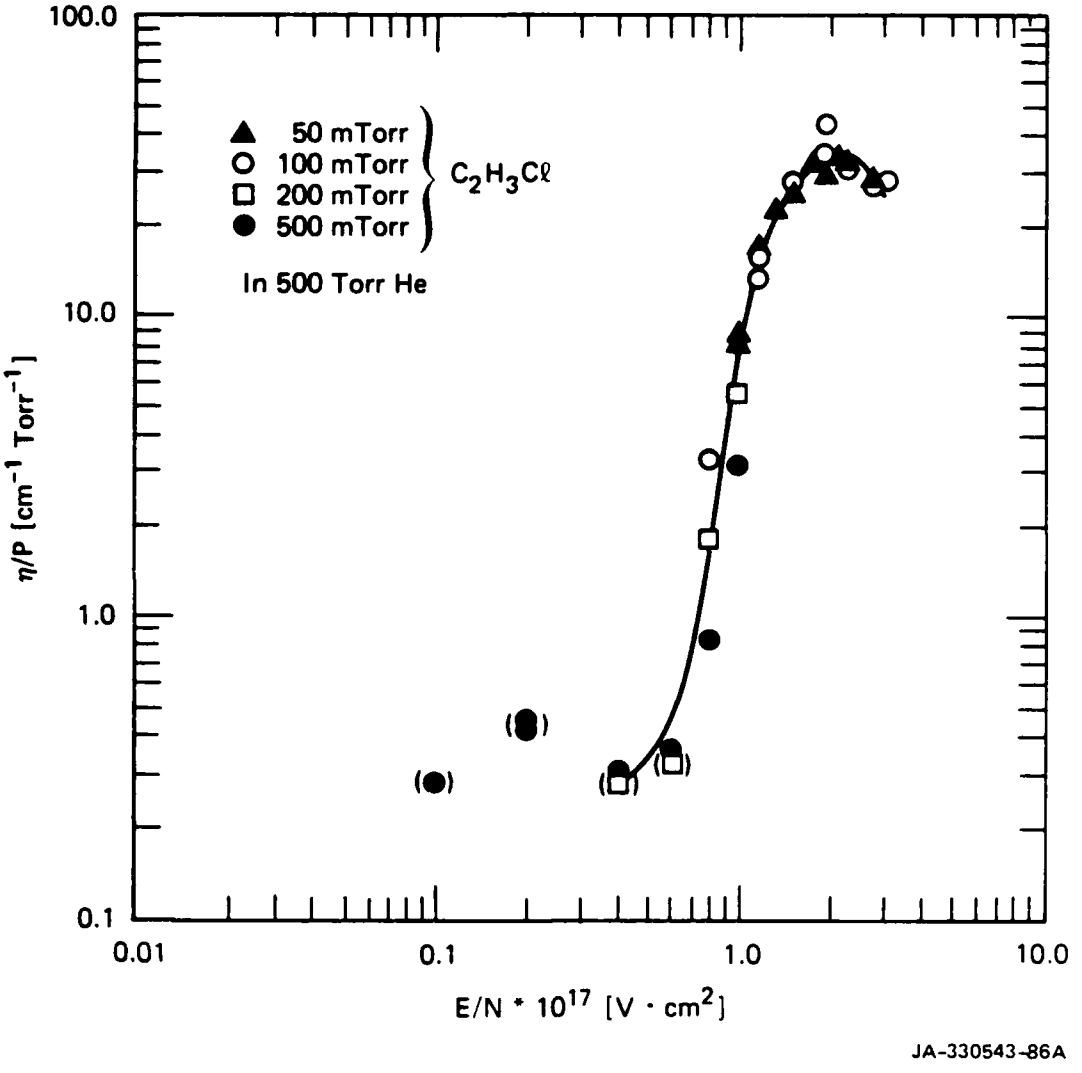

FIGURE 3-3 DISSOCIATIVE ELECTRON ATTACHMENT COEFFICIENT FOR DIFFERENT CONCENTRATIONS OF VINYLCHLORIDE (C_2H_3Cl) AT A CONSTANT BUFFER GAS PRESSURE OF 500 Torr He AND 300 K

measurable attachment, whereas the maximum of η/P occurred at 2.2 Td with η/P = 34 cm^{-1} $Torr^{-1}$. The values in parentheses for low E/N values in Figure 3-3 represent upper limits for η/P. With a value of 7.2×10^5 cm/s as drift velocity in helium at 2.2 Td, we calculate a rate constant of 7.6×10^{-10} cm^3 s^{-1} which is in good agreement with the value measured by McCorkle et al. (6×10^{-10} $cm^3 s^{-1}$) [MC84]. Our value was obtained at 300 K in helium, whereas McCorkle's values were measured at 373 K in Ar. A difference exists in the average electron energy of the attachment maximum, that is 0.91 eV for our measurement and 1.3 eV for the referenced experiment. However, this difference is not surprising because the electron energy distribution functions are different for He and Ar.

Qualitatively, similar results were obtained for TFE, whose η/P values remained near 1 cm^{-1} $Torr^{-1}$ for E/N = 0.4 to 5 Td. At higher values of E/N the attachment coefficient steeply rises to 15 cm^{-1} $Torr^{-1}$ at 9 Td, the maximum reduced field strength allowed before breakdown (200 mTorr TFE in 200 Torr He). These results, shown later in Figure 3-11, indicate the onset of the multiplication regime. We found no literature values with which to compare our results for TFE.

Laser Experiments

We first performed a reference experiment by irradiating 500 Torr of "pure" helium with 5 mJ/cm^2 at 193 nm in parallel to the electrodes (through the Brewster window); the recorded signal indicated a large contribution due to the presence of heavy charge carriers between the electrodes. We verified that the source of this signal was associated with the buffer gas and that it was most probably due to multiphoton ionization of some polyatomic impurity because this signal vanished at power levels of 1 mJ/cm^2 or less. Therefore, we further purified the buffer gas by passing it through a quartz-titanium element at 950°C and trapping the impurities at 77 K. This procedure eliminated residual signals even for high power levels of a few mJ/cm^2.

Next, we performed a laser experiment using 4 mTorr of VCl in 500 Torr of He. Again, a large signal was recorded due to the presence of heavy charge carriers at pulse energies of $\leq$1 mJ/cm^2. From our quantitative multiphoton ion-yield determination at 193 nm (Appendix B), we concluded that positive ions

were not responsible for the measured signal. Therefore, we interpreted this result as photoenhanced electron attachment due to the presence of excited attachers following the 193-nm excitation of VCl. Thus, the slowly varying signal was attributed to the presence of negative ions.

To rule out heterogeneous attachment processes, that is, attachment events occurring on the surface of the cathode, we compared the time-dependent signals for volume excitation (Brewster- window illumination), side-window illumination, and the combined Brewster- and side-window excitation. Figure 3-4 shows the results for 4.1 mTorr VCl in 500 Torr He at 0.38 mJ/cm^2 at 193 nm and 0.165 Td. The side-window illumination mode (Trace A) shows a small degree of attachment, whereas the Brewster-window illumination mode (Trace B) shows a large degree of attachment. The total charge generated by the Brewster-window illuminatiion is only about 20% due to scattered light striking the surface of the cathode as opposed to direct illumination of the cathode through the side window (i.e., $\leq 100\ \mu J/cm^2$ across the side window). The combined illumination mode (Trace C) shows a degree of attachment similar to that obtained using the Brewster window.

This experiment shows first that the total charge generated in Trace C is the sum of the respective values for Trace A and Trace B; that is, I(C) = I(A) + I(B) within experimental scatter. Second, the extent of attachment Trace B (volume excitation) is obtained when electrons are supplied through direct irradiation of the cathode. The value of ηd, which is a measure of the absolute number of attachment events undergone during the drift of the probing electrons across the distance d, is additive within experimental error; that is, $\eta d(C) = \eta d(A) + \eta d(B)$. The small degree of attachment for Trace A means that side-window illumination generated some excited attachers that were interacting with the photoelectrons being generated at the cathode surface when the beam passed on to the cathode. For geometrical reasons this situation is unavoidable at 193 nm and for side-window illumination. This result indicates that the attachment is a homogeneous process taking place primarily in the gas phase. Were the process heterogeneous, we would have observed a high degree of attachment for Trace A because the process would have taken place on the cathode surface.

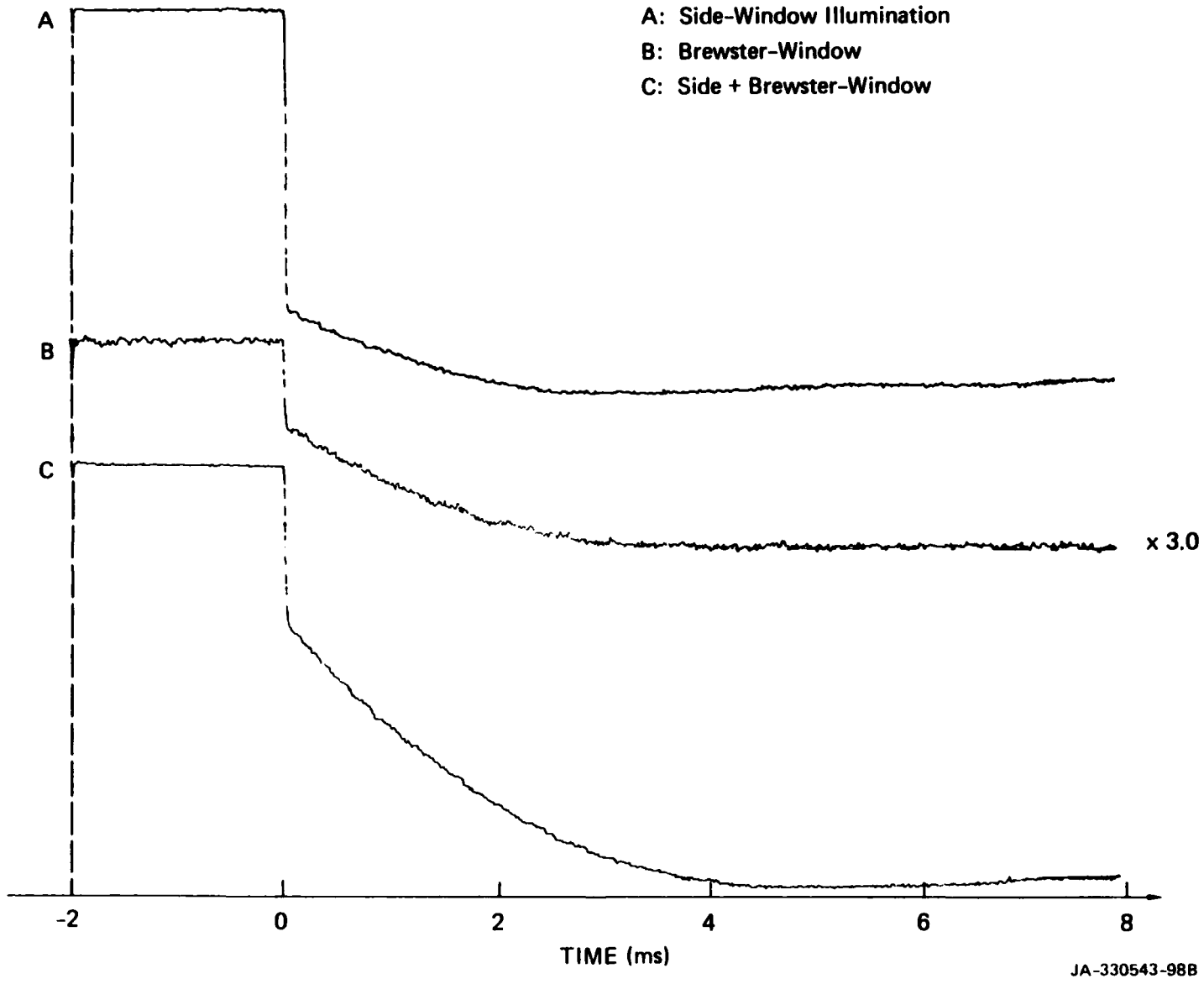

FIGURE 3-4 193-nm PHOTOENHANCED ELECTRON ATTACHMENT OF C_2H_3Cl (4.1 mTorr in 500 Torr He UHP) AT 0.38 mJ/cm^2 AND 0.165 Td

The total charge generated when pure helium is irradiated at 193 nm is only a few percent compared with the situation when VCl is present in the gas mix under conditions where the multiphoton ionization contribution is negligible, that is, a fraction of one percent ($\Phi \leq 1$ mJ/cm^2 for a few millitorr VCl). Figures 3-5 and 3-6 show the pressure dependence of I^{tot}, the total charge generated in the discharge gap. For VCl we observe a saturation phenomenon for both low-power (0.9 mJ/cm^2) and high-power (3.4 mJ/cm^2) conditions. The situation is even more pronounced for TFE, which shows a decrease of I^{tot} with increasing pressure after going through the maximum value. The results for TFE are particularly revealing because of the absence of multiphoton ionization processes for the conditions of Figure 3-6.

These results suggest that absorption of Raleigh scattered photons by unexcited gas at 193 nm decreases the yield of photoelectrons. The irradiated slab was 6.5 mm thick with the edges about equidistant from the respective electrodes (spacing 1.5 cm), so more than 4 mm separated the electrode surface from the nearest volume element of excited attachers. We explain this conspicuous drop in I^{tot} at high pressures due to the presence of absorbers in this "dark" region. This then means that the Raleigh scattering cross section for VCl and TFE at 193 nm must have an important resonance contribution that makes those species effective scatterers of 193-nm radiation.

The power dependence for both VCl and TFE obeys the law $I^{tot} = \Phi^2$, where Φ is the fluence at 193 nm in mJ/cm^2. This formal intensity law was obtained over the fluence range of 0.4 to 6 mJ/cm^2 in both cases. One possible interpretation could be that the single-photon-generated photodissociation products absorb another photon at 193 nm and thus reradiate short-wavelength photon energy that can be used to release photoelectrons from the cathode efficiently. In any case, it will be difficult to distinguish between fluorescence emission and Raleigh scattering in the absence of any wavelength-resolved emission data.

Under typical experimental conditions of 4 mTorr of VCl in 500 Torr He and a fluence of 0.9 mJ/cm^2, we calculate an absolute multiphoton ionization (MPI) yield of 1.3×10^6 ions between the electrodes in the drift cell. This yield is low compared with the signal corresponding to the total charge obtained in

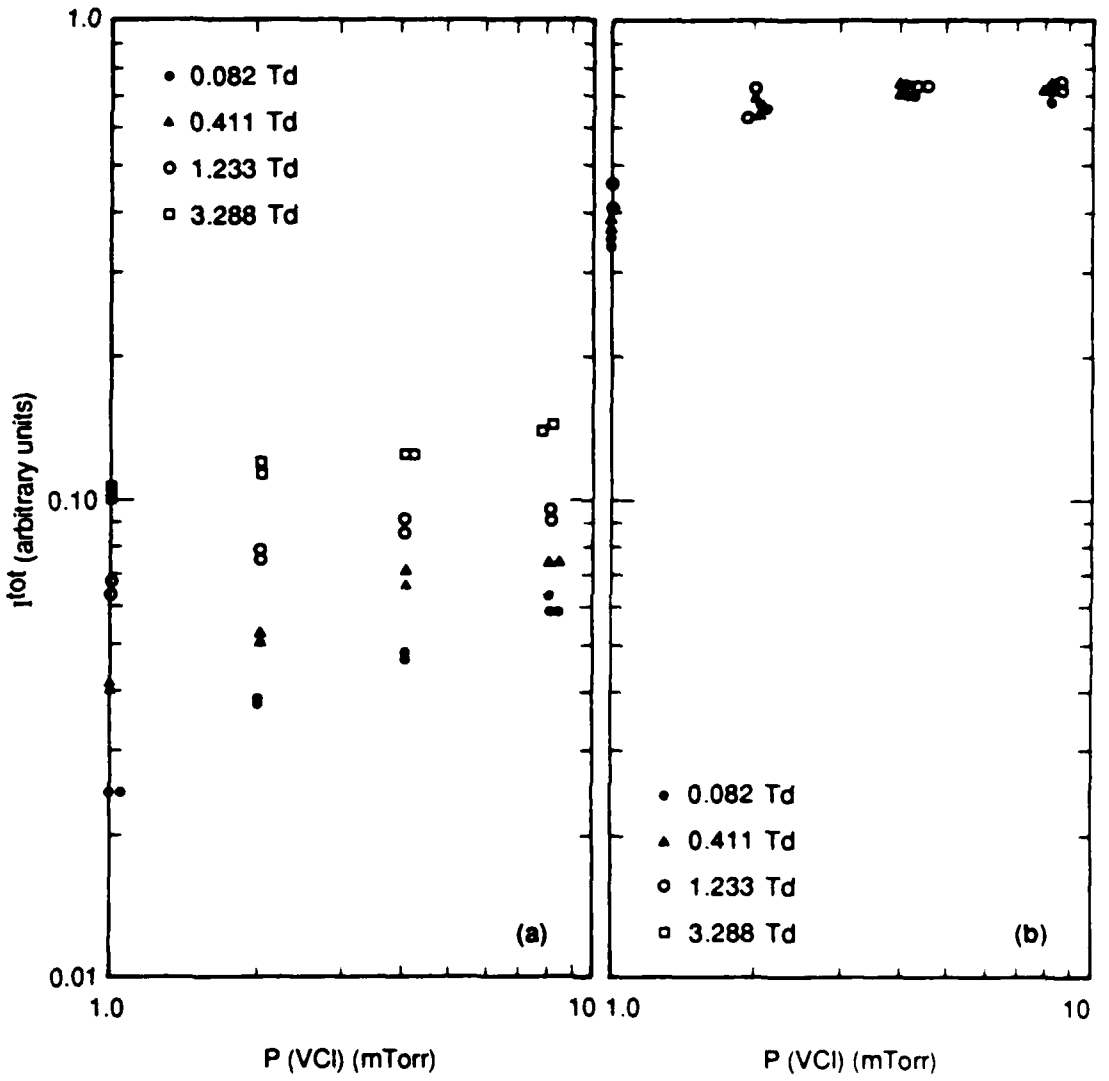

FIGURE 3-5 TOTAL SIGNAL I^{tot} IN ARBITRARY UNITS VERSUS VINYLCHLORIDE (C_2H_3Cl) PRESSURE AT 500 Torr He BUFFER GAS PRESSURE

(a) Corresponds to 0.9 mJ/cm^2, whereas (b) corresponds to 3.4 mJ/cm^2 irradiaton of the gas volume between the discharge electrodes. The cross section of the irradiated volume was 2.2 cm by 0.6 cm (1.3 cm^2).

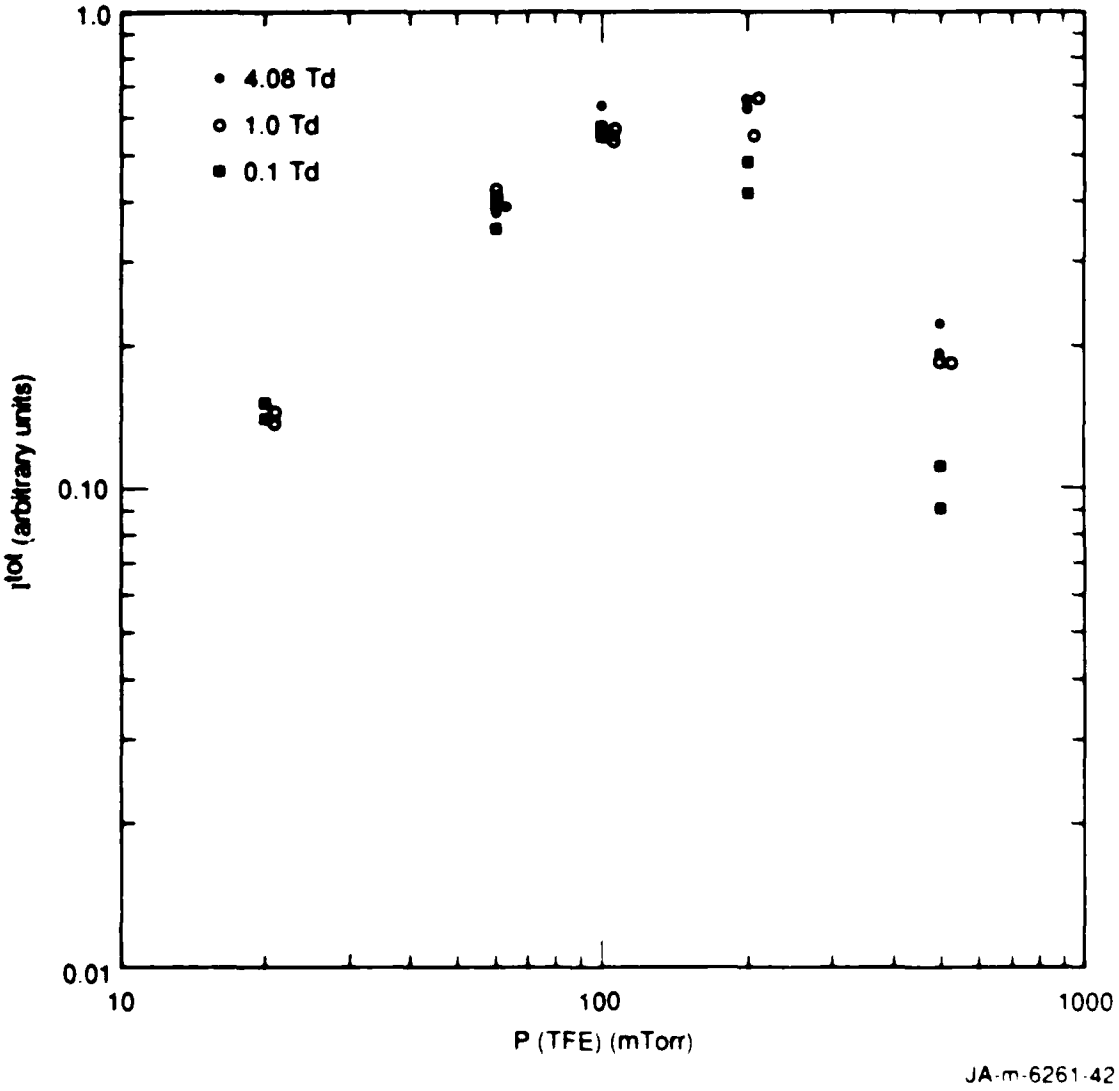

FIGURE 3-6 TOTAL SIGNAL I^{tot} IN ARBITRARY UNITS VERSUS TRIFLUOROETHYLENE (C_2F_3H) PRESSURE 100 Torr He BUFFER GAS PRESSURE

The laser (0.9 mJ/cm^2 at 193 nm) irradiated a cross section of 2.2 cm by 0.6 cm (1.3 cm^2).

the photoenhanced electron attachment experiment, which typically equals 4×10^7 electrons per laser shot. Thus, only 3% of the total charge reaching the anode originates from MPI of VCl. However, at 3 mJ/cm^2 the number of ions essentially equals the total charge generated in the attachment experiment, so that we anticipate a major problem in interpreting our time-dependent signal because the experiment is not able to distinguish between positive and negative ions.

For TFE the situation is similar. Because the absorption cross section of TFE is seven times lower than that of VCl, higher pressures of TFE must be used with the buffer gas to maintain the concentration of excited molecules at a comparable level with the VCl case. Typical experimental conditions are 100 mTorr of TFE exposed to 0.75 mJ/cm^2 of 193-nm laser radiation that lead to 2×10^5 ions generated by MPI corresponding to 0.5% ionization in terms of total charge carriers generated in the attachment experiment. However, at 4.6 mJ/cm^2 this number rises to 4×10^7 ions produced by MPI, which is again comparable to the total charge created in the photoenhanced electron-attachment experiment. As a consequence, we consider only attachment data that were obtained at low power levels and, therefore, under negligible MPI influence.

Photoenhanced Electron Attachment in Vinylchloride

Figure 3-7 shows the photoenhanced attachment coefficients for VCl as a function of the reduced electric field strength for various VCl pressures at 500 Torr buffer gas pressure of He. The laser energy was 0.9 mJ/cm^2 at 193 nm, corresponding to the excitation of 1.53% of the indicated VCl concentration using 1.7×10^{-17} cm^2 as absorption cross section at 193 nm [BE74]. In the absence of any detailed knowledge of VCl photochemistry at those wavelengths, we chose to express the attachment coefficient per Torr of ground state species; even then the enhancement in η/P is impressive with respect to the ground state attachment curve, which is also shown in Figure 3-7 for comparison. When η/P is expressed in terms of excited species, the η/P values in Figure 7 have to be multiplied by 65.

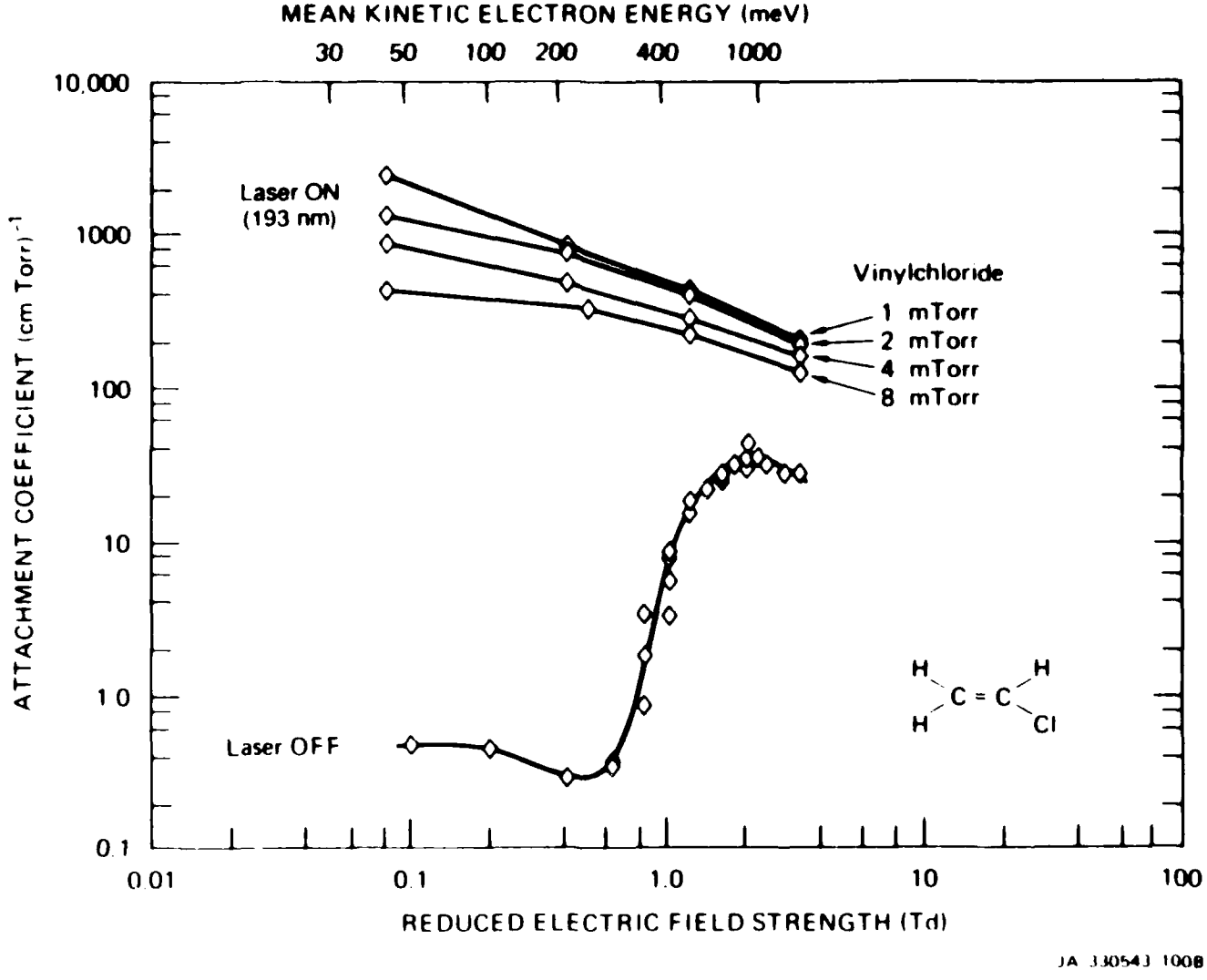

FIGURE 3.7 193-nm PHOTOEHNHANCED ELECTRON ATTACHMENT COEFFICIENT FOR VARIOUS CONCENTRATIONS OF VINYLCHLORIDE IN 500 Torr HELIUM BUFFER AT 0.92 Td AS A FUNCTION OF E/N

The lower group of points represents data for unexcited mixtures obtained for vinylchloride pressures from 50 to 500 mTorr in 500 Torr He. The upper group of points represents data for photoenhanced attachment expressed in terms of the ground state density for 0.9 mJ/cm^2 at 193 nm.

Figure 3-8 presents η/P versus E/N at two He buffer gas pressures. The attachment coefficient depends only slightly on buffer gas pressure, and the largest difference is at low E/N, where it is less than a factor of two. The enhancement factor is 20,000 at 0.1 Td and 16 at the maximum of the ground state attachment curve at 2.2 Td, 4 mTorr of VCl, and 0.9 mJ/cm^2 when η/P is expressed in terms of ground state VCl. This enhancement factor must be multiplied by 65 when η/P is expressed in terms of excited VCl molecules, and the intrinsic photoenhanced attachment coefficient will probably be even higher because not every excited VCl molecule will give rise to an electron attacher

The attachment coefficient was found to be a function of VCl pressure at constant buffer gas pressure. Figure 3-7 presents some data that show this trend. The results of a systematic study of the pressure dependence of η/P are presented in Figure 3-9, where η/P is plotted in semilogarithmic fashion as a function of VCl pressure. The apparent dependence of the quenching efficiency on E/N arises in a circumstantial way: at low values of E/N the electron drift time is longer; that is, the electrons reach the excited sample at later times, thus giving more time for quenching collisions. Likewise, the residence time of the probing electrons in the irradiated volume is longer, so more quenching can occur at low E/N. Therefore the slope of the curve in Figure 3-9 is expected to be a function of E/N.

Because the semilogarithmic plot of η/P versus P(VCl) data is not a straight line, we must question the conveniently held assumption that the quenching process is first order in VCl. We first assume that the buffer gas, helium, is not quenching on the time scale of the attachment experiment, that is, t_e, the drift time of the electrons. We are exploring two quenching reaction models, one pseudo-unimolecular and the other bimolecular in HX^*, the excited attacher. Reactions (3-4) and (3-5) represent the pseudo-unimolecular model:

$$HX^* + VCl \rightarrow HCl + VCl \quad (k_q) \qquad (3\text{-}4)$$

$$e^- + HCl^* \rightarrow H + Cl^- \quad (k_a) \qquad (3\text{-}5)$$

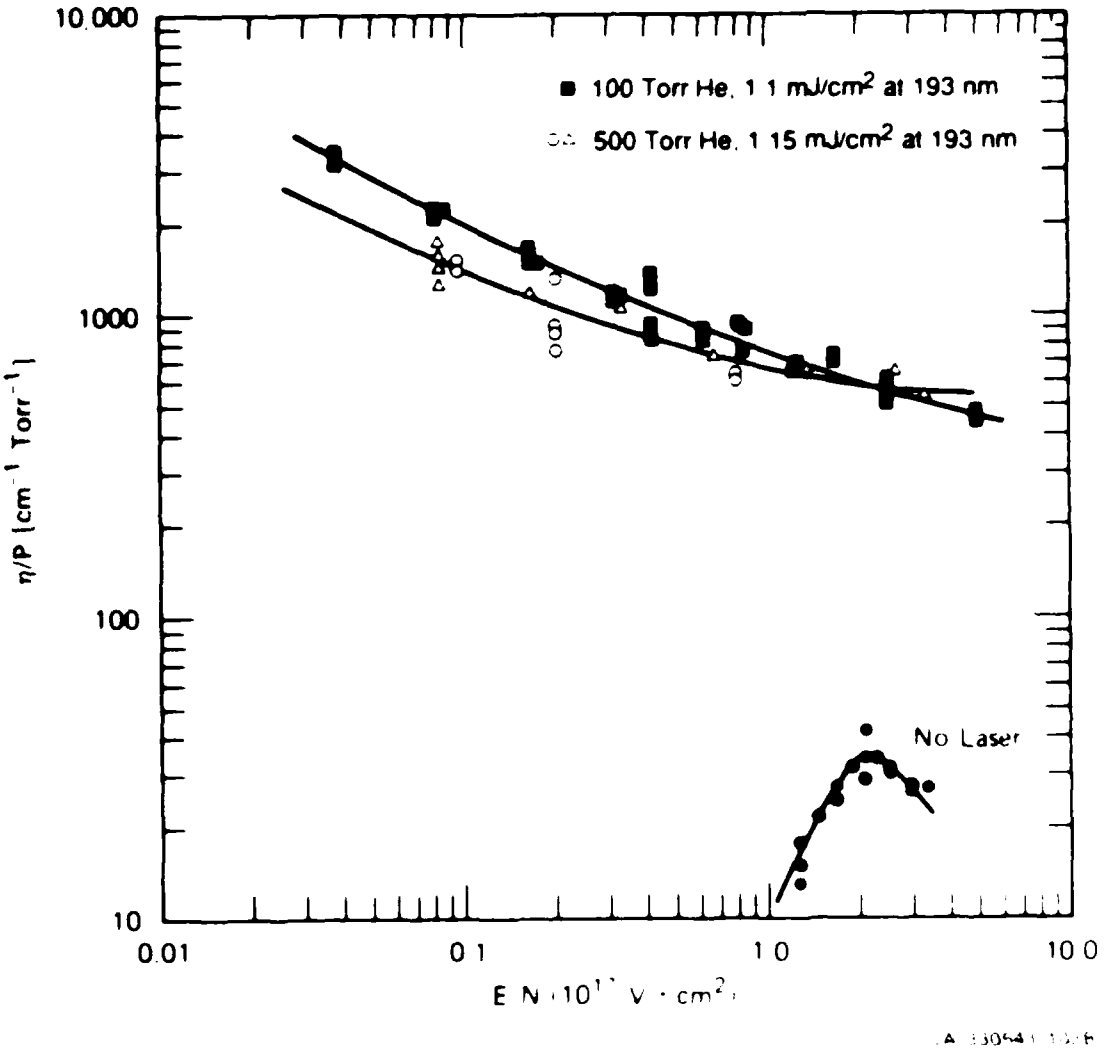

FIGURE 3-8 193-nm LASER PHOTOENHANCED ELECTRON ATTACHMENT COEFFICIENT (expressed as ground state density) FOR 4 1 mTorr VINYLCHLORIDE AT TWO HELIUM BUFFER GAS PRESSURES

The lower data group corresponds to dissociative electron attachment for the ground state of vinylchloride (data for FIGURE 3-3)

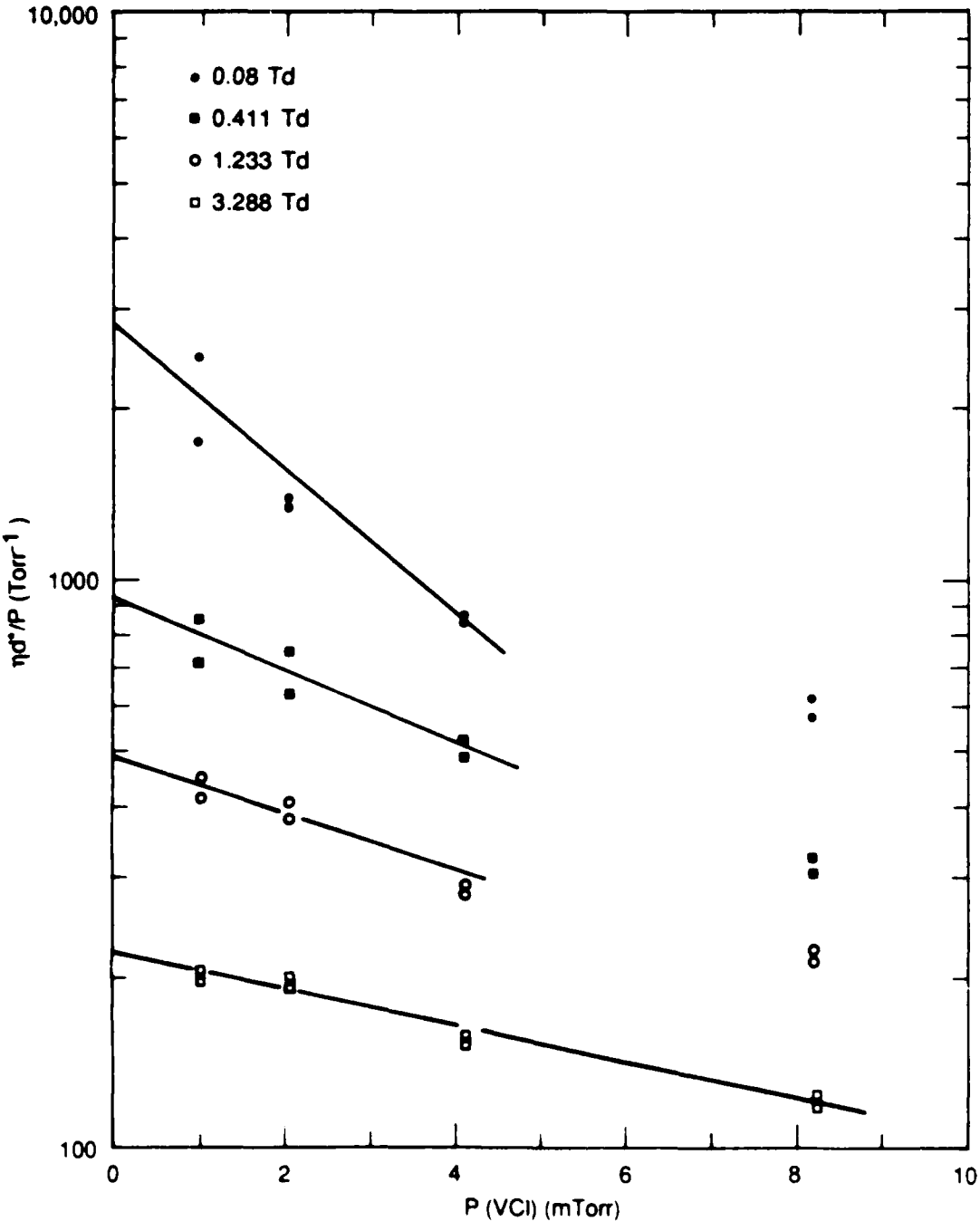

FIGURE 3-9 SEMILOG PLOT OF THE PRESSURE DEPENDENCE OF THE PHOTOENHANCED ELECTRON ATTACHMENT COEFFICIENT FOR VINYLCHLORIDE IN 500 Torr He AT 0.9 mJ/cm^2 (193 nm) AND FOR A CROSS-SECTIONAL AREA OF 2.2 cm BY 0.6 cm (1.31 cm^2) AT DIFFERENT REDUCED ELECTRIC FIELD STRENGTHS (E/N)

In the present pressure-dependence experiments, the HX^* density at a given time t is related to the density at t = 0 $[HX^*(0)]$ in the following way:

$$[HX^*(t)] = [HX^*(0)] \exp(-k_q P t) \tag{3-6}$$

At t = 0 the attachment coefficient η is given by the following relation:

$$\eta_0 = k_a[HCl^*(0)]/w_e \tag{3-7}$$

and at t this converts to:

$$\eta = k_a[HCl^*]/w_e \tag{3-8}$$

where η_0 is a function of E/N and $[HCl^*]$ at t = 0. The E/N values effectively control the time scale of the quenching experiment, and substituting equations (3-7) and (3-8) into (3-6) results in the following relation:

$$\eta = \eta_0 \exp(-k_q P d/2w_e) \tag{3-9}$$

Equation (3-9) expresses η as a function of E/N at constant pressure and describes the accelerated decrease of η at decreasing w_e (decreasing E/N) for a given pressure. The parametric dependence on the VCl pressure can be easily included and results in the following expression for the variation of the attachment coefficient η/P as a function of pressure and E/N:

$$\ln(\eta/P) = \ln(\eta_0/P) - k_q P(d/2w_e) \tag{3-10}$$

Following data points at constant E/N in Figure 3-9 is equivalent to varying P in equation (3-10), whereas a vertical cut through the data points at constant pressure explores the dependence of η/P on w_e, the drift velocity of the swarm electrons, which is a function of the gas mixture and E/N. The intercept η_0/P is the limiting value for the quantity k_a/w_e, which represents the intrinsic attachment rate constant in the absence of quenching of the excited attacher by VCl. The slope of the semilogarithmic plot is proportional to k_q, the quantity of interest. A more rigorous treatment of the attachment process leads to the conclusion that the effective distance over which electron attachment takes place is $0.5d^*$ with $d^* = 1.51$ cm.

The simple formula (3-10) treats the irradiated volume as being collapsed in the middle of the drift cell, symmetrically between the two electrodes. Table 3-1 presents the concentration-dependent data plotted in Figure 3-9, where the initial portion of the curve was approximated as a straight line. Because 193-nm photodissociation of VCl leads to highly excited molecular photofragments, we expect the photoproducts to cascade downward during collisional relaxation. We do not expect a straight line in the semilogarithmic plot and limit ourselves to discussing only the initial slope corresponding to the initial quenching rate constant of the multilevel system.

We used the electron drift velocities for highly diluted helium from the appendix of reference [HC74], which represent only an approximation to the true electron drift velocities in our gas mixture. We did not perform quantitative measurements of w_e for our gas mixtures. The average quenching rate constant for VCl was found to be $(5.3 \pm 1.3) \times 10^{-9}$ cm^3 s^{-1}, which is commensurate with quenching of highly excited species by polyatomic molecules. We believe that the systematic trend in the k_q values is due in part to the approximation to the true w_e values valid for the present gas mixtures. However, the data in Figure 3-9 present the change in initial slope of the straight line with E/N predicted by equation (3-10).

CONCENTRATION-DEPENDENT ATTACHMENT DATA FOR VINYLCHLORIDE AND TRIFLUOETHYLENE

Table 3-1

E/N(Td)	η_0/P (cm^{-1} $Torr^{-1}$)	w_e ($cm\ s^{-1}$)	Slope, m	k_q ($cm^3\ s^{-1}$)
Vinylchloride				
0.082	2800	1.3 (5)	8.98 (-15)	3.9(-9)
0.411	920	3.1 (5)	4.37 (-15)	4.5(-9)
1.23	420	5.3 (5)	3.59 (-15)	6.3(-9)
3.29	222	9.0 (5)	2.18 (-15)	6.5(-9)
Trifluoroethylene				
0.10	390	1.45 (5)	9.07 (-16)	4.4(-10)
0.82	200	4.35 (5)	6.52 (-16)	9.5(-10)
4.10	110	9.9 (5)	5.28 (-16)	1.7(-9)
8.20	100	1.4 (6)	2.85 (-16)	1.3(-9)

Because of the uncertainty in the interpretation of the quenching data in terms of a pseudo-unimolecular quenching model, we also applied a bimolecular quenching model in which deactivation of HX^* was brought about in collisions with fellow HX^* molecules. The pertinent kinetic equations are given in (3-11) and (3-12):

$$HX^* + HX^* \rightarrow 2\ HX \text{ or other products } (k_b) \qquad (3\text{-}11)$$

$$e^- + HX^* \rightarrow H\cdot + Cl\cdot \ (k_a) \qquad (3\text{-}12)$$

In the bimolecular quenching model the variation of $[HX^*]$ with time is given by the simple integrated rate law outlined in equation (3-13):

$$1/[HX^*] - 1/[HX^*_0] = k_b t \qquad (3\text{-}13)$$

After algebraic manipulation and substitution we arrive at equation (3-14) describing a linear dependence of the reciprocal attachment coefficient on pressure:

$$P/\eta d^* = w_e/\alpha k_a d^* + (k_b/2k_a)P \qquad (3\text{-}14)$$

where α is defined as $[HX^*_0]/P$, which is the pressure-independent photodissociation yield per 193-nm laser pulse. In contrast to the pseudo-unimolecular quenching model, the absolute concentration of the excited attacher is a necessary piece of input information due to the bimolecular rate law. The reciprocal plots are good straight lines whose slopes, however, systematically change by almost a factor of three over the E/N values explored in the plot due to the E/N dependence of k_a. The intercept $w_e/\alpha k_a d^*$ yields the

absolute value of k_a when an a prior estimate of α is entered. With the fluence of 1.2 mJ, an irradiated area of 1.3 cm^2, and an absorption cross section of 1.7×10^{-17} cm^2 for VCl [BE74], we arrive at a first estimate of 0.01984 for α, which is the fraction of excited VCl molecules. The value of both rate constants thus calculated is about 10^{-7} cm^3 s^{-1}, which is unusually high for the quenching process although it must be conceded that the quenching process involves very hot species not normally encountered in kinetic studies. Specifically, the average bimolecular quenching rate constant can be calculated as $(4.3 \pm 0.7) \times 10^{-7}$ cm^3 s^{-1}.

Table 3-2 presents the original data on which this evaluation is based. At this point, one quenching model does not appear more appropriate than the other. The bimolecular quenching model seems slightly more suggestive in view of the good linearity of its reciprocal plots, whereas the strong variation of k_q with the degree of internal excitation of the attacher, which the strong nonlinearity of the semilogarithmic plots of Figure 3-9 seem to indicate, is certainly also unexpected.

The power dependence of the VCl attachment coefficient could not be measured because of the increasing importance of multiphoton-ionization processes. At fluences ≤2 mJ per pulse, we verified that the attachment coefficient increased linearly with laser fluence. At fluences exceeding 2 mJ/pulse (equivalent to 1.5 mJ/cm^2), the apparent attachment coefficient levels off with 4 mTorr VCl. This effect can be understood by the increased importance of multiphoton-ionization, which should yield $q = I^{tot}/I^e = 2$ in the absence of any attachment (see Appendix B). With attachment this q value can only increase and can, therefore, never attain values ≤2. This is the experimentally observed situation for higher laser fluences, and we take this as an indication of the increasing importance ot ionization processes with increasing 193 nm laser fluence.. Therefore, we cannot interpret the slowly varying portion of the signal as due exclusively to negative ions, and another method is needed to measure the power dependence of η/P. This alternative method is discussed below.

Table 3-2

ORIGINAL DATA FOR VINYLCHLORIDE FOR BIMOLECULAR QUENCHING MODEL

E/N (Td)	Slope, m	Intercept c(Torr)	k_a (cm^3s^{-1})	k_a (cm^3s^{-1})	k_q η_0/P
0.082	0.182	3.5 (-4)	9.6 (-7)	3.5 (-7)	4746
0.411	0.256	1.0 (-3)	8.0 (-7)	4.1 (-7)	1661
1.233	0.331	2.0 (-3)	6.9 (-7)	4.5 (-7)	834
3.288	0.475	4.4 (-3)	5.4 (-7)	5.1 (-7)	383

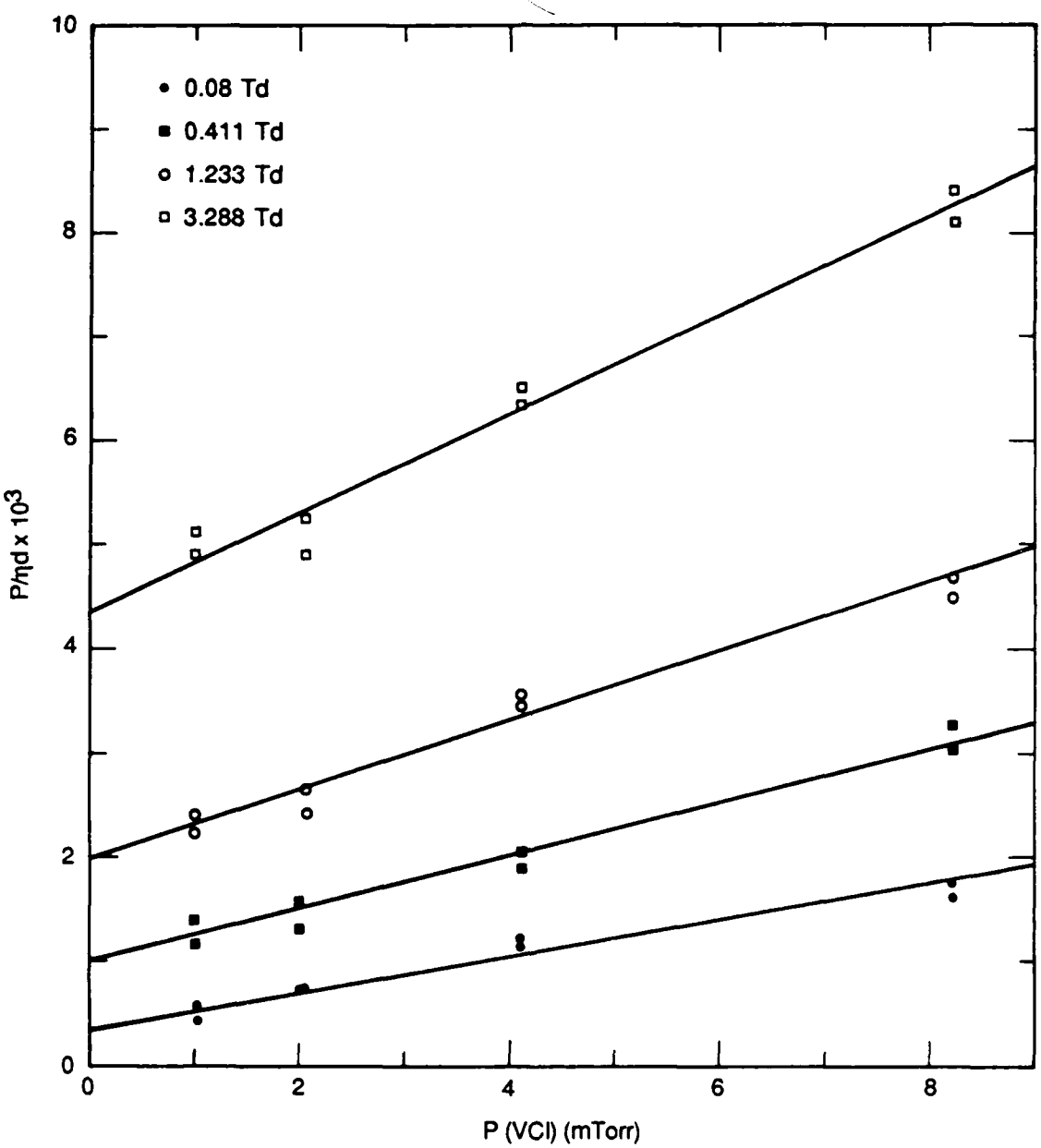

FIGURE 3-10 RECIPROCAL PLOT OF THE PRESSURE DEPENDENCE OF THE PHOTOENHANCED ELECTRON ATTACHMENT COEFFICIENT FOR VINYLCHLORIDE IN 500 Torr He AT 0.9 mJ/cm^2 (193 nm)

Photoenhanced Electron Attachment in Trifluoroethylene

We subjected TFE to 193-nm laser pulses and studied the attachment behavior of the irradiated volume. Because TFE is a weaker absorber at 193 nm by a factor of 7 ($\sigma_{193} = 2.44 \times 10^{-18}$ cm^2 [BS71]), the TFE attachment experiments were performed at a pressure that was roughly an order of magnitude higher than the pressure used in the VCl experiments to achieve roughly the same number density of excited attachers. An important consequence of the higher pressure was the apparent higher degree of quenching as the pressure was varied.

Figure 3-11 presents our data on dissociative attachment of TFE at 100 Torr of helium buffer gas and 100 mTorr of TFE. The attachment to ground state TFE is described by the lower group of points in the η/P versus E/N graph. The attachment coefficient is initially low, 1 cm^{-1} Torr^{-1}, but gradually increases to 10 cm^{-1}Torr^{-1} starting at 3 Td. Breakdown in these TFE-He mixtures is occurring at E/N values in excess of 10 Td, so the rise in apparent attachment for E/N $\leq$5 Td suggests the start of the multiplication regime. The results for the photoenhanced case is represented by the upper group of data points obtained at a laser fluence of 0.68 mJ/cm^2, corresponding to a fractional excitation of 1.36×10^{-3}.

The η/P values are expressed in terms of ground state TFE pressure, so the intrinsic attachment coefficient must be multiplied by a factor of 734 corresponding to an excited state population of 5×10^{12} cm^{-3}. Note that the general functional dependence of the photoenhanced η/P values on E/N is a gentle decline by a factor of 4 similar to the situation in VCl. The photoenhancement factor is 40 at 9 Td under the conditions of Figure 3-11. An enhancement by more than three orders of magnitude is found at lower E/N based on the pressure of excited TFE molecules, a situation that is similar to the one in VCl.

Figure 3-12 presents the pressure dependence of η/P plotted in a semilogarithmic fashion using the first-order quenching model outlined in detail above. Table 3-1 presents the corresponding quantitative data with an average monomolecular quenching rate constant of $(1.1 \pm 0.4) \times 10^{-9}$ cm^3 s^{-1}, which is about a factor of 4 lower than in the analogous VCl case. As in the

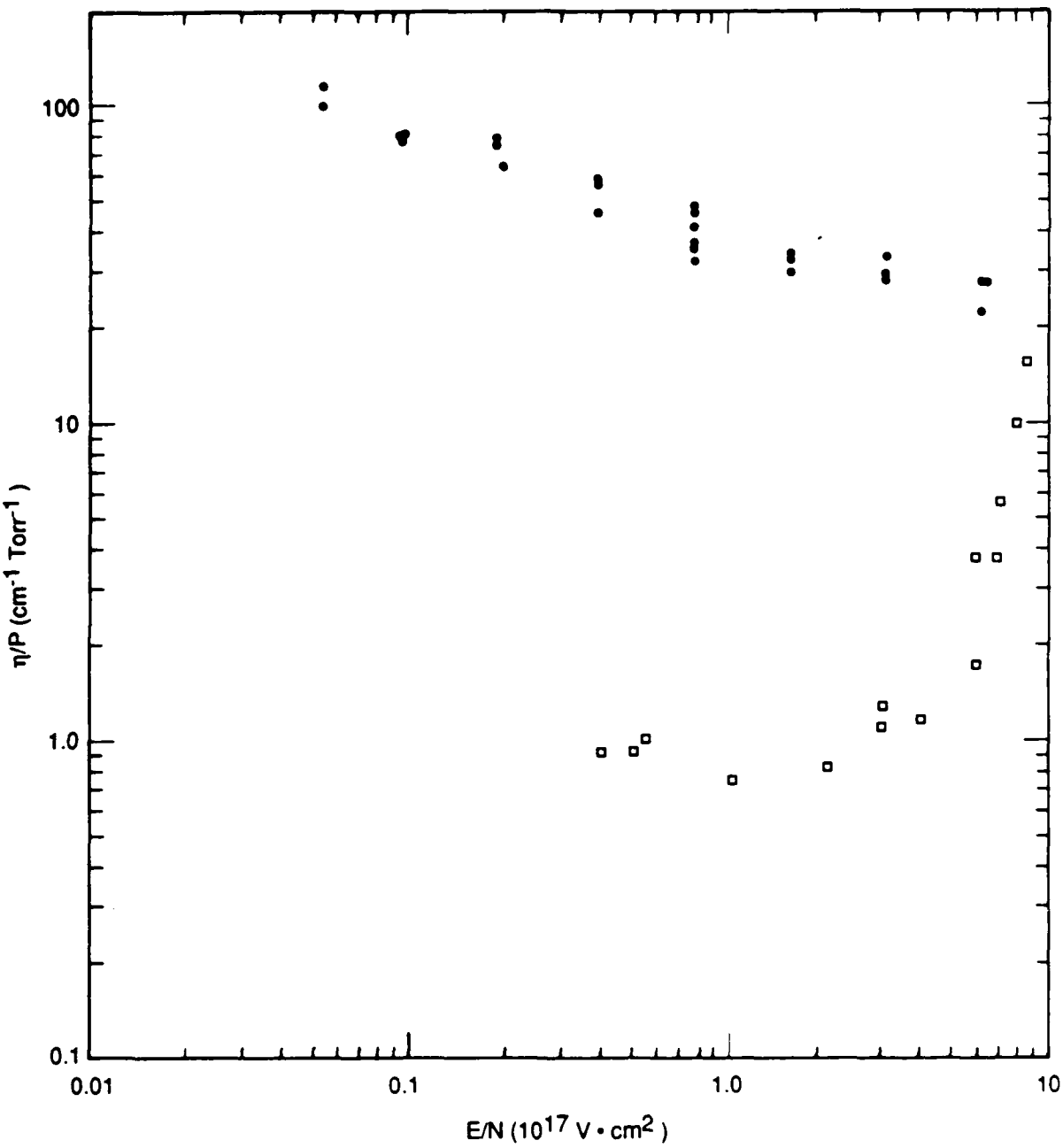

FIGURE 3-11 PHOTOENHANCED ELECTRON ATTACHMENT COEFFICIENT (expressed as ground state density) of 100 mTorr TRIFLUOROETHYLENE (TFE) IN 100 Torr He BUFFER GAS AT 0.7 mJ/cm^2 (193 nm) AS A FUNCTION OF E/N (•)

The lower data group (□) corresponds to dissociative electron attachment of ground state TFE.

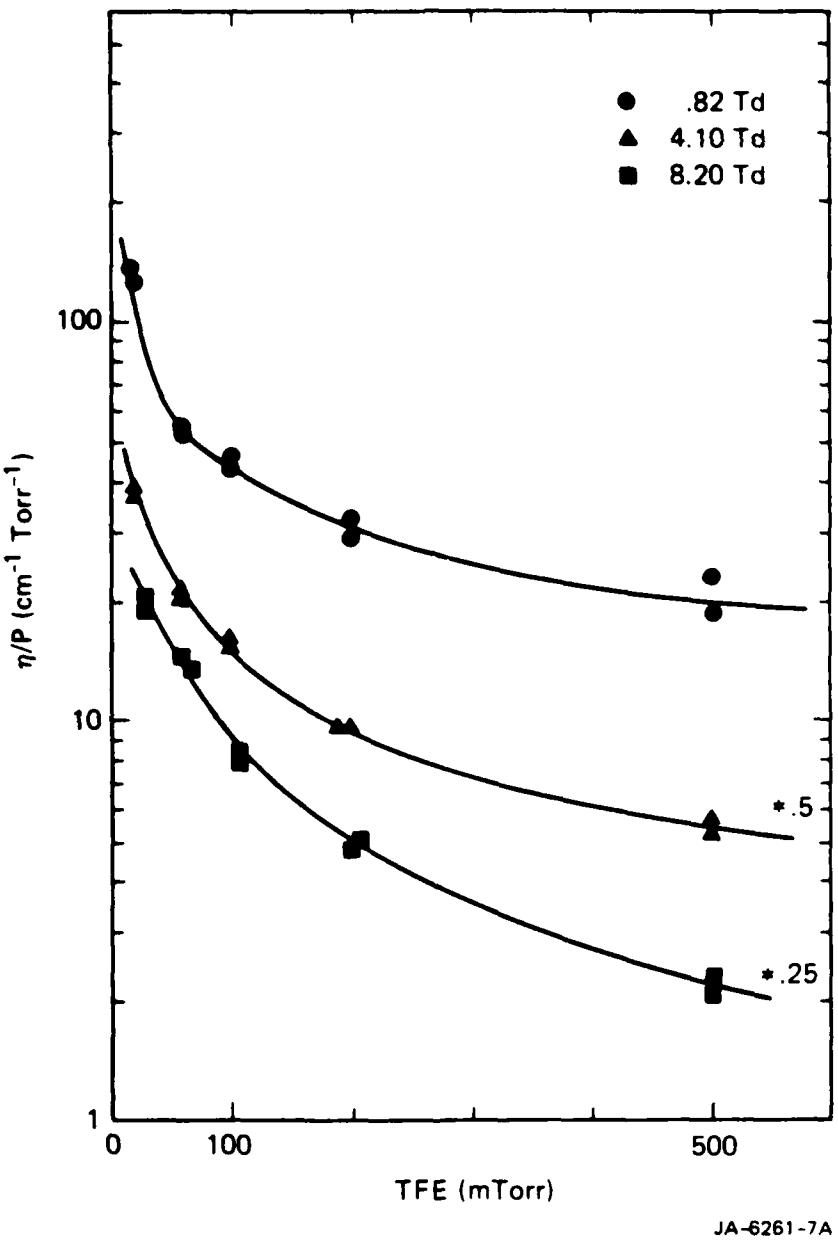

FIGURE 3-12 SEMILOG PLOT OF THE PRESSURE DEPENDENCE OF THE PHOTOENHANCED ELECTRON ATTACHMENT COEFFICIENT OF TRIFLUOROETHYLENE (TFE) IN 100 Torr He BUFFER GAS AT 0.76 mJ/cm^2 (193 nm) AND FOR DIFFERENT (E/N) VALUES

VCl case, the electron drift velocities in those concentrated TFE gas mixtures may not adequately reflect the true electron drift velocities. Furthermore, highly excited HF^* relaxes toward the ground state by a collisional cascade mechanism that could lead to a highly nonlinear semilogarithmic plot, as shown in Figure 3-11.

The average unimolecular quenching rate constant is a factor of 4 lower than that for VCl, a fact that is commensurate with the somewhat lower degree of excitation expected for TFE based on the higher endothermicity of the HF elimination in TFE on 193-nm photolysis in comparison with the analogous HCl elimination in VCl. The second-order analysis also outlined for VCl photoenhanced attachment did not produce consistent results. In particular, the data did not result in straight lines when analyzed in terms of equation (3-14), and when a straight line was imposed on the data, the resulting values for the rate constants were between one and two orders of magnitude too large. We thus conclude that a monomolecular quenching model is appropriate for TFE attachment and that we can exclude a second-order analysis.

Photoenhanced Electron Attachment in VCl and TFE at High Fluence

The nature of our present experiment precludes the distinction of positive from negative heavy charge carriers contributing to the slowly varying signal due to the displacement current. To overcome this limitation, we had to resort to a trick that enables one to emphasize the effect of the negative ions at the expense of the positive ones. The signal is proportional to the product of the density times the distance to the respective "final destination" or discharge electrode. To emphasize the positive ion contribution to the signal, we must create the positive charges in a volume as close as possible to the anode when positive (MPI) and negative (attachment) ions are generated through laser irradiation of the gas volume. In our case, we wanted to eliminate the positive ion contribution to the signal by irradiating a 1-mm-thick slab as close as possible to the cathode ($\leq$0.5 mm from cathode). This does not mean, however, that the positive ions will not exist or are not generated; rather the experiment is insensitive to their existence because the respective displacement current is vanishingly small.

This simple trick enabled us to study the photoenhanced electron attachment process under high-power irradiation, that is, under conditions where charge separation by multiphoton ionization is equal to or even exceeds the generation of photoelectrons by whatever mechanism is operating under these conditions. However, this simple modification also means that we sacrifice sensitivity with respect to ground state attachment because the effective attachment length is now only 1 mm out of 15 mm, the total gap length. Thus, we need to increase the pressure of the precursor and, therefore, the pressure of the excited attachers by roughly tenfold.

The consequence of increasing the pressure of the precursor is that the two experiments, the large cross-section (6-mm) low-laser-fluence irradiation (1 mJ/cm^2) experiment and the narrow-slit (1-mm) high-laser-fluence ($\geq$ 1 mJ/cm^2) experiment, become nonequivalent based on the large quenching rate constants. Especially in our case, this situation can lead to uncertainties because of the inability to reliably describe the quenching behavior in terms of an unambiguous rate law. The net result of this required pressure increase is the increased importance of ground state attachment that takes place in the nonirradiated volume. The ground state contribution has to be subtracted from the total attachment coefficient, which means that accurate ground state attachment data must be obtained under identical experimental conditions.

Under high-fluence conditions charge separation should occur predominantly by multiphoton ionization (MPI). Consequently, a plot of I^{tot} versus fluence Φ_0 should result in a formal intensity law that is indicative of MPI. Figure 3-13 is a plot for 45 mTorr VCl in 500 Torr He under slit irradiation conditions and shows an intensity exponent very close to the one measured by monitoring the positive ions (Appendix B). In a log-log plot the exponential law with the highest exponent is emphasized. This means that the data in such a plot may still contain a quadratic dependence of I^{tot} on Φ_0 due to the scattering contribution measured at low power (see the previous Laser Experiments subsection).

Figure 3-14 shows the E/N dependence of η/P for VCl at high laser fluence, high precursor pressure, and slit irradiation near the cathode. The general functional dependence of η/P is similar to the result obtained at low power

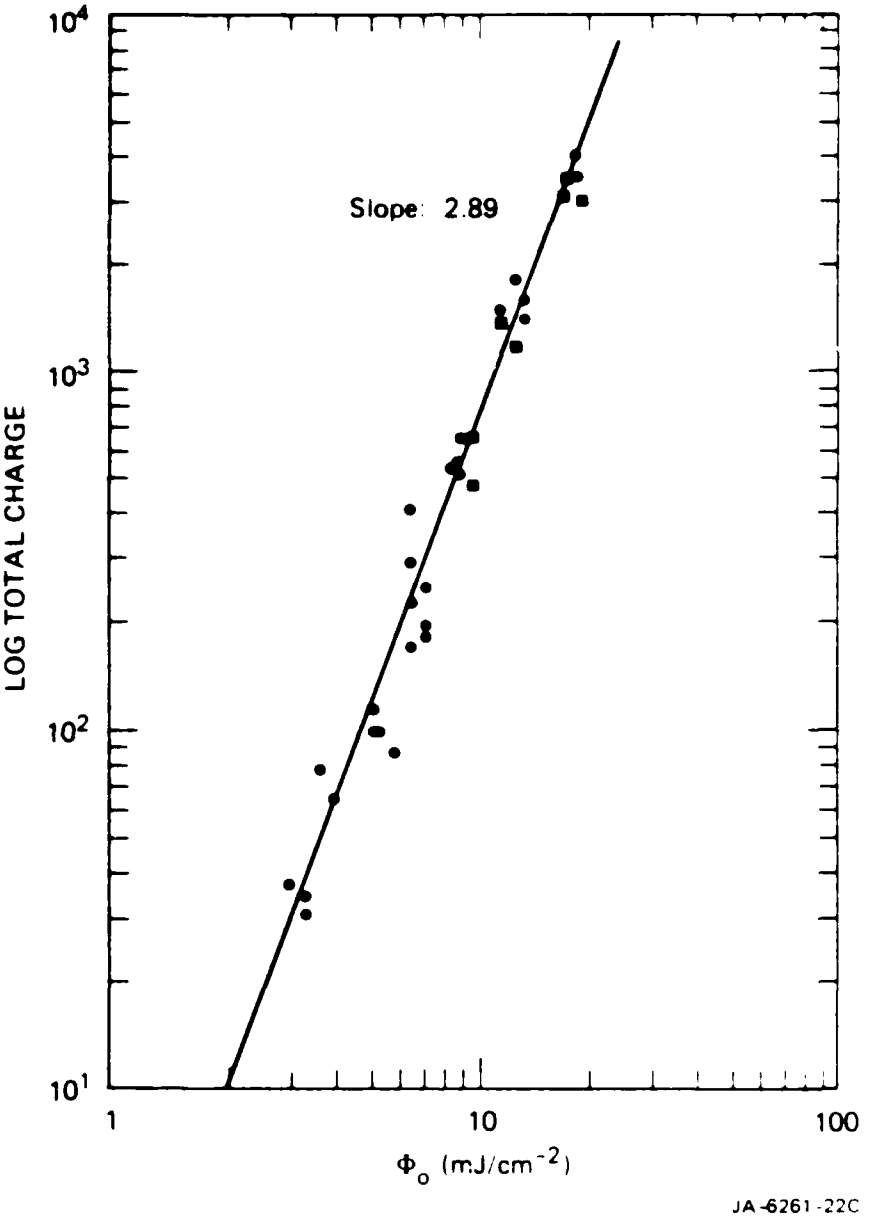

FIGURE 3-13 TOTAL CHARGE (I_{tot}) VERSUS 193-nm LASER FLUENCE IN 45 n.Torr VINYLCHLORIDE IN 500 Torr He AT 0.08 Td AND WITH 1-mm SLIT IRRADIATION

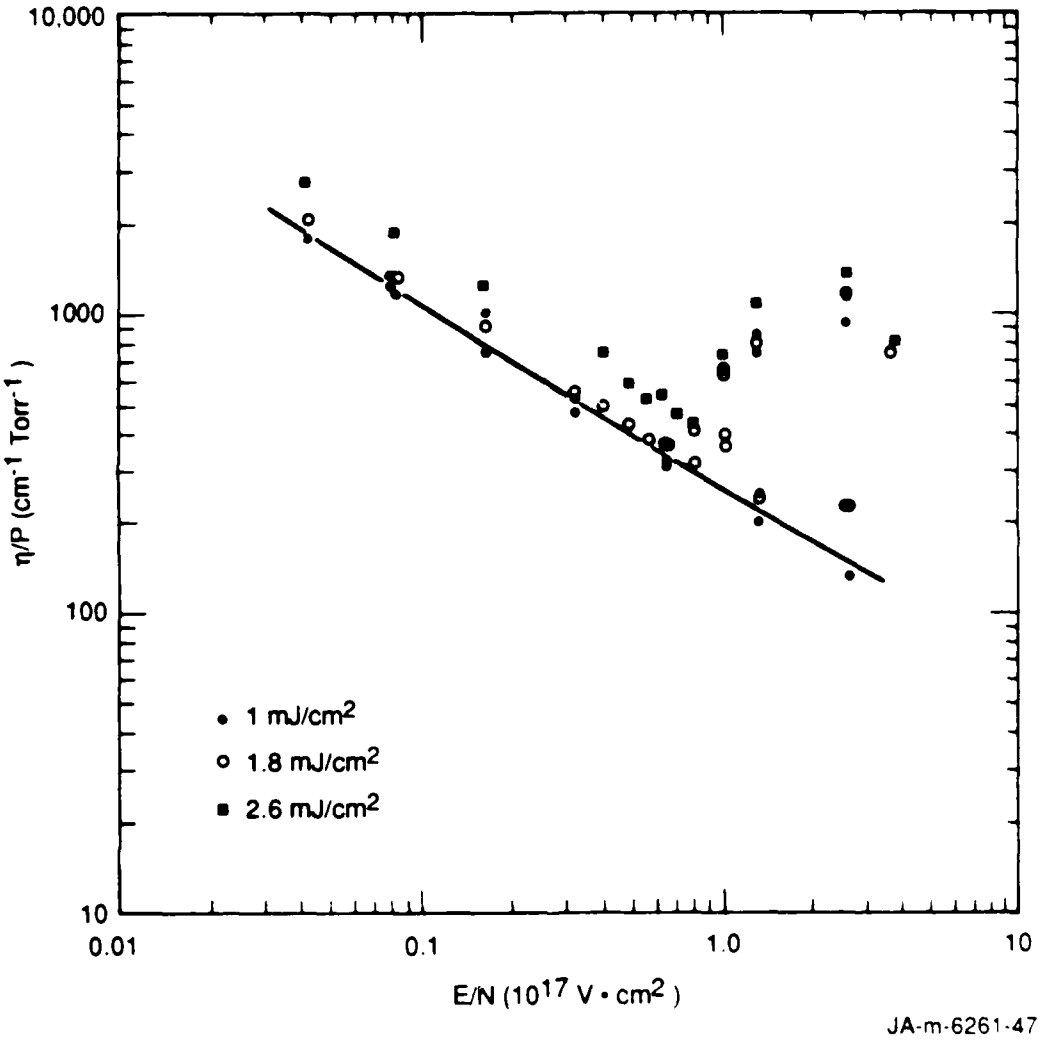

FIGURE 3-14 E/N DEPENDENCE OF THE PHOTOENHANCED ELECTRON ATTACHMENT COEFFICIENT FOR 44mTorr OF VINYLCHLORIDE (VCl) AT DIFFERENT LASER FLUENCES (193 nm) FOR 1-mm SLIT-IRRADIATION (see text)

For E/N ≥ 0.8 Td, the data (o,•) have been corrected for the ground state contribution to dissociative electron attachment of VCl.

irradiation (Figure 3-7). Clearly, the maximum in η/P around 2 Td is due to VCl ground state dissociative attachment, and after subtraction of this ground state contribution, the maximum disappears. For the subtraction the data of Figure 3-3 were used, and the corrected η/P dependence shows a monotonic decline. Two different data sets were collected for the pressure dependence of η/P at four E/N values. The average quenching rate constant k_q based on an unimolecular quenching model was measured as $(1.36 \pm 0.76) \times 10^{-9}$ cm^3 s^{-1} for 2.1 mJ/cm^2, and at 3.8 mJ/cm^2 it was $(1.21 \pm 0.79) \times 10^{-9}$ cm^3 s^{-1}. This represents a decrease of a factor of 4 compared with our low pressure results. This decrease in k_q with increasing pressure is expected in view of the strongly nonlinear semilogarithmic plot for collisional quenching of excited VCl or its 193-nm photodissociation product.

Figure 3-15 shows the E/N dependence of η/P for TFE at high laser fluence, high precursor pressure, and slit irradiation. As in VCl, the general shape of the attachment curve is similar to that obtained at low TFE pressure (Figure 3-11). Here the upturn of the attachment coefficient at field strengths >2 Td is certainly a consequence of the importance of the ground state attachment process (Figure 3-11). However, in this instance we did not attempt to subtract the ground state attachment effect because we did not have sufficient data obtained under the proper experimental conditions. The buffer gas pressure for the data of Figure 3-15 was 500 Torr He, whereas that for the data of Figure 3-11 was 100 Torr He.

The pressure dependence of η/P in 500 Torr He was measured for 4.5 mJ/cm^2 and slit irradiation conditions. The average k_q was found as $(1.4 \pm 0.35) \times 10^{-11}$ cm^3 s^{-1}, which is about a factor of 100 smaller than the average rate constant presented in Table 3-2. This decrease on k_q may seem excessive, but recall that for TFE k_q is a strong function of TFE pressure (Fig. 3-12). Futhermore, the total buffer gas pressure differs by a factor of five. In contrast to VCl, it is not clear which quenching model for excited TFE should be used because neither unimolecular nor bimolecular model seems to work well. Excited TFE quenching seems to be characterized by a very steep initial decrease of k_q with pressure.

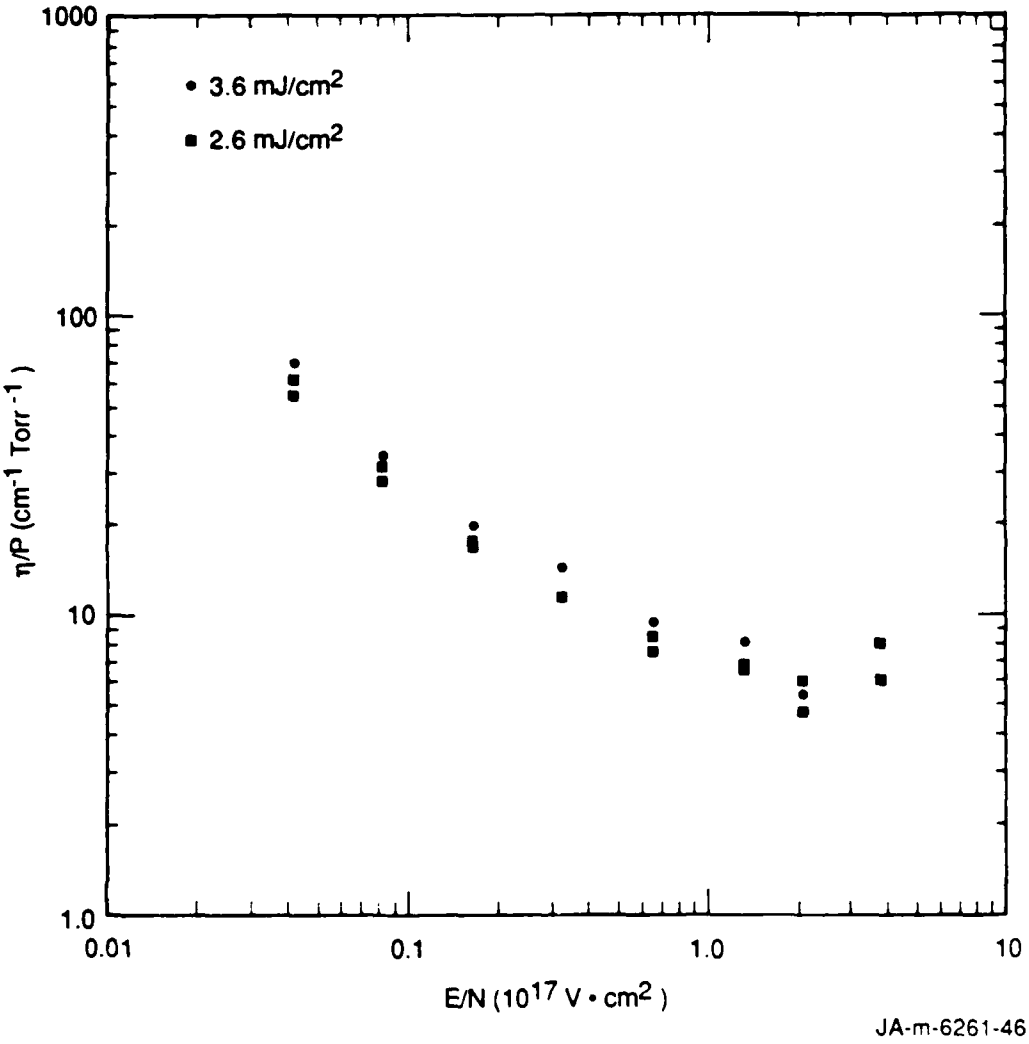

FIGURE 3-15 E/N DEPENDENCE OF THE PHOTOENHANCED ELECTRON ATTACHMENT COEFFICIENT FOR 1 Torr OF TRIFLUOROETHYLENE (TFE) IN 500 Torr He BUFFER GAS AT TWO LASER FLUENCES FOR 1-mm SLIT IRRADIATION (see text)

Two-Laser Experiment in VCl Photoenhanced Electron Attachment

The idea behind the two-laser experiment is to generate photoelectrons by 248-nm laser irradiation in oblique incidence and to let this electron swarm interact with a gas volume excited at 193 nm. The time delay can be varied smoothly from positive Δt (the 193-nm laser is fired first) to negative Δt (the 248-nm laser is fired first) to observe the transient nature of the photoenhanced electron attachment effect. The irradiation geometry was such that the 193-nm volume-exciting laser irradiated a 1-mm slit positioned as close to the cathode as possible to avoid detection of the positive ions generated by MPI processes. The photoelectron-releasing 248-nm laser irradiated an area on the cathode that was adjacent to the 193-nm excited volume. The initial experiment indicated that about 2.7 times as many electrons were not interacting with the excited volume than were interacting with the volume because of the mismatch between irradiation geometries. This factor of 2.7 was measured by comparing the "photoenhancement effect" I^n/I^{tot} for the two-laser experiment with that of the one-laser experiment at 193 nm. I^n is the fraction of the signal due to the negative ions, whereas I^{tot} corresponds to the total signal. In this procedure we assumed that the photoelectrons generated from volume excitation at 193 nm were all interacting with the excited volume created by the same laser.

At long delay times, it is possible to distinguish between both electron swarms, the swarm released through 193-nm excitation and the second swarm released through 248-nm irradiation of the cathode. Figure 3-16 shows the oscilloscope traces of signals from a two-laser experiment in 4.1 mTorr VCl, 500 Torr of He, and 0.082 Td. It is clear that the 248-nm irradiation of the cathode leads to I^{tot} values that are an order of magnitude larger than the corresponding ones from 193-nm irradiation. Photoenhanced attachment resulting from the action of both lasers is immediately obvious in that I^e for Trace C is significantly smaller than I^e for Trace A that displays the signal for the 248-nm triggered release of electrons from the cathode. This situation is evident in Figures 3-16(a) and (b), which show the drift time of the electrons and negative ions, respectively. The time delay Δt between the 193-nm and 248-nm laser beams was chosen as 15 μs for the conditions of Figure 3-16, and because

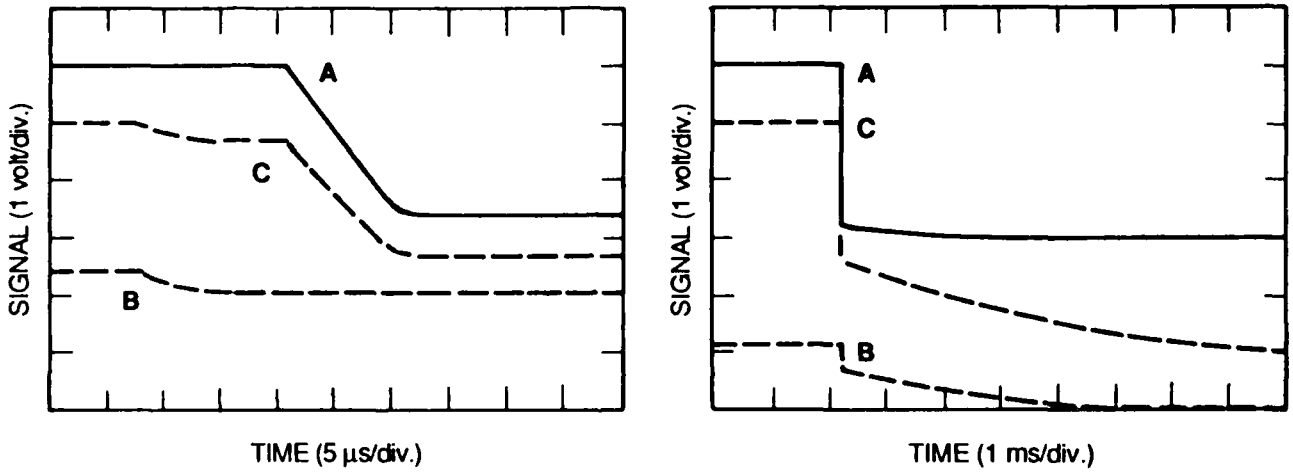

FIGURE 3-16 OSCILLOSCOPE TRACES OF TRANSIENT VOLTAGE FOR 4.1 mTorr VINYLCHLORIDE IN 500 Torr He BUFFER GAS AT 0.082 Td

The 193-nm laser irradiated a cross section of 1.0 cm by 0.1 cm at 6 mJ/cm^2. Trace A corresponds to the transient voltage obtained by 248-nm laser and trace B to 193-nm laser irradiation individually. In trace C the 248-nm laser was delayed by 15 μs with respect to the 193-nm laser.

of its magnitude the drift of the two electron swarms can be clearly resolved in time. Therefore, we applied an additive correction to all other two-laser attachment data because we are basically dealing with two attachment experiments separated by Δt. We focused on the attachment behavior of the 248-nm laser-generated electron swarm; thus, when reviewing data from the two-laser experiments, we subtract the effect of the 193-nm laser-generated electron swarm from the two-laser attachment trace.

We define a "photoenhancement effect" by I^n/I^{tot}, which is a quantity that describes the importance of electron attachment with respect to total charge generated by the probe. Figures 3-17 and 3-18 present the results in terms of I^n/I^{tot} as a function of the delay time Δt on the microsecond time scale, whereas Figure 3-19 presents that same kind of data on a longer time scale (tens of microseconds). The VCl pressure chosen was 42 mTorr in 500 Torr He at 0.082 Td. The photoenhancement effect essentially vanishes at negative time delays of a few microseconds, which is equivalent to probing the volume before irradiation, and generation of excited attachers. The negative delay time of a microsecond or so means that it takes the average swarm electron about that amount of time to drift into the average position where the excited attachers are found. In other words, at $\Delta t = 0$ the swarm electrons (248-nm irradiation) are generated a microsecond before the excited attacher, which is generated essentially instantaneous, because it takes the electrons about that long to drift into the excited volume.

The error bars in Figures 3-17 and 3-18 are significant because of the subtraction procedure outlined above. Because this measurement is important to our concept of photoenhanced electron attachment, we obtained several independent data sets to confirm the effect. The chosen scale is indeed compressed for decreasing $I^nI/^{tot}$, which, for convenience, is related to I^{tot}/I^e by equation (3-15):

$$(1 - I^n/I^{tot})^{-1} = I^{tot}/I^e \qquad (3\text{-}15)$$

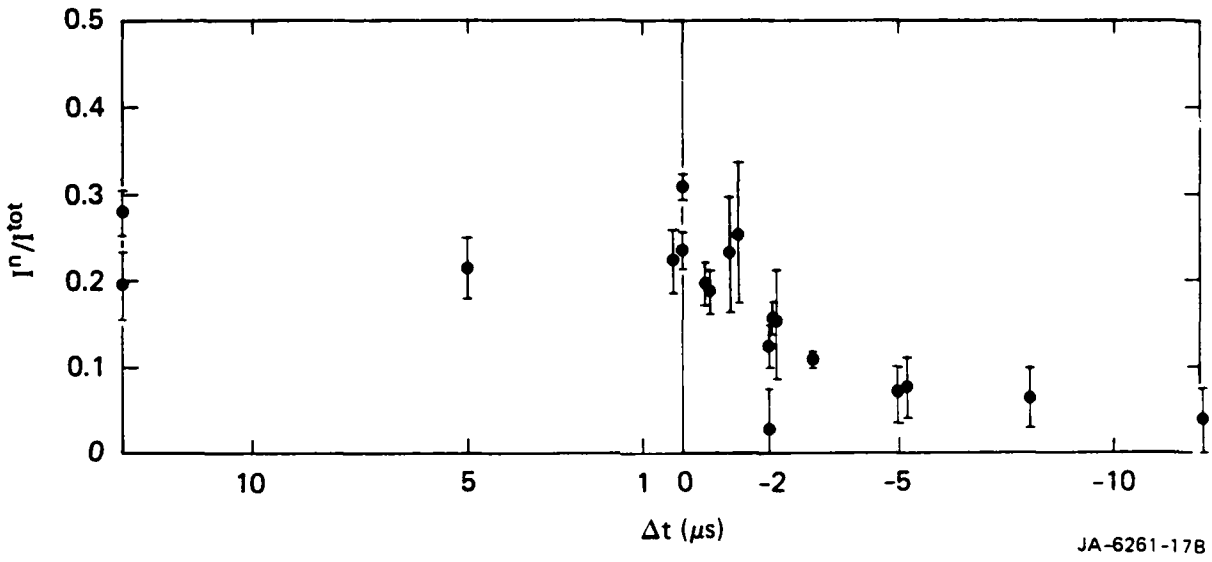

FIGURE 3-17 RATIO OF NEGATIVE ION CHARGE VERSUS TOTAL CHARGE AS A FUNCTION OF DELAY TIME BETWEEN 193-nm AND 248-nm LASER AT 6 mJ/cm^2 (193 nm)

Positive Δt means that the 193-nm laser (for generation of excited electron attachers) was fired first. 42 mTorr C_2H_3Cl in 500 Torr He at 0.08 Td.

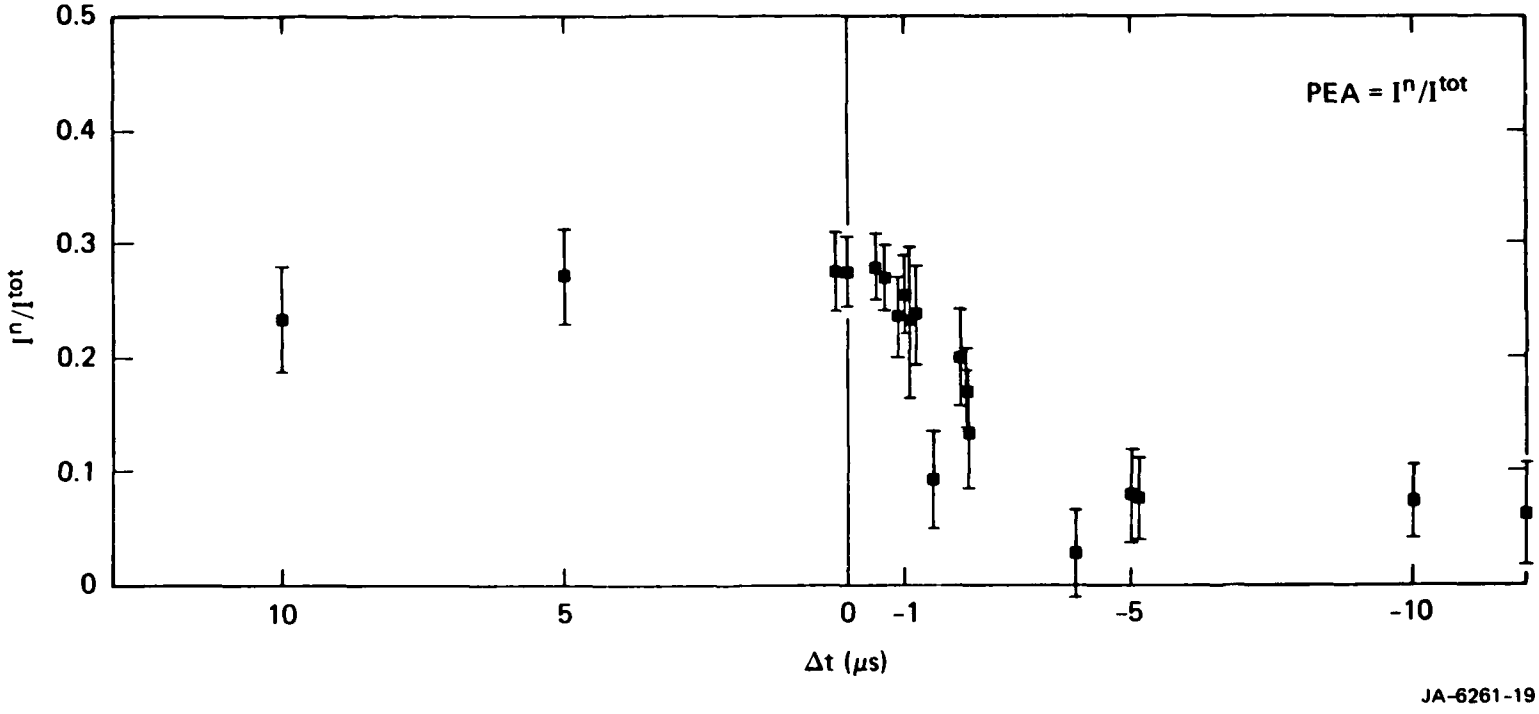

FIGURE 3-18 RATIO OF NEGATIVE ION CHARGE VERSUS TOTAL CHARGE AS A FUNCTION OF DELAY TIME BETWEEN 193-nm AND 248-nm LASER AT 12 mJ/cm^2 (193 nm)

Positive Δt means that the 193-nm laser (for generation of excited electron attachers) was fired first. 42 mTorr C_2H_3Cl in 500 Torr He at 0.08 Td.

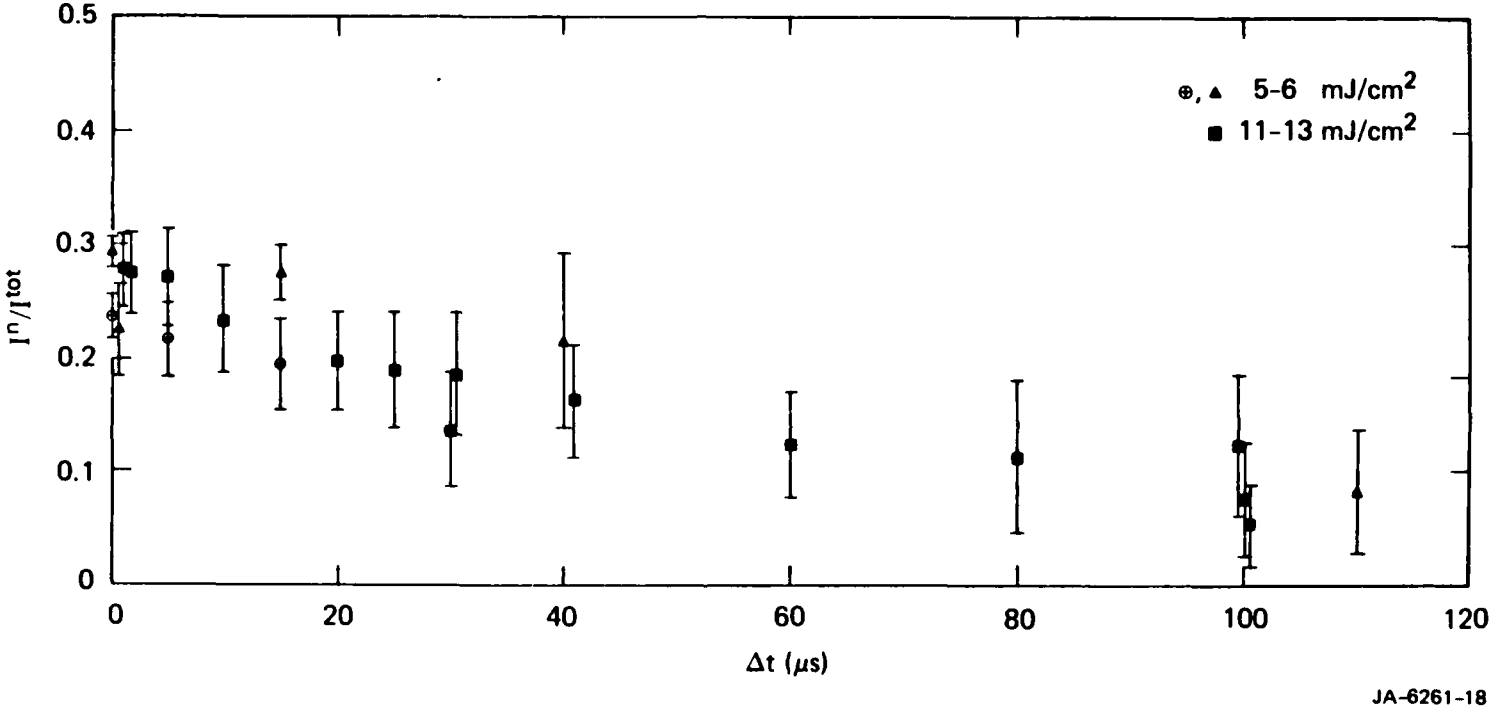

FIGURE 3-19 RATIO OF NEGATIVE ION CHARGE VERSUS TOTAL CHARGE AS A FUNCTION OF DELAY TIME BETWEEN 193-nm AND 248-nm LASER AT 5-6 AND 11-13 mJ/cm^2 (193 nm)

42 mTorr VCl in 500 Torr He at 0.08 Td.

For the long positive time delays shown in Figure 3-19, the photoenhancement effect lingers for 100 μs or longer, a fact that is surprising in view of the initial quenching rate constants from the low pressure low laser fluence data (see the subsection Photoenhance Electron Attachment in Vinylchloride). The data of Figure 3-19 have been converted to attachment coefficients using the ground state pressure of VCl and have been plotted in a semilogarithmic fashion in Figure 3-20. Because of the scatter in the data, it is not clear whether the data follow first-order kinetics or some other rate law. To the extent that a straight line represents our experimental data for these conditions, we derive a lifetime of 56 μs for the excited attacher. This lifetime is much longer than expected from our low pressure quenching experiments indicated above, and it can be transformed into a bimolecular quenching rate constant of 1.3×10^{-11} cm^3 s^{-1}, compared the low pressure of k_q with 5.3×10^{-9} cm^3 s^{-1}. Because of the different pressure regimes and reaction times involved, this discrepancy is not surprising because the low pressure quenching rate constant corresponds to the steep initial rate that describes quenching of very highly excited species, whereas the high pressure quenching rate constant is more characteristic of quenching of species with a moderate excitation energy.

Figure 3-21 shows the power dependence of the photoenhancement effect. The upper group of data refers to the single laser experiment when only the 193-nm laser is fired. The lower group of data points describe the photoenhancement effect achieved in the two-laser experiment when 42 mTorr of VCl is irradiated in 500 Torr of He at 0.08 Td. These data are scattered because the signal due to 193-nm laser alone had to be subtracted from the signal obtained in the two laser experiment. Each data point is an average of 3 to 5 experiments. When the photoenhancement effect is converted into the corresponding attachment coefficient, the plot in Figure 3-22 results. This plot shows that the attachment coefficient η/P scales linearly with laser fluence at the given conditions and shows signs of saturation at fluences above 15-20 mJ/cm^2, corresponding to 25 to 33% excitation. The solid line has been drawn to guide the eye, and the degree of saturation depends on the slope of the line. This result is gratifying because it agrees with the expectation of a single-photon process for VCl at 193 nm, which is discussed in terms of the VCl photochemistry in more detail in Appendix C.

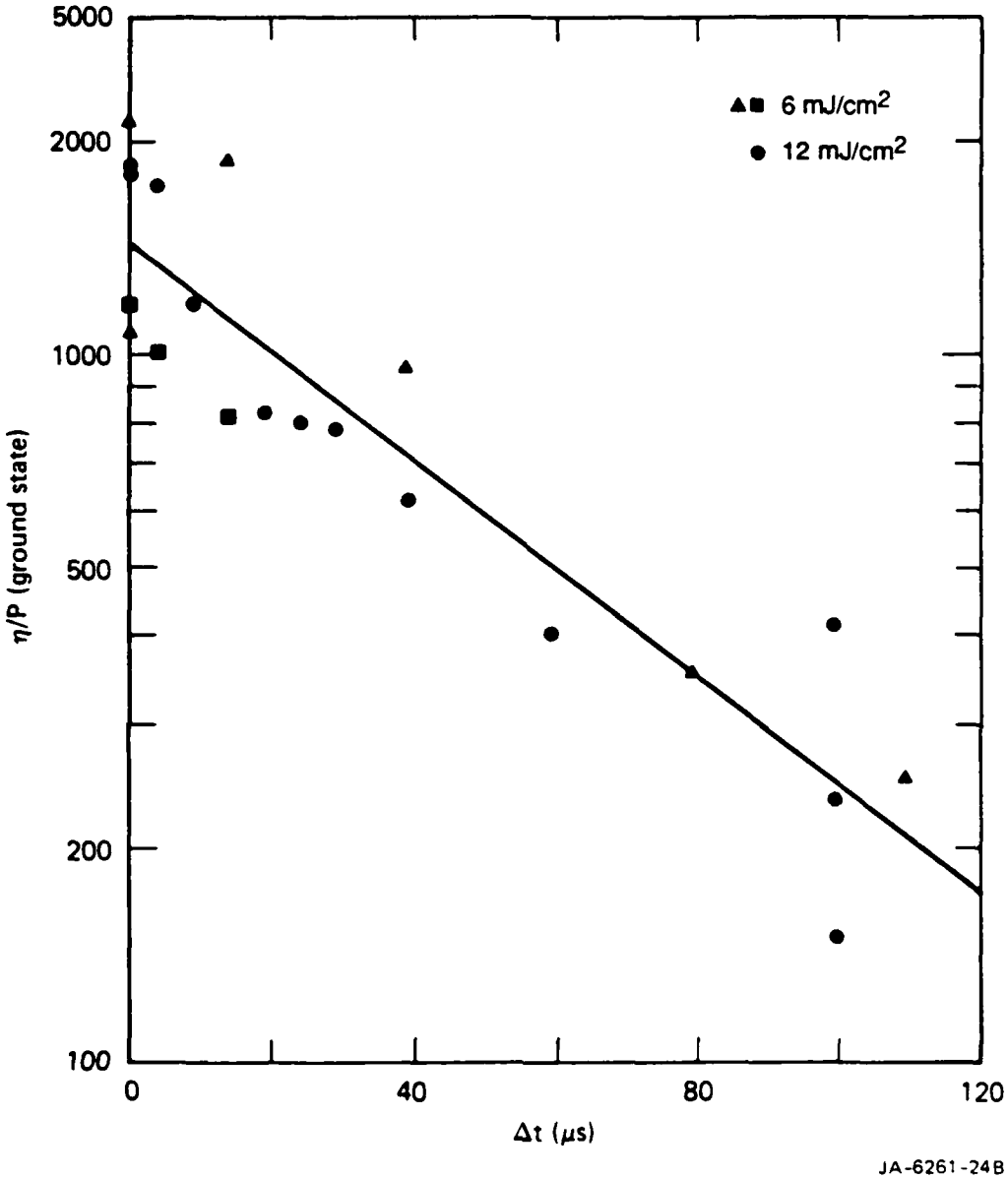

FIGURE 3-20 DECAY OF THE PHOTOENHANCED ELECTRON ATTACHMENT COEFFICIENT (expressed as ground state density) OF 42 mTorr VINYLCHLORIDE IN 500 Torr HELIUM BUFFER GAS AT 0.082 Td FOR 1-mm SLIT IRRADIATION AT 6-12 mJ/cm^2 (193 nm)

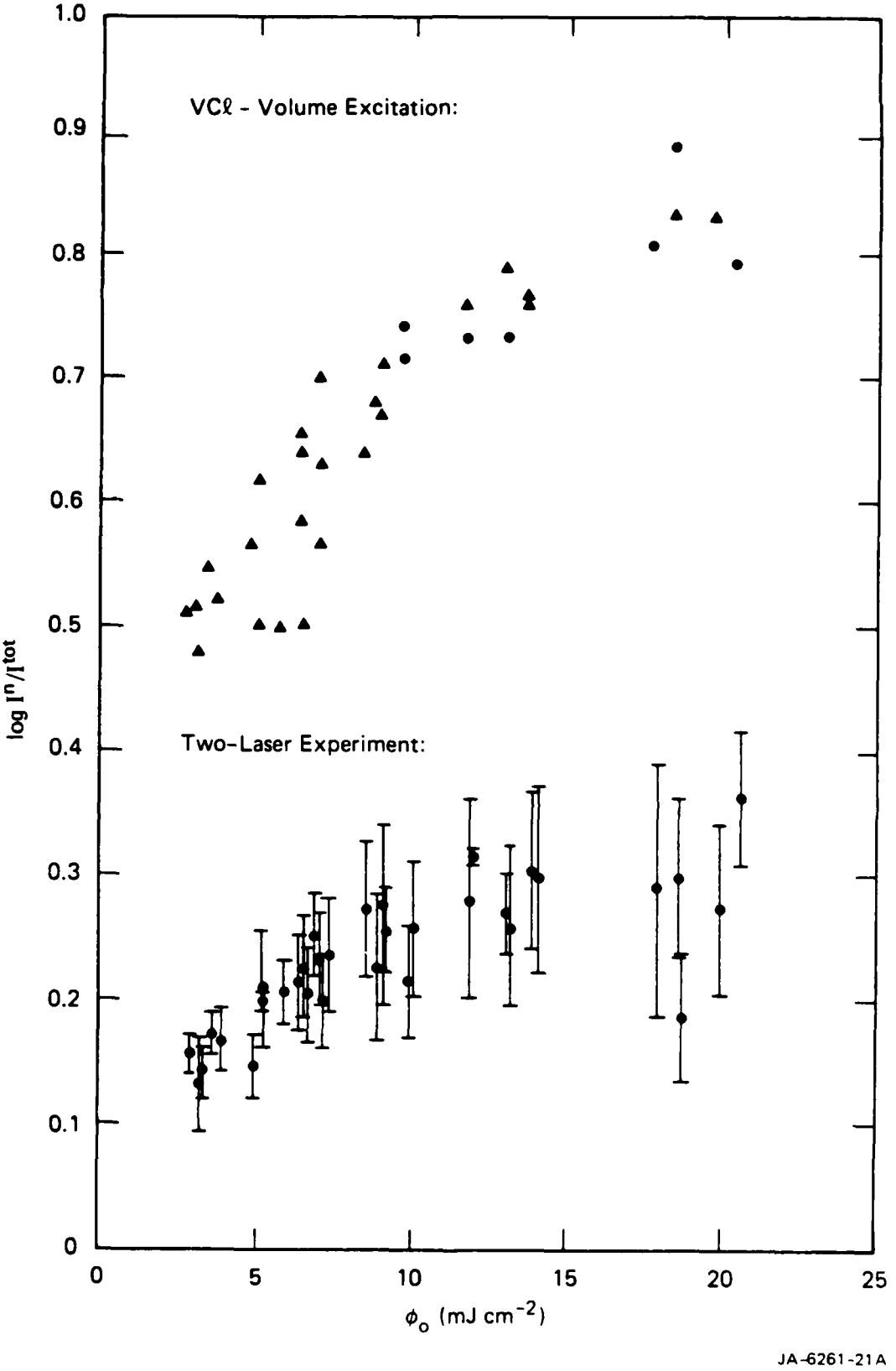

FIGURE 3-21 POWER DEPENDENCE OF THE PHOTOENHANCED ATTACHMENT EFFECT AT 193 nm FOR 42 mTorr VCl IN 500 Torr He AT 0.08 Td

▲ 193-nm experiment: single laser; ● Two-laser experiment with Δt = -0.5 μs.

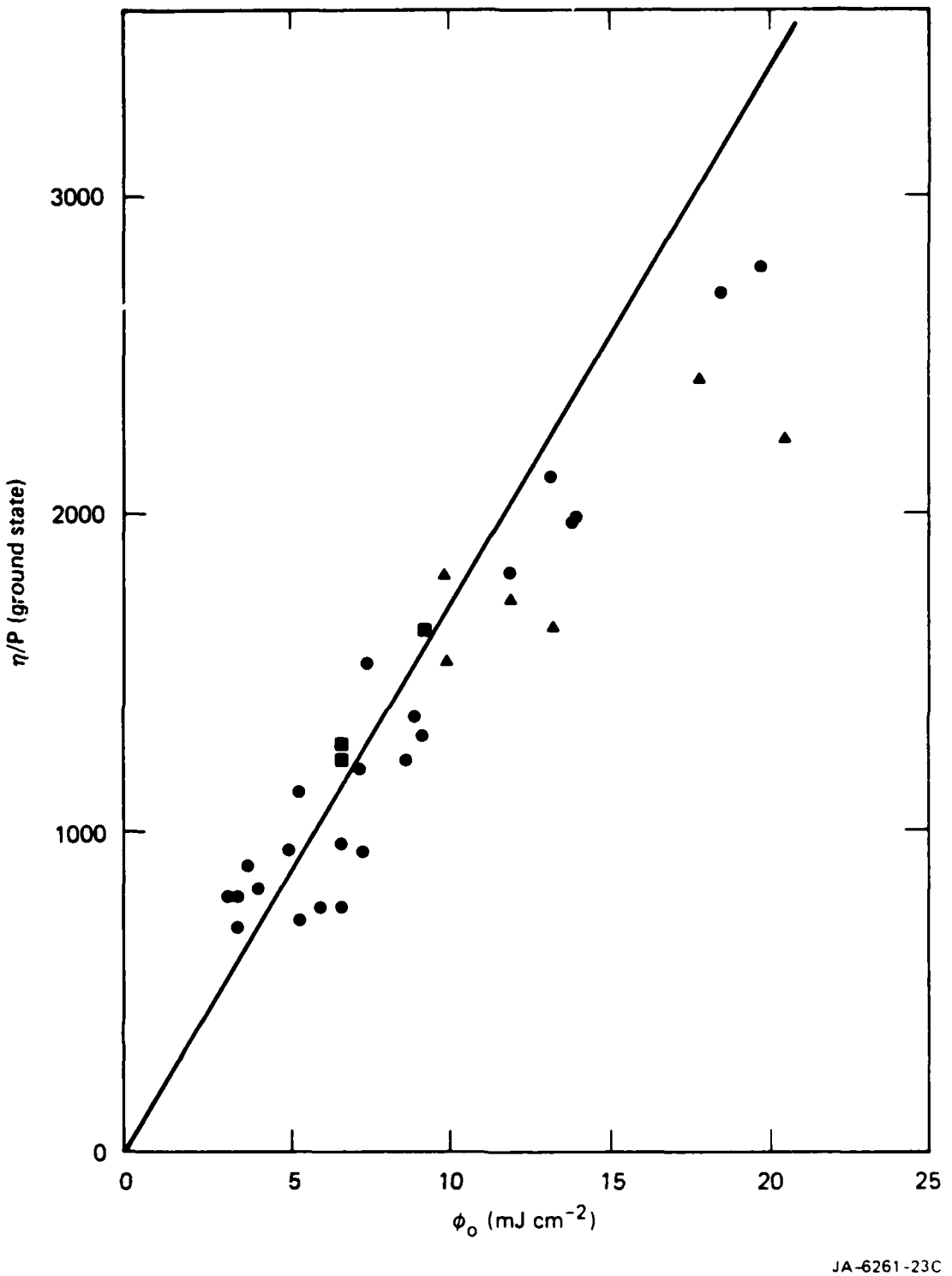

FIGURE 3-22 POWER DEPENDENCE OF 193-nm PHOTOENHANCED ATTACHMENT COEFFICIENT AT 42 mTorr VCl IN 500 Torr He AT 0.08 Td BASED ON THE TWO-LASER DATA OF FIGURE 3-21

Discussion

In both gases the observed enhancement in the attachment coefficient on 193-nm photoexcitation is attributed to the formation of vibrationally excited attaching photofragments from the photodissociation of the substituted ethylene. The expected photochemistry for vinylchloride at 193 nm is given by equations (3-16) and (3-17):

$$C_2H_3Cl \rightarrow C_2H_2^* + HCl^* + \leq 5.4 \text{ eV} \qquad (3\text{-}16)$$

$$C_2H_3Cl \rightarrow C_2H_3\cdot + Cl + \leq 2.5 \text{ eV} \qquad (3\text{-}17)$$

Reaction (3-16) is the photochemical analog to the thermal unimolecular decomposition of VCl for which many analogous examples exist in the literature. The thermal activation energy is estimated at 55 kcal/mol, and after photoexcitation the reacting system has to distribute an excess of 125 kcal/mol over the available translational, rotational, and vibrational degrees of freedom. The large excess energy in reaction (3-16) reflects the small endothermicity of ΔH^0_r = 23.2 kcal/mol, whereas that same quantity for reaction (3-17) is increased to 90 kcal/mol, which corresponds to the C-Cl bond strength in VCl.

Among the recent studies on the photochemistry of VCl are the measurements of the kinetic energy release in chloroethylene fragmentation on 193-nm photolysis by Umemoto et al. [US85], the VUV and UV emission studies of chlorine-containing compounds on 193-nm irradiation by Kenner et al. [KH86], and the FTIR emission study of VCl excited at 193 nm by Donaldson and Leone [DL86]. According to Umemoto et al., the two primary pathways of the 193-nm photofragmentation are as follows [US85]: Cl· atom ejection [reaction (3-17)] occurs by internal conversion of the single-photon prepared state to a highly excited predissociating $^1(\pi\pi^*)$ state, which releases the Cl· with high kinetic energy, whereas the molecular elimination [reaction (3-16)] occurs by internal

conversion through an electronically excited $^1(\pi\pi^*)$ state, in this case the lowest singlet state in VCl, and on to high-lying vibrational states of the electronic ground state, from which HCl elimination takes place. The kinetic energy distribution in the molecular elimination pathway (3-16) shows a broad maximum at 15 kcal/mol and suggests a similar distribution in the remaining degrees of freedom, namely, rotation and vibration of both photofragments. This conclusion is supported by the results of Donaldson and Leone [DL86], which show a broad distribution of vibrationally excited HCl on 193-nm photolysis of VCl. They specifically measured the emission from HCl v = 1-4 states, but their vibrational population distribution suggests significant population in higher vibrational levels.

UV and VUV emission spectra of Cl-containing molecules, which were irradiated by unfocused 193-nm laser light, indicate the importance of photodissociation and subsequent electronic excitation of the photofragment species in a multiphoton excitation process [KH86]. Kenner et al. specifically ruled out a nonladder switching mechanism in the case of the 193-nm photolysis of $CHCl_3$ and CH_2Cl_2, which results in 230-nm emission from HCl ($B^1\Sigma^+$) following single-photon absorption from highly vibrationally excited states of the ground potential energy surface of HCl ($X^1\Sigma^+$). This mechanism of HCl excitation is similar to our three-photon ionization scheme of VCl discussed in Appendix B. Also, the branching ratio between the two competing reaction channels, reactions (3-16) and (3-17) is discussed in detail in Appendix B.

The choice of VCl as a parent for HCl and Cl· is a lucky circumstance in that the presence of Cl· atom will not initiate a chain reaction because the hydrogen abstraction reaction by Cl· from VCl is endothermic by 7 kcal/mol and will therefore be slow at room temperature. Even if vinyl radical is generated by 193-nm photolysis of VCl, we can show that the photoenhanced attachment process is not dominated by vinyl radical, C_2H_3·. Assuming a thermal rate constant of about 2×10^{-10} cm^3 s^{-1}, which is an upper limit for vinyl radical recombination based on the well-known value for CH_3·, we estimate the half-life for vinyl radical toward recombination as follows. For irradiation conditions of 4 mJ/cm^2 into 10 mTorr VCl at 500 Torr He, the initial vinyl radical density is 2.8×10^{12} cm^{-3} and the half-life is 11 ms. Clearly, the photoenhanced

attachment to VCl cannot be due to the presence of the vinyl radical by virtue of its expected long lifetime under our conditions. Therefore, we believe that the species responsible for attachment in the photoexcited system must be vibrationally excited HC· and/or C_2H_2, which is consistent with the measured fast quenching rate constants.

The fluoroethylenes are not as well investigated as to their thermochemistry and their laser-induced photochemistry. The relevant photoelimination reaction is given by reaction (3-19), whose endothermicity has been estimated at 58 ± 5 kcal/mol:

$$F_2C{=}CFH \rightarrow F\text{-}C{\equiv}C\text{-}F^* + HF^* \qquad (3\text{-}19)$$

The activation energy for thermal unimolecular decomposition of TFE according to reaction (3-19) is estimated to be 65 kcal/mol, which means that HF may contain significant vibrational energy. The photoexcited system has an excess energy of 90 kcal/mol beyond its endothermicity, which leaves enough energy to be distributed into internal excitation in both photofragments. From our multiphoton ionization study of TFE (Appendix B) we concluded that a competing photodissociation reaction (3-20) took place:

$$F_2C{=}CFH \rightarrow CF_2^* + CFH^* \qquad (3\text{-}20)$$

Following the same arguments as above for the vinyl radical, we can safely exclude a dominant role of both carbenes in the photoenhanced attachment to TFE due to their slow recombination kinetics. Therefore, we conclude that the attaching species in photoenhanced electron attachment to TFE are vibrationally excited HF and/or C_2F_2.

Section 4

MULTIPHOTON IONIZATION STUDIES

During excimer laser irradiation of the electrode gap of the drift tube apparatus, it became apparent that multiphoton ionization of vinylchloride (C_2H_3Cl, VCl) and trifluoroethylene (C_2F_3H, TFE) generated as many ions and electrons at fluences above 1 mJ/cm^2 as there were electrons generated at the cathode through the photoelectric effect. Therefore, it was necessary to quantify the MPI under our irradiation conditions to minimize its interference in our experiment. Thus, we set up a time-of-flight mass spectrometer in which a molecular beam interacted with a laser beam at right angles. The strategy was to compare VCl and TFE MPI with benzene (C_6H_6, Be) at 193 nm, the primary wavelength of interest. To put our beam data on an absolute scale, we measured Be MPI at 248 nm in our apparatus so that we could compare our relative signals with the absolute yields obtained for Be at 248 nm by Bischel et al. [BJ85].

The significant results of our work are as follows. The fractional photoionization of Be at 248 nm decreased with respect to the predicted yield for laser powers $\geq 10^7$ W/cm^2. The model curve was obtained from the low power data of Bischel et al. [BJSE85], and we interpret the yield depression as being due to a competing photodissociation process (not resulting in ions) of a superexcited state that is the precursor to molecular and fragment ions of Be. At 193 nm, the Be two-photon ionization cross section depends on the laser pulse duration, and for a typical laser pulse width of 15 ns FWHM, the yield is only 1/30 of that obtained using 248-nm MPI under similar irradiation conditions.

The MPI of VCl and TFE at 193 nm is a three-photon process resulting in HCl^+ for VCl and CF^+ and CFH^+ forTFE. No molecular ions were observed in either case under unfocused conditions, and when cold, ground state HCl in He was irradiated, no molecular ion was detected. These experiments showed that highly vibrationally excited HCl ($v = 6$ or higher) undergoes two-photon ionization and are proof that some vibrationally excited HCl is indeed formed as a result of 193-nm excitation of VCl. Quantitative absolute MPI cross sections

for Be, VCl, and TFE at 193 nm are given in two publications, one of which has appeared and one of which has been submitted recently (Appendices A and B).

Section 5

LASER DC-GLOW DISCHARGE INTERACTION

During this contract, we observed that a DC-glow discharge using a hollow cathode can be extinguished by a pulse of unfocused 193-nm light when a 2% VCl in He mixture is discharged at a few torr total pressure and several hundred volts of applied voltage. We also observed that multiphoton ionization of VCl can initiate the discharge. A mode was observed at applied voltages below breakdown of the discharge gap where one laser pulse could "turn on" the discharge while the following one could extinguish it. This appears to be a first application of our concept of controlled photo-induced electron attachment. In pure helium or argon, a DC discharge can be initiated (through MPI) but cannot be extinguished through laser irradiation. We used a variety of discharge tube geometries, and the parameter space was delineated with respect to applied voltage, flow rate, pressure, and discharge current. Subsequently, we found that 248-nm irradiation is active in extinguishing the discharge as well, and absorption measurements at 254-nm confirm the presence of absorbing species at 248 nm in an active discharge of VCl and helium.

A paper based on these results has been submitted to Appl. Phys. Lett.; a copy of the preprint is appended as Appendix D.

Section 6

PHOTOENHANCED ELECTRON ATTACHMENT TO ELECTRONICALLY EXCITED METASTABLE TRIPLET STATES OF p-BENZOQUINONE AND CHLORANIL

Introduction

An abundance of parent negative molecular ions are formed as a result of a thermal or epithermal electron-molecule interaction [CH84a]. However, the case of p-benzoquinone ($C_6H_4O_2$) and of a few other molecules [CH84b] is unique in that higher energy electrons lead to the formation of stable negative ions. Those negative ions are metastable toward the reverse process, autoionization, and lifetimes of a few tens of microseconds have been measured [CC70; CC69].

The attachment process has been characterized as proceeding in the field of an excited electronic state of the parent molecule, thus simultaneously promoting an electron of the neutral molecule into a higher orbit as a result of the electron-molecule interaction. Therefore, the initial kinetic energy of the incoming electron is stored to a large extent in potential energy of the metastable core excited state of p-benzoquinone (BQ) so that effectively conditions of thermal electron attachment are restored. This process is known as electron-excited Feshbach resonance or core-excited Type I resonance and occurs at 2.1 eV in the case of BQ. The origin of the electronically excited metastable triplet state of BQ of either $^3B_{1g}(T_1)$ or $^3A_u(T_2)$ symmetry lies at approximately 2.3 eV, so an apparently good correspondence of the optically detected state with the negative ion resonance results. Recently, a detailed time-resolved electron spectroscopic study investigated the fate of BQ in the aftermath of an energetic electron-BQ collision, essentially confirming the longevity of the BQ negative ion in agreement with the earlier results cited above [AL83; AL84].

We decided to test this attachment behavior by preparing the electronically excited metastable state by optical pumping and investigating the electron-attachment properties of that optically prepared state of BQ in our high pressure swarm apparatus. We also investigated the electron attachment

properties of its tetrachloro derivative, chloranil ($C_6Cl_4O_2$, CA), because it is similar to BQ except that it has a different electronic structure [GJ84]. Both species lead to stable negative ions as a result of their large positive electron affinities.

Background

The gas phase photophysics of BQ is well known [IT85; BM73], whereas no gas phase photokinetics of CA seems to have been published. Therefore data on solution photodynamics were taken as an approximation to the corresponding gas-phase values [KG77]. Briefly, BQ quantitatively transforms into vibrationally excited triplet when excited into its $^1B_{3g}$ band, which corresponds to its lowest ($\pi\pi^*$) state. At low pressure a sizable fraction returns to the $^1B_{1g}(n\pi^*)$ state by reverse intersystem crossing because the phosphorescence quantum yield approaches zero and the fluorescence quantum yield increases with decreasing pressure. However, with added amounts of buffer gas vibrational relaxation in the triplet manifold occurs, and the phosphorescence quantum yield approaches its maximum value, which means that essentially the excited state population is quantitatively transferred into the relaxed phosphorescing state (^3A_u).

By analogy, we are assuming that the same is true for CA excited at 350 nm, an assumption that is borne out in fluid solutions in which essentially all excited CA molecules convert into the lowest excited triplet state. Therefore, we have the situation in both quinones that optical pumping into the S_2 excited state effectively transfers all the excited population quantitatively into their lowest triplet states at high buffer gas pressure. For BQ and CA in solution we used $\sigma = 1.15 \times 10^{-18}$ cm^2 for BQ at 308 nm and $\sigma = 8.0 \times 10^{-18}$ cm^2 for CA at 350 nm [ST67]. Unfortunately, BQ absorbs only very weakly at 350 nm, so we had to use different excitation wavelengths for each quinone.

Experimental

The drift tube experimental apparatus is described in Section 3. The drift tube (drift distance = 1.5 cm) and associated gas handling system was

wrapped with heating to conduct attachment experiments at elevated the temperatures required because of the low vapor pressures of BQ and CA. The temperatures were monitored using chromel-alumel thermocouples that were slipped in between the glass apparatus wrapped with aluminum foil and the heating tape. The highest and the lowest readings of the temperature were 4K apart, and an average of the three thermocouple readings was taken to represent the temperature of the drift tube. The quinones were placed in a 3-cm^3 side arm that could be heated separately and that controlled the vapor pressure of the substance. We were careful to maintain at least a 30K temperature differential between the vapor-pressure-controlling vessel and the remainder of the drift tube to eliminate cold spots in the apparatus.

The measurements were performed with a static gas fill that was frequently replaced because of apparent photochemical exhaustion of the sample. The contents of the drift cell were pumped out using an auxiliary rotary vane pump/zeolite filter combination after which a 270 L/s turbo molecular pump took over. We noticed that the flash-lamp irradiation through the side window led to more rapid depletion of the sample compared with excimer laser irradiation. This rapid depletion apparently is a result of the short wavelength emission of the flash-lamp (EG&G Litepak and lamp FX-200U) that led to rapid photochemical decay of the quinones. The excimer lasers used were a Lambda Physik EMG 101 for 350-nm irradiation of CA and an EMG 50 for 308-nm irradiation of BQ. The pressure of BQ was measured by a 100-Torr full-scale Baratron 227AHS-100, whereas the vapor pressure for CA was calculated according to the following formula found in the 52^{nd} edition of the Handbook of Chemistry and Physics (Chemical Rubber Corporation):

$$\log P/\text{Torr} = -0.2185\ A/K + B$$

with A = 21514.3 and B = 13.673 for 70.7, $343.7 \leq T/K \geq 435$. The transient displacement current was recorded in its entirety on a waveform recorder, and then the data were processed and averaged by a microcomputer.

Results and Discussion

The first task we undertook was to measure the ground state electron attachment to BQ and CA in He at subatmospheric pressures. The details of the measurements as well as the method of data reduction are discussed in a Section 3, Experimental Details. The electron attachment to BQ has been measured in a variety of buffer gases (Ar, N_2, C_2H_4), whereas our measurements for CA represent the first attachment data for that compound. We began with the ground state attachment behavior to compare the photoenhanced situation with the ground state attachment properties of both quinones and thus provide baseline data against which to evaluate the enhancement effect on the attachment rates due to electronic excitation.

Figure 6-1 shows the ground state attachment results for BQ and CA. With 110 mTorr of BQ in 500 Torr of He at 298K, the attachment coefficient shows the characteristic maximum at about 3 Td corresponding to 1.23 V average swarm energy. This maximum is undoubtedly related to the above-mentioned resonance at 2.1 eV, which has been interpreted as an electron-excited Feshbach resonance [CC69; CC70; AL83]. The attachment coefficients for the ground state of CA were obtained at 372K and pressures of 0.8 to 1.3 Torr of CA. The helium pressure was 600 and 300 torr, respectively.

Although the physicochemical properties of both BQ and CA are similar, the ground state attachment behavior is very different. There is no indication that the attachment coefficient would increase with increasing E/N as in the case of BQ, and this fact is all the more surprising in view of the similar excited electronic states, with respect to both character (symmetries) and energetics. Also, the electron affinities of both quinones are very similar, 1.88 eV for BQ and 2.44 eV for CA. One of the differences is the electronic structure of the ground state. The frontier orbitals for CA have π character, $\pi_4(b_{3u})$, and $\pi_3(b_{1g})$, whereas those for BQ have lone-pair character, $n^-(b_{3g})$ and $n^+(b_{2u})$. In this respect, it would be very interesting to investigate the attachment behavior of 2,6-dichloro-1,4-p-benzoquinone, which resembles BQ as far as the nature and sequence of its frontier molecular orbitals is concerned.

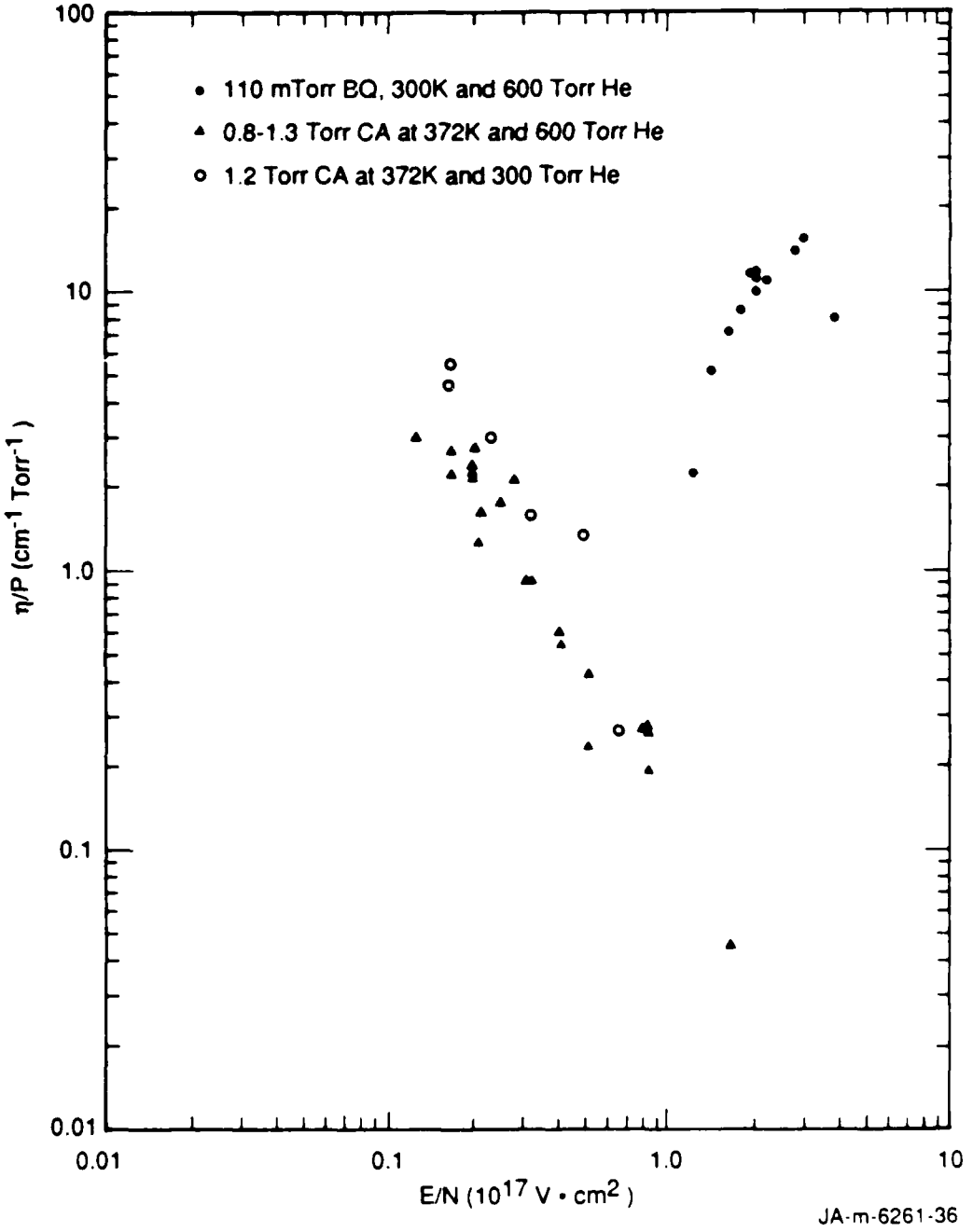

FIGURE 6-1 COEFFICIENT FOR DISSOCIATIVE ELECTRON ATTACHMENT OF p-BENZOQUINONE (BQ) AND CHLORANIL (CA) AT 300 AND 600 Torr He BUFFER GAS PRESSURE

Figure 6-1 also reveals a significant difference in the attachment coefficient with changing buffer gas pressure. However, this difference has to be understood in terms of a change in the electron energy distribution function (EEDF) with CA/buffer gas mixing ratio. More extensive data on the ground-state attachment behavior of BQ at higher temperatures are presented below.

Next, we examined the attachment behavior of triplet excited CA using 350-nm laser radiation. The laser beam excited a volume with a 1.2×2 cm^2 cross section in which 1.2 cm of 1.5 cm, which corresponds to the electrode distance, was illuminated. The laser alone produced a strong signal without the need to generate photoelectrons from the irradiation of the cathode by the short-pulse high-intensity flash-lamp. In fact, the flash-lamp signal was only a few percent of the laser-induced signal, so the flash-lamp could not be used in conjunction with the laser related experiments.

In anticipation of results described below, we may note that this laser-induced signal did not originate from three-photon ionization of CA because the fluence levels were about 2-4 mJ/cm^2. Therefore, we subtracted the CA ground state attachment contribution from the observed attachment coefficient η/P to obtain that fraction of η/P that was due to laser excitation. The resulting attachment coefficient was small and depended strongly on the value of η/P for ground state CA. Thus, we concluded that the photoenhanced attachment effect was either small or nonexistent over the E/N range explored (0.1 to 3.0 Td). In agreement with this finding was the fact that the observed η/P was independent of laser power. The power dependence of the total signal, I^{tot}, which corresponds to the sum of all charged species generated by the laser pulse, was inconclusive because of the small fluence range explored. The power exponent n in the relation $I^{tot} - \Phi^n$ with Φ being the fluence in mJ/cm^2 at 350 nm was found to lie between 1 and 2.

To perform spatially resolved illumination experiments close to either electrode, we reduced the irradiated volume into a 1-mm-thick slab. When the irradiated volume was positioned within less than a mm of the cathode, heavy charge carriers caused a large signal. Under the conditions used (proximity to cathode, 1.7 mJ/cm^2, 0.6 Torr CA), the contribution of positive ions from whatever source was kept below 5%, so the ion current is interpreted as solely

due to the formation of negative ions. However, after subtraction of the ground state contribution to η/P, the uncertainty in the vapor pressure obscured the presence of any photoenhanced attachment effect.

When the irradiated slab was moved within 1 mm of the anode, the total charge (I^{tot}) was smaller, but a large fraction of the signal had to be attributed to positive ions. However, the time dependence of the slow portion of I^{tot} showed a peculiar behavior in that it displayed a "plateau" that depended on E/N. This time lag in the displacement current clearly shows that the mechanism of formation of those positive ions is not taking place in the gas phase. The flat portion of the time-dependent displacement current lasted from 200 μs to 1 ms for E/N values ranging from 0.4 to 0.2 Td. Thus, we believe that scattered photons are responsible for the surface generation of positive ions that subsequently desorb by a mechanism that has both thermal as well as field desorption characteristics. Those surface processes may be facilitated by the well-known tendency of this type of organic molecule to coat a metal surface.

In summary, the follwoing four observations from our CA attachment data support of the hypothesis that the electrons generated as a result of the laser-gas interaction inside the drift gap have their origin in scattered light or fluorescence from CA and not in three-photon ionization at 350 nm:

- I^{tot} increases linearly with the laser fluence in the range 14 to 39 mJ/cm^2.
- I^{tot} increases by a factor of two for a factor of 4 increase in pressure.
- I^{tot} is lowest when the irradiated slab is farthest away from the cathode.
- Direct irradiation of the anode by 350 nm laser light causes a large I^{tot} signal.

These observations are easiest to rationalize in terms of scattered photons from the primary gas-phase irradiation hitting the cathode and releasing photoelectrons. Higher pressure of CA leads to reabsorption, thus lowering the

I^{tot} in analogy to the situation in vinylchloride and trifluoroethylene. Whether the nature of the scattering process is resonance enhanced, Rayleigh scattering or fluorescence is still an open question. However, we tend to rule out fluorescence or phosphorescence because of its long wavelength nature in CA.

Having confirmed the absence of a photoenhanced attachment effect in the experiments described above, we decided to obtain attachment data from two "back-to-back" experiments because of the difficulty of keeping the pressure constant from one gas fill to another. High precision data are required because of the subtraction procedure that is necessary to account for the attachment of ground state CA. Therefore, we gathered data using a laser to irradiate a 1-mm-thick slab near the cathode, then we obtained flash-lamp data on the same gas mix, after which the gas mixture was changed and another pair of attachment experiments were undertaken. As pointed out above, we used the photoelectrons produced by scattered photons impinging onto the cathode to probe the attaching gas in the discharge gap.

Figure 6-2 shows the back-to-back attachment data for BQ irradiated at 308 nm at about 2 mJ/cm^2 and at 620 Torr of He buffer gas pressure on one hand and for flash-lamp-triggered release of photoelectrons on the other hand. The temperature of the drift cell was 373K, and the superposition of the flash-lamp data of Figure 6-2 with the corresponding data of Figure 6-1 reveals a minor shift of the attachment peak for both axes. Most important, however, the data clearly show the absence of any significant enhancement of the electron attachment to BQ under those conditions.

In an analogous way, back-to-back data were gathered for CA irradiated at 350 nm. Figure 6-3 shows data on CA obtained at 373K and 600 Torr He irradiated with 20 to 40 mJ/cm^2 at 350 nm and flash-lamp illumination. Here also the data do not show any photoenhancement of the attachment coefficient. Lowering the buffer gas pressure by a factor of 5 leads to an order of magnitude increase in η/P, but again no photoenhancement is observed at 21 mJ/cm^2. The increase in η/P with decreasing total pressure and constant mixing ratio is not immediately understandable without quantitative modeling of the reaction system. However, we need to perform more pressure measurements before we will

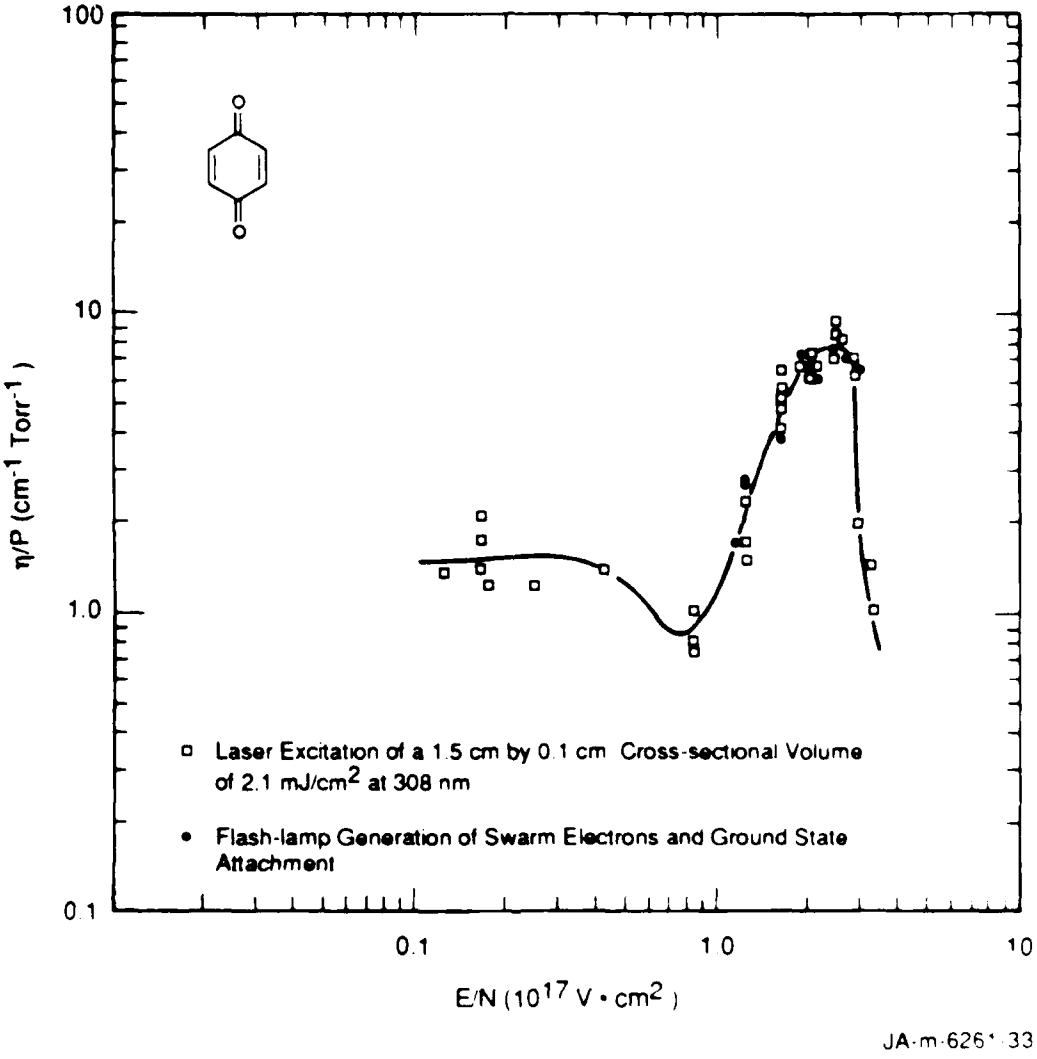

FIGURE 6-2 BACK-TO-BACK MEASUREMENT OF THE ELECTRON ATTACHMENT COEFFICIENT FOR p-BENZOQUINONE AT 373K AND 620 Torr He BUFFER GAS PRESSURE

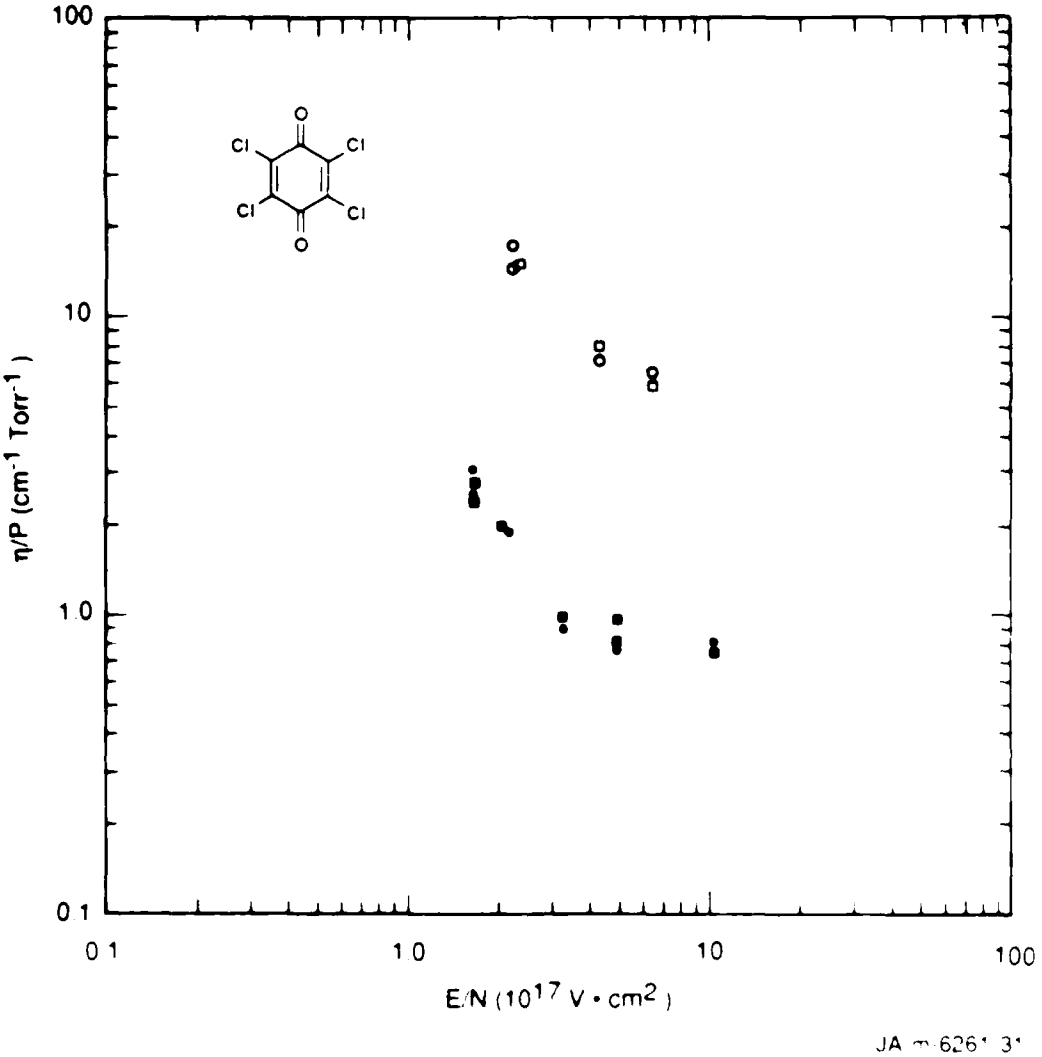

FIGURE 6-3 BACK-TO-BACK MEASUREMENT OF THE ELECTRON ATTACHMENT COEFFICIENT FOR CHLORANIL (CA) AT 373K, 120 AND 600 Torr He BUFFER GAS PRESSURE

- 350-nm laser excitation of a 1.5 cm by 0.1 cm cross-sectional gas volume at 20-35 mJ/cm^2, 620 Torr He and 450-500 mTorr CA
- Flash-lamp generation of swarm electrons at 620 Torr He, 450-500 mTorr CA and ground state attachment
- ▫ 350-nm laser excitation at 21 mJ/cm^2, 120 Torr He and 120 mTorr CA
- ○ Flash-lamp excitation at 120 Torr He, 120 mTorr CA and ground state attachment

be able to conclusively make any quantitative statements about pressure effects. At 20 mJ/cm^2, 28% of the irradiated CA molecules are excited, and the literature indicates that quenching is not a major loss process for the triplet states of BQ and CA. Therefore, insignificant number densities of excited attachers cannot be responsible for the absence of any photoenhancement of electron attachment to those quinones. However, one possible reason for the absence of any measurable photoenhancement of η/P could be the fact that the photogenerated vibrationally excited triplet state is not quenched by the helium buffer and therefore reverts to its singlet state by reverse intersystem crossing with ensuing fast dissipation of singlet energy in non-radiative pathways [IT85]. This situation is primarily the result of our use of helium as a buffer gas which is known to be an inefficient quencher for vibrational excitation in polyatomic molecules [MP83].

At this point, we were interested to determine whether collisional relaxation could be an important factor process for the excited triplet attacher population during the electron drift time. At 600 Torr He and 0.5 Torr CA at 400K the CA-CA gas collision frequency is calculated as 6.9×10^6 s^{-1} assuming a hard sphere collision diameter of 7 Å for CA. This represents a time between collisions of 146 ns. At low E/N the electron drift time can be as large as 1 μs which leads to 7 collisions between a pair of CA molecules. The collisions of CA with He are supposed to be benign, even though the time between collisions is only 50 ps. At 120 Torr He and 0.12 Torr CA at 400K CA-CA collisions occur at a frequency of 1.64×10^6 s^{-1}, corresponding to a mean time between collisions of 600 ns. Under these conditions the excited triplet chloranil experiences only 1 or so collisions during the electron drift time across the irradiated slab. From this discussion we conclude that the interaction of the electron with the excited triplet CA takes place under nearly CA-CA collision-free conditions at those lower pressures. However, there are many buffer gas-CA collisions on that time scale.

Our next experiment consisted of measuring BQ attachment under 308-nm laser irradiation using N_2 as a buffer gas. The experiments were performed again back-to-back to each other, as described above with first the laser

(1-mm-thick irradiated slab) and then the flash-lamp. Figure 6-4 shows the results of this experiment in a plot of the attachment coefficient η/P versus the reduced electric field strength E/N. In nitrogen as a buffer gas the ground state of BQ does not attach electrons at low E/N under our conditions, whereas the laser-excited attacher [Figures 6-5(a) and (c)], gives rise to strong attachment. At higher E/N the ground state of BA begins to slightly attach electrons [Figure 6-5 (d)]. The low pressure data in Figure 6-4 (140mTorr BQ) are corrected for the concurrent ground state attachment effect. For 140 mTorr of BQ in 620 Torr of N_2 no dependence of η/P on E/N is observed, whereas the data pertaining to 530 mTorr of N_2 in 600 Torr of N_2 strongly depend on E/N. This E/N dependence of the high pressure photoenhanced attachment data (530 mTorr BQ) stems from the fact that the overall η/P values of Figure 6-4 show the increasing contribution of BQ attachment at higher E/N and the fact that electron attachment in the laser excited small volume is comparable to ground state attachment in the unexcited part of the drift volume. These raw η/P values of Figure 6-4 at higher pressure could not be corrected for this ground state contribution of unexcited BQ to the electron attachment due to lack of flash-lamp data for BQ in this pressure range. Of importance is further the fact that quenching processes seem to be important for electron attachment to $^3BQ^*$. The laser fluence in both cases was 6.7 mJ/cm^2, leading to a 1.2% excitation of the irradiated volume. Thus, the sample is optically thin, and the electron attachment coefficient of Figure 6-4 is expressed per Torr of ground state of BQ. To arrive at the true attachment coefficient for the triplet excited BQ, we must multiply the abscissa by about a factor of 100, which leads to η/P values of between 1,000 and 10,000 $cm^{-1}Torr^{-1}$ under the assumption that each excited BQ molecule is converted to a triplet. In case that this may not be so, the above numbers have to be regarded as lower limits. We observe, thus, a photoenhanced attachment effect in this case, and the future will show if these impressive numbers will hold up against further scrutiny.

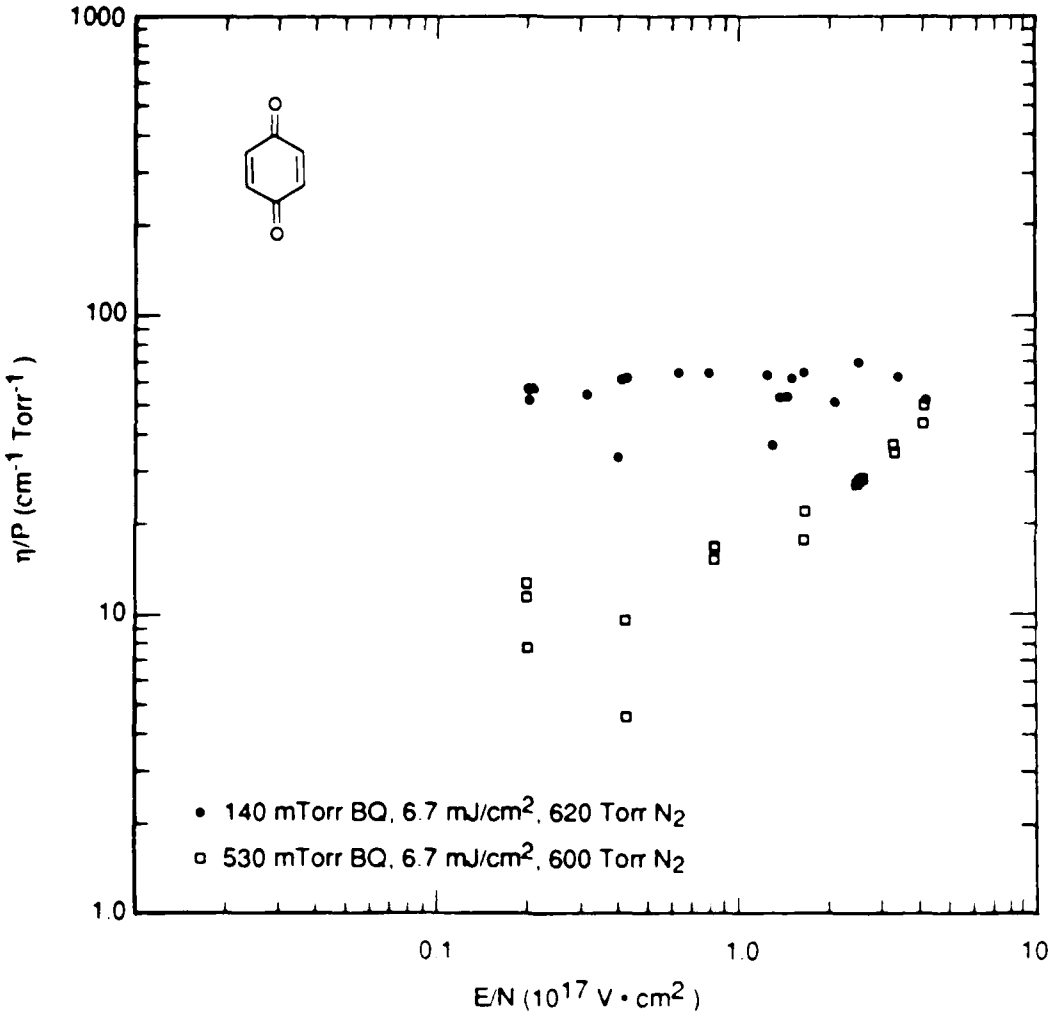

FIGURE 6-4 E/N-DEPENDENCE OF PHOTOENHANCED ELECTRON ATTACHMENT COEFFICIENT FOR p-BENZOQUINONE (BQ) IN 600-620 Torr OF N_2 AT 372K EXCITED AT 308 nm IN A GAS VOLUME OF 1.5 cm BY 0.1 cm CROSS SECTION

The attachment coefficient is expressed in terms of ground state BQ.

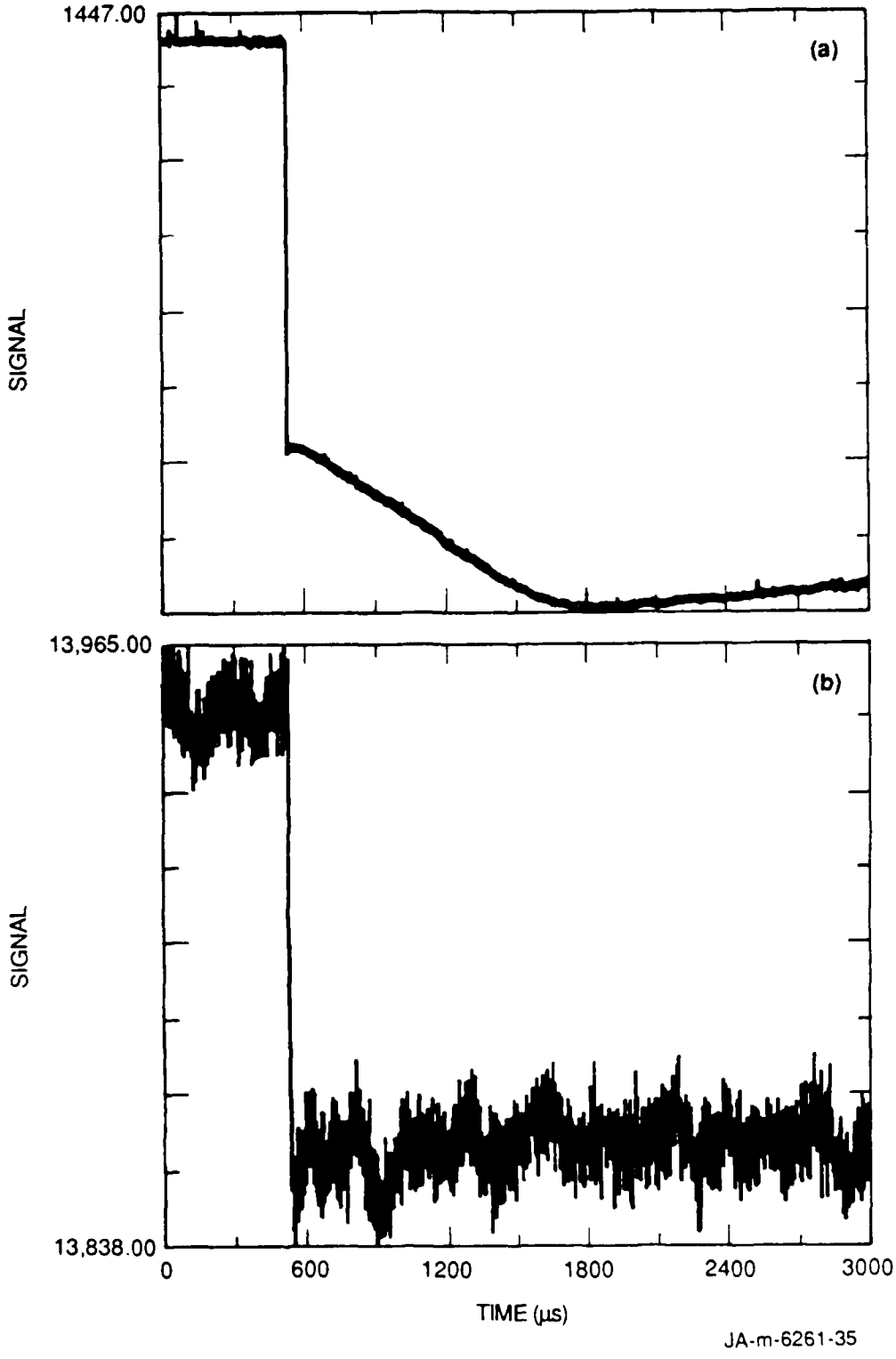

FIGURE 6-5 OSCILLOSCOPE TRACES OF THE TRANSIENT VOLTAGE FOR 140 mTorr OF p-BENZOQUINONE IN 620 Torr N_2 and 372K (continued)

(a) 308-nm laser excitation (20 shots) of gas volume at 1.24 Td of 1.5 cm by 0.1 cm cross section.

(b) Flash-lamp excitation of cathode (200 shots) at 1.24 Td.

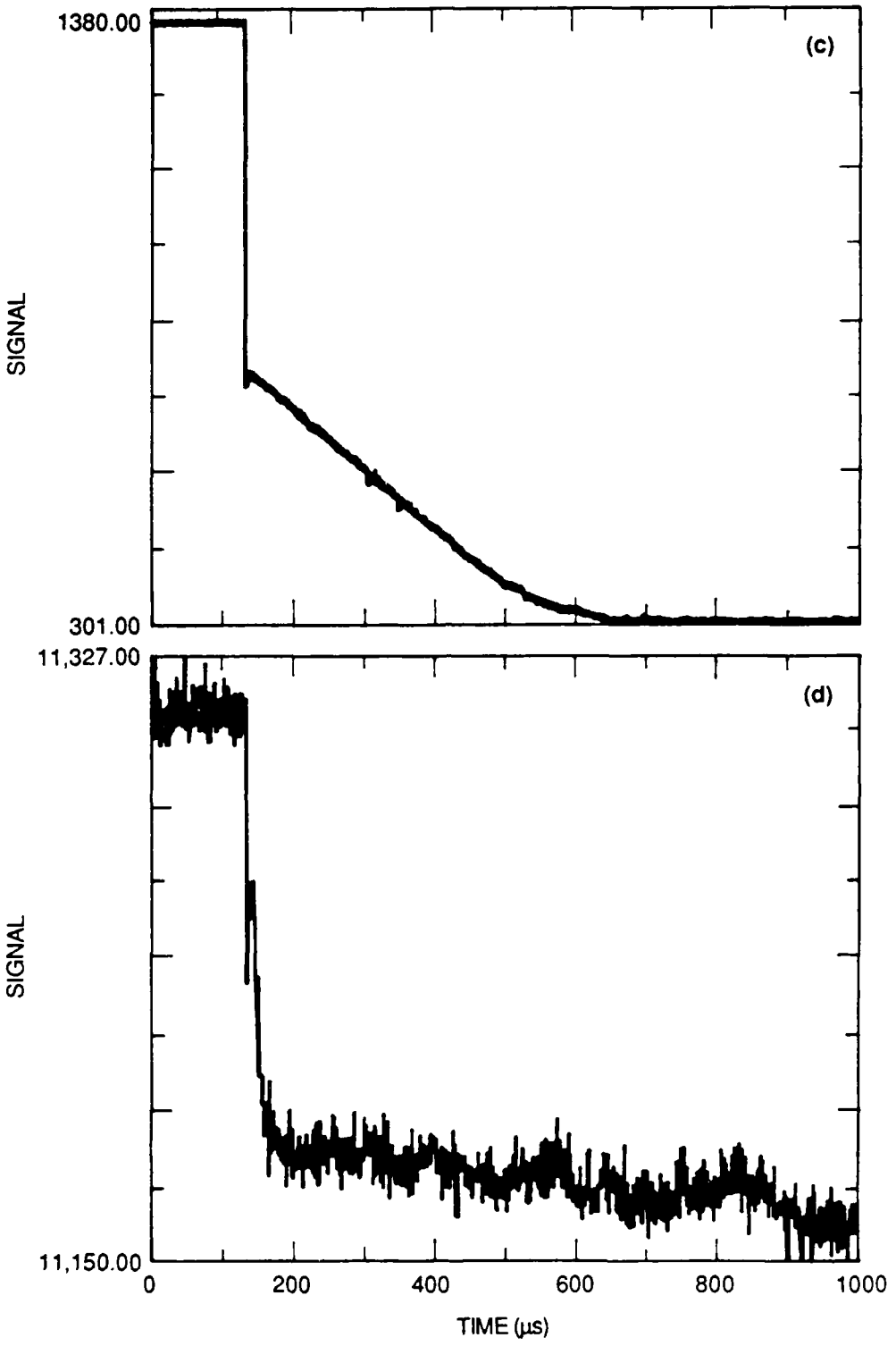

FIGURE 6-5 OSCILLOSCOPE TRACES OF THE TRANSIENT VOLTAGE FOR 140 mTorr OF p-BENZOQUINONE IN 620 Torr N_2 and 372K (concluded)

(c) 308-nm laser excitation (20 shots) at 3.30 Td.

(d) Flash-lamp excitation (200 shots) at 3.30 Td.

Section 7

CONCLUSIONS

This section deals with the conclusions of our work on photoenhanced electron attachment processes to vibrationally and electronically excited polyatomic molecules in relation to the performance of diffuse discharge opening switches. Only qualitative conclusions will be reached here as far as loss processes and opening times are concerned because discharge modeling studies are outside the scope of this report.

Inductive energy storage is attractive in pulsed power applications because of its intrinsic high energy density compared to capacitive energy storage systems. The key technological problem for the realization of such an inductive energy storage device is the development of opening switches, especially for repetitive operation. A promising candidate for a repetitive opening switch is a laser-assisted e-beam sustained diffuse discharge, that opens when the external ionization source is turned of. The time scale on which complete switch opening and therefore commutation of the electrical power stored in the inductor into the load circuit is occurring should be in the submicrosecond range because of power considerations. In order to achieve this goal at typical electron densities of $\leq 10^{14}$ cm^{-3}, the dominant loss mechanism must be electron attachment as opposed to ion-electron recombination. This means that the switch gas mixture must contain an electronegative gas which in turn increases the power loss during the conduction phase. However, both conflicting requirements, namely fast opening times and low power losses during the conduction (closed) phase can be reconciled with the following requirements:

- The attachment rate coefficient should be small and the the electron drift velocity large during the conduction phase, that is at low E/N in order to minimize losses.

- At high E/N characteristic of a diffuse discharge switch in the opening phase, the attachment rate coefficient should increase and the electron drift velocity should decrease in order to favor the rapid switch opening process.

This in turn means that the diffuse discharge opening switch ideally is recombination dominated in the conduction phase with low or no power losses occurring (low E/N), whereas the gas medium changes to attachment dominated at higher E/N in the opening phase. A possible solution to this ideal situation is to use a laser synchronously with the turn-off of the external ionization source (e-beam) in order to convert the gas medium from non-attaching to highly attaching within the laser pulse width. We would like to stress that we use the laser only for a very short duration and a specific phase of the switch cycle in order to switch the attaching properties of the gas medium at one point in time. Lasers are too inefficient at this time to qualify as a sustainment method for a diffuse discharge, although schemes based on a combination of photodetachment and photoionization processes have been proposed.

As an illustration we explore the laser power requirements for generation of an equal density of highly excited attachers based on the 193 nm photolysis of vinylchloride and of dicharge electrons in a diffuse discharge at 0.1 Td (conduction phase) and 1 atmosphere helium. With an assumed current density of 20 A/cm^2 the electron density is calculated as 8.6×10^{14} electrons cm^{-3}, which in turn means that we have to have an equal density of attachers in order to satisfy our minimum requirement of a 1:1 correspondence between excited attachers and discharge electrons. Using 40 mTorr of vinylchloride we will have to use approximately 100 mJ/cm^2 of 193 nm laser radiation in order to create 10^{15} cm^{-3} of excited attachers. It is seen that this laser requirement is modest and can be reached with todays technogy, where doses of 100 mJ/cm^2 can be achieved at 500 Hz with commercially available laboratory lasers. The attenuation of the laser beam is 1.2% per cm so that large diameter and/or pathlength switch devices could be irradiated.

Another illustration serves to underline the electron attaching properties of the laser irradiated system versus the ground state system at a specific pressure and reduced electric field strength (E/N). The electron attaching properties will be expressed in terms of percentage attachment of an electron swarm per cm of drift distance.

One mTorr of vinylchloride in 500 Torr of helium irradiated with 1.2 mJ/cm^2 of 193 nm laser radiation at 0.082 Td leads to 93.9% attachment, whereas the same conditions at 1.23 Td will lead to 39.3% attachment reflecting the gradual drop of the photoenhanced attachment curve with increasing E/N. The ground state values which have to be given for reference purposes are 0.04% attachment at 0.10 Td and 1.69% attachment per cm linear drift distance at 1.23 Td at the above cited pressure of 1 mTorr of vinylchloride in 500 Torr of helium.

Another example concerns the electron attachment to the metastable electronically excited state of p-benzoquinone (BQ) with 6.7 mJ/cm^2 at 308 nm. At 0.2 Td 99.96% of the electrons will be attached per cm drift distance at 140 mTorr of BQ in 620 Torr of molecular nitrogen, and this number is the same at 2.5 Td (99.98%). The ground state system will attach 18.9% at 0.2 Td and 69.1% at 2.5 Td. The important difference between laser excited BQ and vinylchloride is the fact that the attachment curve does not seem to vary with increasing E/N in the former case, wheareas there is no significant ground state attachment in the latter case.

As a conclusion we believe that both attachment schemes explored in the course of this work lead to very promising gas media in diffuse discharge opening switches when coupled with laser radiation emitted by existing lasers. However, questions concerning gas integrity and load characteristics under realistic conditions have to be addressed prior to assessing the full potential of the outlined technological solution to the problem of repetitive diffuse discharge opening switches.

Section 7

CONCLUSIONS

This section deals with the conclusions of our work on photoenhanced electron attachment processes to vibrationally and electronically excited polyatomic molecules in relation to the performance of diffuse discharge opening switches. Only qualitative conclusions will be reached here as far as loss processes and opening times are concerned because discharge modeling studies are outside the scope of this report.

Inductive energy storage is attractive in pulsed power applications because of its intrinsic high energy density compared to capacitive energy storage systems. The key technological problem for the realization of such an inductive energy storage device is the development of opening switches, especially for repetitive operation. A promising candidate for a repetitive opening switch is a laser-assisted e-beam sustained diffuse discharge, that opens when the external ionization source is turned of. The time scale on which complete switch opening and therefore commutation of the electrical power stored in the inductor into the load circuit is occurring should be in the submicrosecond range because of power considerations. In order to achieve this goal at typical electron densities of $\leq 10^{14}$ cm^{-3}, the dominant loss mechanism must be electron attachment as opposed to ion-electron recombination. This means that the switch gas mixture must contain an electronegative gas which in turn increases the power loss during the conduction phase. However, both conflicting requirements, namely fast opening times and low power losses during the conduction (closed) phase can be reconciled with the following requirements:

- The attachment rate coefficient should be small and the the electron drift velocity large during the conduction phase, that is at low E/N in order to minimize losses.

- At high E/N characteristic of a diffuse discharge switch in the opening phase, the attachment rate coefficient should increase and the electron drift velocity should decrease in order to favor the rapid switch opening process.

This in turn means that the diffuse discharge opening switch ideally is recombination dominated in the conduction phase with low or no power losses occurring (low E/N), whereas the gas medium changes to attachment dominated at higher E/N in the opening phase. A possible solution to this ideal situation is to use a laser synchronously with the turn-off of the external ionization source (e-beam) in order to convert the gas medium from non-attaching to highly attaching within the laser pulse width. We would like to stress that we use the laser only for a very short duration and a specific phase of the switch cycle in order to switch the attaching properties of the gas medium at one point in time. Lasers are too inefficient at this time to qualify as a sustainment method for a diffuse discharge, although schemes based on a combination of photodetachment and photoionization processes have been proposed.

As an illustration we explore the laser power requirements for generation of an equal density of highly excited attachers based on the 193 nm photolysis of vinylchloride and of dicharge electrons in a diffuse discharge at 0.1 Td (conduction phase) and 1 atmosphere helium. With an assumed current density of 20 A/cm^2 the electron density is calculated as 8.6×10^{14} electrons cm^{-3}, which in turn means that we have to have an equal density of attachers in order to satisfy our minimum requirement of a 1:1 correspondence between excited attachers and discharge electrons. Using 40 mTorr of vinylchloride we will have to use approximately 100 mJ/cm^2 of 193 nm laser radiation in order to create 10^{15} cm^{-3} of excited attachers. It is seen that this laser requirement is modest and can be reached with todays technogy, where doses of 100 mJ/cm^2 can be achieved at 500 Hz with commercially available laboratory lasers. The attenuation of the laser beam is 1.2% per cm so that large diameter and/or pathlength switch devices could be irradiated.

Another illustration serves to underline the electron attaching properties of the laser irradiated system versus the ground state system at a specific pressure and reduced electric field strength (E/N). The electron attaching properties will be expressed in terms of percentage attachment of an electron swarm per cm of drift distance.

One mTorr of vinylchloride in 500 Torr of helium irradiated with 1.2 mJ/cm^2 of 193 nm laser radiation at 0.082 Td leads to 93.9% attachment, whereas the same conditions at 1.23 Td will lead to 39.3% attachment reflecting the gradual drop of the photoenhanced attachment curve with increasing E/N. The ground state values which have to be given for reference purposes are 0.04% attachment at 0.10 Td and 1.69% attachment per cm linear drift distance at 1.23 Td at the above cited pressure of 1 mTorr of vinylchloride in 500 Torr of helium.

Another example concerns the electron attachment to the metastable electronically excited state of p-benzoquinone (BQ) with 6.7 mJ/cm^2 at 308 nm. At 0.2 Td 99.96% of the electrons will be attached per cm drift distance at 140 mTorr of BQ in 620 Torr of molecular nitrogen, and this number is the same at 2.5 Td (99.98%). The ground state system will attach 18.9% at 0.2 Td and 69.1% at 2.5 Td. The important difference between laser excited BQ and vinylchloride is the fact that the attachment curve does not seem to vary with increasing E/N in the former case, wheareas there is no significant ground state attachment in the latter case.

As a conclusion we believe that both attachment schemes explored in the course of this work lead to very promising gas media in diffuse discharge opening switches when coupled with laser radiation emitted by existing lasers. However, questions concerning gas integrity and load characteristics under realistic conditions have to be addressed prior to assessing the full potential of the outlined technological solution to the problem of repetitive diffuse discharge opening switches.

REFERENCES

AL83 M. Allan, Chem. Phys. 81, 235 (1983).

AL84 M. Allan, Chem. Phys., 84, 311 (1984).

AN75 D.A. Armstrong and S.S. Nagra, J. Phys. Chem., 79, 2875 (1975).

AW78 M. Allan and S. F. Wong, Phys. Rev. Lett., 41, 1791-1794 (1978).

AW81 M. Allan and S. F. Wong, J. Chem. Phys. 78, 1687-1691 (1981).

BE74 M. J. Berry, J. Chem. Phys. 55, 2055 (1971).

BJ85 W.K. Bischel, L.J. Jusinski, M.N. Spencer, and D.J. Eckstrom, J. Opt. Soc. Am. B., 2, 877 (1985).

BM73 L. E. Brus and J. R. Mcdonald, J. Chem. Phys., 58, 4223 (1973).

BS71 G. Belanger and C. Sandorfy, J. Chem. Phys., 55, 2055 (1971).

BW83 J. N. Bardsley and J. M. Wadehra, J. Chem. Phys., 78, 7227-7234 (1983).

CC68 L.G. Christophorou, R.N. Comptou, and H.W. Dickson, J. Chem. Phys., 48, 1949 (1968).

CC69 L.G. Christophorou, J. G. Carter, and A. A. Christodoulides, Chem. Phys. Lett., 3, 237 (1969).

CC70 P. M. Collins, L. G. Christophorou, E. L. Chaney, and J. G. Carter Chem. Phys. Lett., 4, 646 (1970).

CC79 C. L. Chen and P. J. Chantry, J. Chem. Phys., 71, 3897-3907 (1979)

CH79 P. J. Chantry, J. Chem. Phys. 71, 2746-2759 (1979).

CH84a Electron-Molecule Interactions and Their Applications, Vol. I and II, L. G. Christophorou, Ed. (Academic Press, 1984).

CH84b Electron-Molecule Interactions and Their Applications, L. G. Christophorou, Ed., Volume 1, Chapter 6 (Academic Press, 1984).

CH85 L. G. Christophorou, J. Chem. Phys., 83, 6543 (1985).

CJ74 L. G. Christophorou, D. R. James, R. Y. Pai, R. A. Mathis, I. Sauers, D. H. Smith, L. Frees, M. O. Pace, D. W. Bouldin, C. C. Chan, A. Fatheddin, and D. Maughan, Oak Ridge National Laboratory Report ORNL TM-7405 (1974).

CP67 J. C. Y. Chen and J. L. Peacher, Phys. Rev. 163, 103-111 (1967).

DA85 R. Dressler, M. Allan, and E. Haselbach, Chimia 39, 385 (1985).

DL86 D. J. Donaldson and St. R. Leone, manuscript submitted to Chem. Phys Lett.

FB63 W. L. Fite and R. T. Brackmann, Proc. Int. Conf. on Ionization Phenomenon in Gases, Paris, 1, 21-27 (1963).

GJ84 M. Guerra, D. Jones, G. Distefano, and A. Modelli, Chem. Phys. 85, 389 (1984).

Gr69 R. Gruenberg, Z. Naturforski, 24a, 1039 (1969).

HC74 "The Diffusion and Drift of Electrons in Gases," L. G. Huxley and R.W. Crompton, (John Wiley, 1974).

IT85 T. Itoh, Mol. Phys., 55, 799 (1985).

KG77 H. Kobashi, H. Gyoda, and T. Morita, Bull. Chem. Soc. Jap., 50, 1731 (1977).

KH86 R. D. Kenner, H. K. Haak, and F. Stuhl, J. Chem. Phys. 85, 1915 (1986).

MC84 D. L. McCorkle, A. A. Christodoulides, and L. G. Christophorou, in Gaseous Dielectrics IV, pg. 12, L. G. Christophorou and M. O. Pace, Eds. (Pergamon Press, 1984).

MP83 M.J. Rossi, J. R. Plaskiewicz, and J. R. Barker, J. Chem. Phys., 78, 6695 (1983).

MS82 D. L. McCorkle, I. Szamrej, and L. G. Christophorou, J. Chem. Phys. 77, 5542-5548 (1982).

OM67 T. F. O'Malley, Phys. Rev., 155, 59-63 (1967)

SC85a S. M. Spyrou and L. G. Christophorou, J. Chem. Phys. 83, 2829 (1985).

SC85b S. M. Spyrou and L. G. Christophorou, J. Chem. Phys. 82, 1048 (1985).

SC86 K. L. Stricklett, S. C. Chu, and P. D. Burrow, Chem. Phys. Lett., 131, 279 (1986).

SH86 H. Shimamaui and H. Holta, J. Chem. Phys. 85, 4480 (1986).

ST67 P. E. Stevenson, J. Mol. Spectry. 23, 191 (1967); M. A. Slifkin, R.A. Sumner, and J. G. Heathcote, Spectrochim. Acta, 26A, 1135 (1970); H. P. Trommsdorff, P. Sahy and J. Kahane-Paillous, Spectrochim. Acta 23A, 1751 (1967).

US85 M. Umemoto, K. Seki, H. Shinohara, U. Nagashima, N. Nishi, M. Kinoshita, and R. Shimada, J. Chem. Phys. 83, 1657 (1985).

APPENDIX A

Photoenhanced electron attachment of vinylchloride and trifluoroethylene at 193 nm

M. J. Rossi, H. Helm, and D. C. Lorents
Chemical Physics Laboratory, SRI International, Menlo Park, California 94025

(Received 8 April 1985; accepted for publication 21 June 1985)

We show that the electron attachment properties of a gas mixture of helium containing vinylchloride or trifluoroethylene can be altered from nonattaching to strongly attaching by irradiation with a low-energy laser pulse at 193 nm. These molecules are photodissociated producing vibrationally excited HCl or HF and other fragments that strongly attach low-energy electrons.

This study was motivated by the possibility that vibrationally or electronically excited molecules can be photolytically produced that attach electrons with a significantly higher cross section than their ground-state counterparts. This possibility of optical control of the electron attachment suggests a practical means of externally switching the conductivity of a diffuse discharge.

The work demonstrates that the attachment rate of a gas mixture can be optically enhanced by several orders of magnitude. A nonequilibrium population of attaching species is generated in high-lying vibrational states by photodissociation of nonattaching parent molecules and their attachment rate constants are measured in a drift tube. Specifically, the electron attachment of highly excited HCl and HF formed by irradiating vinylchloride and trifluoroethylene with a laser pulse at 193 nm is examined.

Our measurements of the photoenhanced electron attachment were performed in a Grunberg-type[1] drift tube apparatus (Fig. 1). Grünberg's method for the measurements of electron attachment rates is based on the analysis of the transient waveform induced by the movement of charged carriers in a parallel plate electrode gap, and on the temporal separation of electrons from ions due to their different drift velocities. For this purpose a swarm of electrons is released from one electrode and the remaining electrons, as well as the negative ions formed in the gap by electron attachment are collected at the opposite electrode. A broadband xenon flashlamp was used for photoelectron production and typically 10–100 transient waveforms were accumulated before being analyzed. The dynamic range of our measurement of the attachment coefficient η (number of attachment events per cm drift length) is about 400 with a precision of typically 5%.

We tested the apparatus by measuring electron drift velocities in He and attachment in pure O_2. Overall agreement was found with literature data.[1,2]

In order to compare the attachment behavior of the excited with the unexcited "ground-state" sample, we first measured the attachment coefficient of unexcited C_2H_3Cl and C_2HF_3 in a He buffer.

The attachment coefficient of vinylchloride measured as a function of E/N is shown in Fig. 2 by the solid dots. A weak dependence on vinylchloride concentration (10^{-5}–10^{-4}) was observed being most pronounced in the steeply rising portion of the attachment curve around 0.8 Td. The curve drawn through the data in Fig. 2 merely represents a guide to the eye. At the concentrations employed in this experiment attachment was not detectable below 0.5 cm^{-1} Torr^{-1} and the data in Fig. 2 for $E/N < 0.6$ Td have to be considered as upper limits for η/P. Qualitatively similar results were observed in trifluoroethylene, the data being shown by the solid dots in Fig. 3. In this case η/P values remained near 1 cm^{-1} Torr^{-1} for $E/N = 0.4$–5 Td. At higher values of E/N the apparent attachment coefficient rises to 15 cm^{-1} Torr^{-1} at 9 Td, the maximum reduced field strength used. Beyond 9 Td breakdown occurs so it is possible that the rise is due to positive ions produced by the swarm electrons.

Illumination of the gap with a weak excimer laser beam at 193 nm coincident in time with the photoelectron source dramatically altered the attachment properties of the gas samples. This phenomenon was expected since vinylchloride and trifluoroethylene are photodissociated into strongly attaching products at this wavelength. However, the transient current method distinguishes charge carriers only on the basis of their different drift velocities but does not distinguish between positive and negative ions. Hence a variety of control experiments were performed to ensure that the observed phenomena were due to electron attachment to photoproducts in the gas phase. First it was observed that illumination of the gap with light from a KrF laser (248 nm) did not alter

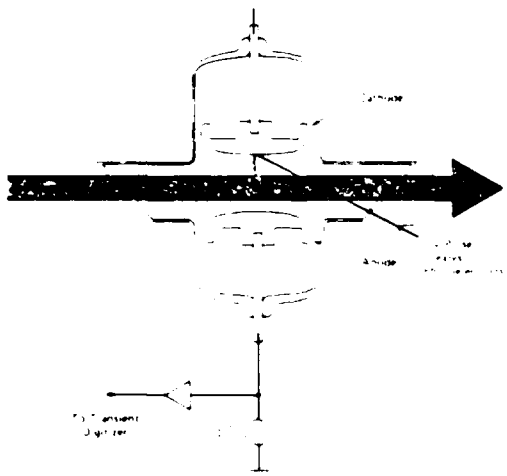

FIG. 1. Schematic drawing of Grunberg-type drift tube apparatus for measurement of photoenhanced electron attachment. The gap distance is [illegible] and the electrode diameter is 5 cm.

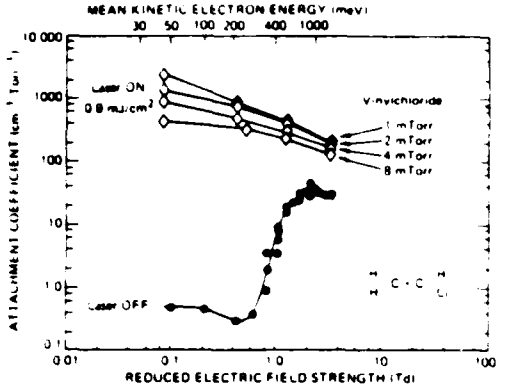

FIG. 2. Attachment coefficient for vinylchloride in helium buffer (500 Torr). The solid points represent the data for unexcited mixtures, obtained at vinylchloride pressures ranging from 50 to 500 mTorr. The photoenhanced attachment coefficient (open points) is expressed in terms of the unexcited vinylchloride concentration.

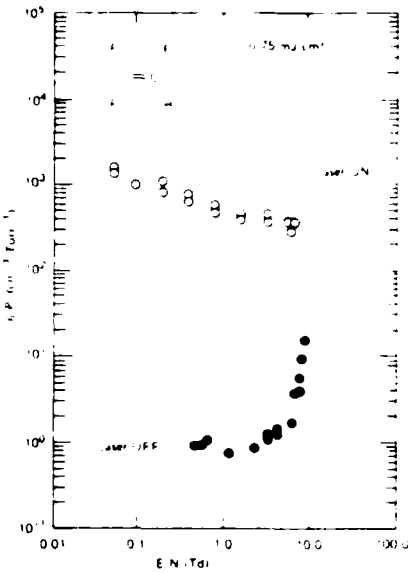

FIG. 3. Attachment coefficient for trifluoroethylene. The solid dots give the values for the unexcited sample (200 mTorr of C_2F_3H in 200 Torr helium). The open circles represent the data for the excited sample (100 mTorr of C_2F_3H in 100 Torr helium). The attachment coefficients are expressed in terms of the unexcited trifluoroethylene pressure.

the attachment properties of the gas samples. As expected neither gas appreciably absorbs in this spectral region. The fraction of the transient current that originated from multiphoton ionization (MPI) at 193 nm was examined in great detail. For this matter the relative MPI yields for vinylchloride, trifluoroethylene, and benzene were measured at 193 and 248 nm using a nozzle beam combined with a time-of-flight mass spectrometer system.[3] Absolute values for the total MPI yield of benzene[4] at 248 nm were used to obtain absolute MPI yields. It was then possible to assess the absolute MPI yield of the compounds of interest under the given experimental conditions. A detailed description of this study will be reported in a separate paper.[5]

Under typical experimental conditions of 4 mTorr of vinylchloride in 500 Torr He and a laser power density of 1.0 mJ/cm^2 at 193 nm, the total MPI yield between the electrodes of the drift cell is 1.5×10^6 ions. This number is to be compared with the total charge of photoelectrons in the attachment experiment, which is typically greater than 5×10^7 *electrons per transient. Thus, less than 3% of the total* charge monitored in each transient originates from MPI of C_2H_3Cl. A similar situation exists for trifluoroethylene which has a cross section for multiphoton ionization an order of magnitude lower than vinylchloride.

The open diamonds in Fig. 2 display our photoenhanced attachment coefficients for vinylchloride as a function of the reduced electric field strength for various sample pressures at 500 Torr total pressure of He. The laser fluence was 0.9 mJ/cm^2 at 193 nm, corresponding to the excitation of $\sim 2\%$ of the indicated C_2H_3Cl concentration using 1.7×10^{-17} cm^2 as absorption cross section at 193 nm.[6] Note that the attachment coefficient is expressed per Torr of ground-state species, nevertheless, the enhancement in the attachment coefficient is very large relative to the ground-state attachment curve. Expressed in terms of the pressure of excited species, the η/P values in Fig. 2 should be multiplied by 50. Thus, the actual enhancement factor per excited molecule is $> 2 \times 10^4$ at 0.1 Td and 5×10^2 at the maximum of the ground-state attachment curve at 2.2 Td for a pressure of 1 mTorr of C_2H_3Cl and 0.9 mJ/cm^2. The effect of quenching of the attaching species by the residual vinylchloride is apparent from Fig. 2.

The results for the photoenhanced electron attachment of trifluoroethylene (C_2F_3H) are quite analogous to the ones for C_2H_3Cl. The basic difference between the two molecules lies in their absorption cross sections at 193 nm with C_2F_3H being the weaker absorber ($\sigma = 2.44 \times 10^{-18}$ cm^2).[7] A sample of our data on C_2F_3H is shown by the open circles in Fig. 3, where η/P has again been expressed in terms of ground-state pressure of C_2F_3H. The photoenhancement amounts to a factor of 40 at 9 Td, when 100 mTorr of C_2F_3H in 100 Torr He were excited at 193 nm with 0.75 mJ/cm^2. More than three orders of magnitude of enhancement is found at low values of E/N. We note from Fig. 3 that the general functional dependence of the photoenhanced η/P values on E/N is a gentle decline by a factor of 4 very similar to the situation in C_2H_3Cl. In terms of the excited state density, the η/P values in Fig. 3 should be multiplied by a factor of 700. A concentration dependence for trifluoroethylene similar to vinylchloride was observed.

In both gases the observed enhancement in the attachment coefficient upon 193-nm photoexcitation is attributed to the formation of vibrationally excited, attaching photofragments from the photodissociation of the substituted ethylene. The expected photochemistry for vinylchloride at 193 nm is

$$C_2H_3Cl \xrightarrow{h\nu} HC \equiv CH^{\ddagger} + HCl \quad \Delta H_r = 23.2 \text{ kcal/mol}, \tag{1}$$

$$C_2H_3Cl \xrightarrow{h\nu} H_2C = C^{\ddagger} + HCl, \tag{2}$$

$$C_2H_3Cl \xrightarrow{h\nu} H_2C = CH^{\ddagger} + Cl \tag{3}$$

The thermal activation energy for reaction (1) is estimated at 55.0 kcal/mol, and after photoexcitation the reaction system has to distribute an excess of 125 kcal/mol over the available translational, rotational, and vibrational degrees of freedom. We estimate that HCl is initially excited to $v = 6 \pm 1$ in analogy to published examples of HF elimination in vinylfluoride and 1,1-difluoroethylene,[5] where the maximum degree of vibrational excitation in HF was observed to correspond (within $\pm$ one vibrational quantum) to the thermal activation energy for the same process. The acetylene may be vibrationally excited as well, but no experimental information is available. Reaction (2) must be included because of the transient existence of vinylidene (C_2H_2), which is calculated to have a few picoseconds of lifetime towards isomerization to acetylene. The final products from the photoelimination according to reaction (2) are the same as for reaction (1) except that the nascent internal energy distribution will be different. The third choice to dispose of the excess energy gained in the photoexcitation requires energies in excess of 90.4 kcal/mol and results in the formation of a Cl atom and a vinyl radical [reaction (3)].[6] The branching ratio between HCl [reactions (1) and (2)] and Cl [reaction (3)] was assessed in a separate experiment. Using gas chromatorgraphic analysis of a static vinylchloride sample irradiated at 1 mJ/cm^2 at 193 nm we measured a branching ratio of 86/14 for formation of HCl vs Cl. The reaction progress of both reactions (1) and (2) was monitored by measuring the amount of acetylene, whereas the extent of reaction (3) was followed by measuring the amount of butadiene C_4H_6, which is the recombination product of the vinyl radical.

The relevant photoelimination reaction in the case of trifluoroethylene is given by reaction (4), whose endothermicity has been estimated at 58.0 $\pm$ 5.0 kcal/mol

$$F_2C = CFH \xrightarrow[h\nu]{193\text{ nm}} FC \equiv CF + HF^{\ddagger} \qquad (4)$$

The activation energy for thermal unimolecular decomposition of trifluoroethylene according to reaction (4) is estimated to be 65 kcal/mol, which means that HF may contain vibrational energy up to $v = 5 \pm 1$ if we proceed in an analogous way as before.[5] Nevertheless, we cannot rule out some degree of vibrational excitation in the difluoroacetylene product, so that we conclude that the attaching species in the photoenhanced attachment of trifluoroethylene are vibrationally excited HF and/or C_2F_2.

In conclusion, we have demonstrated that a certain class of nonattaching molecules can, by laser activated photodissociation, be converted to strongly attaching species. This observation may have significant implications for the optical control of diffuse discharge switches.

Support by ARO is gratefully acknowledged.

[1] R. Grunberg, Z. Naturforsch. **24A**, 1039 (1969).
[2] L. G. H. Huxley and R. W. Crompton, *The Diffusion and Drift of Electrons in Gases* (Wiley, New York, 1974), Chap. 14.
[3] N. Bjerre, R. Kachru, and H. Helm, Phys. Rev. A **31**, 1206 (1985).
[4] W. K. Bischel, L. E. Jusinski, M. N. Spencer, and D. J. Eckstrom, J. Opt. Soc. B (in press).
[5] M. J. Rossi and H. Helm (unpublished).
[6] M. J. Berry, J. Chem. Phys. **61**, 3121 (1974).
[7] G. Belanger and C. Sandorfy, J. Chem. Phys. **55**, 2055 (1971).
[8] E. R. Sirkin and G. C. Pimentel, J. Chem. Phys. **75**, 604 (1981); J. Chem. Phys. **77**, 1314 (1982).
[9] D. F. McMillen and D. M. Golden, Ann. Rev. Phys. Chem. **33**, 493 (1982).

APPENDIX B

Volume 120, number 2 CHEMICAL PHYSICS LETTERS 4 October 1985

QUANTITATIVE ASPECTS OF BENZENE PHOTOIONIZATION AT 248 nm

Michel ROSSI and D.J. ECKSTROM

Chemical Physics Laboratory, SRI International, Menlo Park, CA 94025, USA

Received 10 June 1985; in final form 28 July 1985

We have carefully remeasured the mass distribution of ions resulting from photoionization of benzene at 248 nm. The fragmentation occurs at lower intensities than previously indicated, beginning below 2 MW/cm². At 17 MW/cm² the parent ion constitutes only 12.5% of the total, while at 110 MW/cm², C^+ constitutes 24% of the yield. The functional dependence of the absolute photoionization yield as a function of laser power cannot be described by a simple four-level kinetic model successfully used to describe the absolute MPI yield at low power. Instead, a highly excited neutral intermediate is postulated that can either autoionize or photodissociate upon absorption of an additional photon.

1. Introduction

It is well known that organic molecules produce fragment ions as well as the parent ions when they are multiphoton ionized at high laser intensities [1–5]. However, there is some question about the quantitative accuracy of previous studies carried out using excimer lasers because of the difficulty of accurately specifying the laser intensity in the focal volume of these multimode lasers. Furthermore, there are no quantitative data on absolute ion yields upon resonant two-photon ionization at 248 nm at higher intensities. Such data are urgently needed in order to test or expand models for resonant MPI in polyatomic molecules. Because of the importance of the results to studies of the guiding of electron beams by preionized channels [6], we have repeated the measurements for benzene photoionized by a KrF laser, taking particular care in the determination of the focused laser intensity. In this paper we report on fragmentation patterns of benzene as a function of laser power at 248 nm and on absolute yields for resonant MPI of benzene at high laser power using the low-power results of Bischel et al. [7] as calibration points.

2. Experimental

We used a Lambda-Physik model EMG 101 excimer laser operated with standard stable resonator optics so that it produced 180 mJ pulses of 14 ns full width at half maximum in a beam 0.7 × 2.2 cm². An aperture of 0.35 cm diameter isolated the uniform center of the beam. This aperture was focused with a 5 cm focal length lens unto a second "pinhole" aperture. The calculated focal diameter at the pinhole was 1.13×10^{-4} cm. However, transmission measurements through pinholes of different diameters showed that the focal diameter was, in fact, only marginally smaller than the 0.025 cm diameter pinhole used in all subsequent experiments to define the focal diameter of the laser beam.

The power dependence of the resonant two-photon ionization of benzene was studied by monitoring the ion signal as a function of the distance between aperture II and focusing lens L1 (fig. 1) with aperture II being stationary. For all but the highest power (2.7×10^8 W/cm²), the focused laser beam was vignetted by aperture II so that its homogeneous illumination was achieved throughout the study. We estimate that the maximum power transmitted through the pinhole was larger than the nominal value quoted by about 10–20% due to the fact that the focal diameter was slightly smaller than the 0.025 mm diameter pinhole

0 009-2614/85/$ 03.30

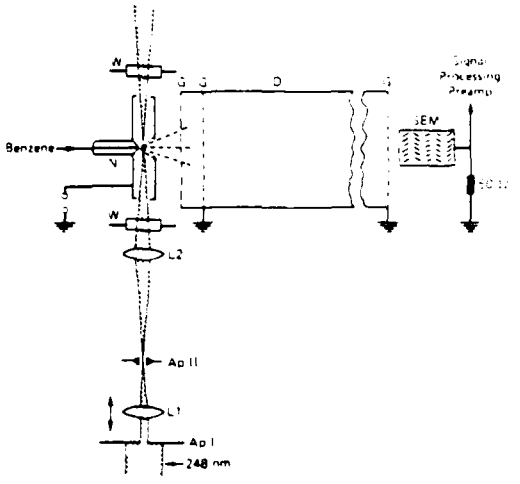

Fig. 1. Schematic of experimental apparatus for the measurement of the MPI fragmentation of benzene at 248 nm. Ap I, II, apertures; L1, L2, lenses; W, quartz window; N, tungsten needle with 40 μm diameter capillary; G, grounded grid; D, field free drift section; SEM, secondary electron multiplier.

(aperture II, fig. 1). This systematic error, however, applies only to the highest power data taken in each run, because vignetting of the beam was achieved for all other (lower) laser powers.

The pinhole aperture was imaged with unit magnification into the center of the ionization region using a 30 cm focal length lens. We measured the laser energy with a Scientech energy meter after the imaging lens but before the cell window. The maximum intensity in the focal volume based on the diameter of the pinhole, the measured laser energy, and the measured fwhm of the laser pulse, was 110 MW/cm^2. We reduced the intensity to values as low as 4.0 MW/cm^2 by moving the first lens away from the pinhole so that the laser beam passed through a focus and was diverging at the pinhole. We also made measurements at 2.3 MW/cm^2 using the apertured beam from the laser with no focusing.

Benzene was introduced into the ionization region through a tungsten capillary nozzle of 40 μm diameter, which was connected to a reservoir containing benzene at lower than ambient temperature, thus maintaining a constant pressure. The ionization chamber was maintained at a pressure of about 10^{-6} Torr, so we assume the benzene formed an effusive collisionless free jet that diverged gradually away from the orifice. The image of the pinhole was adjusted to produce the maximum ion signal for each laser intensity, which presumably occurs when the focus is just at the exit of the orifice. Note that the laser Rayleigh range was much greater than the orifice diameter, so that the intensity should have been uniform across the width of the jet.

As will be discussed later, our irradiation conditions do not lead to either saturation or photobleaching of the irradiated volume, even at the highest laser powers achieved. In view of the fact that we only ionize 10% of the sample at the highest laser powers, we took particular care to align the focal region of the beam with the jet to achieve maximum overlap. This was done by reflecting the laser beam before it entered the TOF mass spectrometer through window W (fig. 1) and searching for the position of the image of aperture II. The position of this image was brought to overlap with the jet by adjusting the position of aperture II and focal lens L2. Final "fine tuning" was achieved by maximizing the total ion signal through laser beam steering.

The ions produced were measured using a time-of-flight mass spectrometer [8] with a 2.9 kV accelerating voltage and a secondary electron multiplier detector. The voltage applied to the SEM was 2.6 kV in most experiments, but was reduced to 2.1 kV for experiments at the highest laser intensities in order to avoid saturation effects. In addition, it was necessary to decrease the stagnation presssure behind the nozzle for experiments at higher laser powers because of space charge effects on the ion flight time. We changed the benzene pressure from 0.8 to 80 Torr by cooling the benzene reservoir from room temperature to [illegible] °C. We assume that all ions were detected with equal sensitivity, regardless of mass. When the focal region was moved vertically so that the laser beam missed the jet, the ion signal decreased essentially to zero, indicating the absence of background ionization.

The entire apparatus is shown schematically in fig. 1.

3. Results and discussion

The distribution [illegible]

AD-A181 055 PHOTON-ENHANCED ELECTRON ATTACHMENT PROCESSES IN DISCHARGE-OPENING SWITCHES(U) SRI INTERNATIONAL MENLO PARK CA M J ROSSI ET AL. FEB 87 ARO-19934.5-PH 2/2

UNCLASSIFIED DAAG29-83-K-0113 F/G 7/4 NL

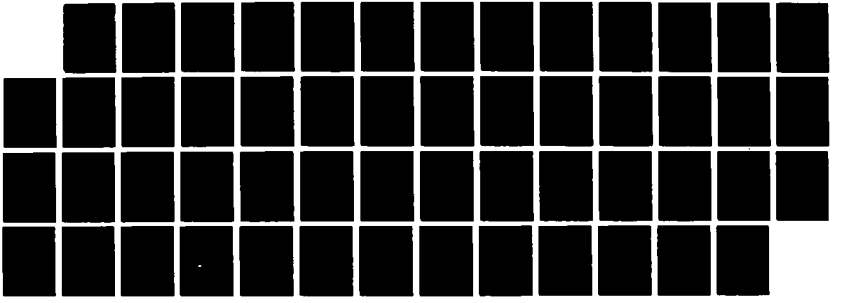

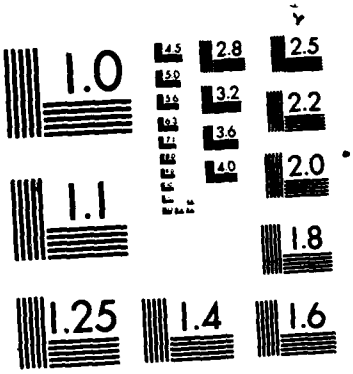

Table 1
Percentage ion mass distribution resulting from 248 nm photoionization of benzene at selected laser intensities (W/cm^2)

Species	Mass	2.3(6)	3.95(6)	7.24(6)	1.64(7)	3.03(7)	4.09(7)	1.11(8)
C^+	12				3.25	9.67	11.91	23.89
CH^+	13				0.29	0.47	0.70	1.32
CH_2^+	14				0.22	0.23	0.26	0.50
CH_3^+	15				0.15			
C_2^+	24				0.65	3.69	4.38	10.25
C_2H^+	25				0.81	1.84	1.93	3.32
$C_2H_2^+$	26		0.20	3.52	3.58	3.32	3.33	4.22
$C_2H_3^+$	27		0.20	3.52	2.93	3.14	3.33	4.52
$C_2H_4^+$	28				0.33	0.28	0.18	0.31
C_3^+	36				6.22	11.44	10.30	12.07
C_3H^+	37			1.06	9.13	9.87	8.83	7.23
$C_3H_2^+$	38			1.06	3.11	2.34	2.31	1.61
$C_3H_3^+$	39	0.89	1.61	2.95	6.22	5.20	5.64	5.22
C_4^+	48				2.96	2.34	2.36	1.61
C_4H^+	49			0.72	5.93	4.35	4.34	2.82
$C_4H_2^+$	50		1.32	6.58	17.50	13.06	12.44	6.84
$C_4H_3^+$	51		4.13	12.19	14.23	10.04	10.09	4.89
$C_4H_4^+$	52	2.69	3.14	4.69	3.56	3.01	2.69	1.20
$C_5H_3^+$	63	0.22	0.40	0.94	0.99	0.43	0.70	
$C_6H_4^+$	76		2.98	2.95	1.01	0.87	0.95	0.40
$C_6H_5^+$	77		13.35	14.79	4.45	4.04	3.47	2.01
$C_6H_6^+$	78	89.84	66.75	41.36	11.57	9.53	9.15	5.22
	79	6.35	5.95	3.69	0.89	0.87	0.76	0.60

laser intensity is listed in table 1, expressed as percent of the total yield at that intensity. The same results are shown in bar graph form in fig. 2 and results for selected ions are plotted versus laser intensity in fig. 3.

The results are qualitatively similar to those of Reilly and Kompa [2]. We report a maximum of 22 different ions, compared to their 18, but the new species we detected were present only in low abundances, presumably below their sensitivity limit. The major and important difference between our results and theirs is in the intensity levels required to produce given fragmentation patterns. A visual comparison of their mass distributions with ours indicates similar patterns when our intensities are about one-tenth their stated values. As indicated above, we suspect that the actual laser intensities in their experiment were much lower than they calculated because the multimode excimer laser did not focus to as small a spot size as expected from simple diffraction theory. Our own experience, described above, shows that the discrepancy between the calculated and measured beam diameter can exceed a factor of 100.

In contrast, our results indicate somewhat less fragmentation at a given laser intensity than do those of Antonov et al. [3]. They report fragmentation of benzene beginning at 0.05 MW/cm^2, and their published mass spectrum at 2 MW/cm^2 shows similar levels of fragmentation as our results at 7 MW/cm^2. They report that $C_6H_6^+$ is the dominant ion at least up to 20 MW/cm^2, in reasonable agreement with our observation that it is dominant up to about 15 MW/cm^2. However, their fragmentation pattern is different in detail from those we observe at any laser intensity. In particular, their pattern for m/e = 76, 77, and 78 (corresponding to $C_6H_4^+$, $C_6H_5^+$, and $C_6H_6^+$), does not match our results for the same range of laser intensities. They made their measurements by reducing their laser beam size using a telescope, and then aperturing the reduced

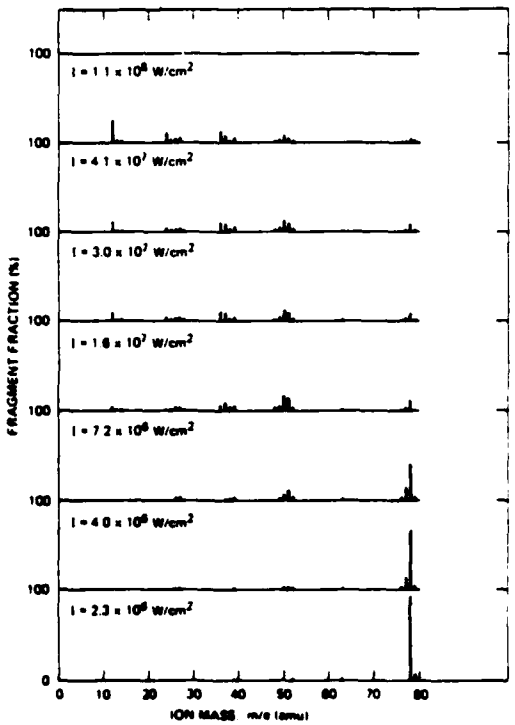

Fig. 2. Ion mass distribution resulting from photoionization of benzene at 248 nm as a function of laser power (14 ns fwhm of laser pulse).

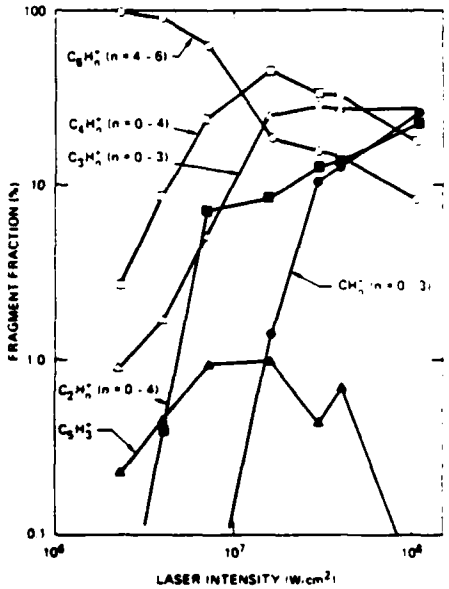

Fig. 3. Ion mass distribution for the most important fragment groups resulting from photoionization of benzene at 248 nm as a function of laser intensity.

beam. In order to achieve high laser intensities, they used up to 50% of the incident laser power. We suspect that the beam was non-uniform in intensity, so that there were "hot spots" in the reduced beam. Their fragmentation patterns would then result from the addition of larger areas of low intensity (primarily responsible for the parent ion signals) and localized areas of high intensity (which would contribute the majority of the fragment ion signals).

As suggested previously [2], benzene photoionization and fragmentation at 248 nm appears to occur by way of formation of the parent ion ($C_6H_6^+$), which subsequently absorbs more photons and decomposes stepwise, even as far as C^+ at the highest intensities. The yield of the parent ion decreases steadily over the entire intensity range. In addition, $C_6H_5^+$ and $C_6H_4^+$, which first appear at 4 MW/cm^2, decrease in constant proportion to $C_6H_6^+$ at higher intensities, as shown in fig. 2. The similarity of appearance intensities, together with their near equality of appearance energies, suggests that these two ions are both formed independently from the parent ion. Furthermore, their constant proportionality to the parent ion suggests that these two product ions undergo photodissociation at the same rate as the parent ion. As can be seen in figs. 2 and 3, the details of the photofragmentation spectrum of $C_6H_6^+$ are a complex function of the laser intensity. It appears that elimination of CH_n ($n = 1-3$) to yield $C_5H_3^+$ is not a favored process over the entire intensity range. Also, the elimination of C_2H_n ($n = 0-4$) seems to be favored over the extrusion of C_3H_n ($n = 0-3$) at intensities below 10^7 W/cm^2. The situation is complicated by the fact that the precursors (ionic or neutral) for the fragment ions are not presently known. However, the general trend can be noted, that the appearance energy for a fragment ion is inversely proportional to its carbon content (with the exception of $C_5H_3^+$).

We have added the contributions of ions of all

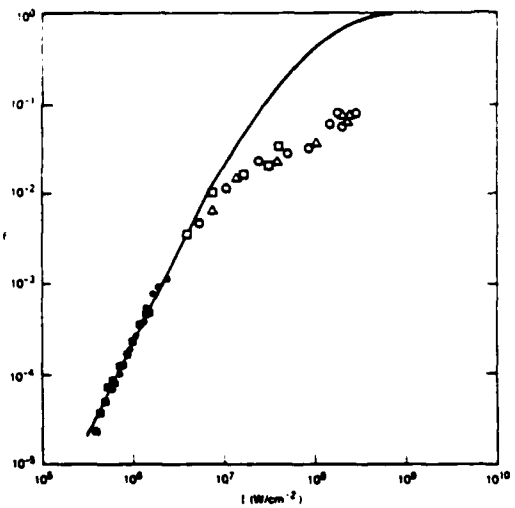

Fig. 4. Absolute ion yield (mass integrated) in resonant two-photon ionization of benzene at 248 nm as a function of laser power I (14 ns fwhm of laser pulse). ●, ■ ...unfocused beam, 80 Torr stagnation pressure, ○, △ ...focused, 0.8 Torr stagnation pressure, □ ...focused, 25 Torr stagnation pressure.

masses at each laser intensity to determine the dependence of total photoionization yield on laser power or intensity. The results are compared in fig. 4 with the predicted variation based on the molecular constants for benzene measured recently by Bischel et al. [7], using our laser pulse shape.

In their work, absolute ionization yields for the two-photon resonant excitation of benzene were measured at laser intensities low enough that no fragmentation occurred. The ion current was found to be strictly second order in laser intensity up to laser fluence of 8 mJ/cm^2, and the results were fitted to a four-level rate equation model of benzene. The assumption was made that photoionization only takes in benzene resulting in benzene molecular ion, $C_6H_6^+$, and therefore ionization of neutral fragments originating from the photodissociation of C_6H_6 or $C_6H_6^+$ would not contribute to the total observed ion current. This assumption also leads to the statement that all fragment ions must have their origin in $C_6H_6^+$, an assumption that may not hold in view of the low ionization potential of many open-shell hydrocarbon species. In fact, Bischel et al. were able to explain their data on the basis of the above assumption (no fragmentation under their experimental condition) and the following four-level model:

$$^1A_{1g} + h\nu \xrightarrow{\sigma_{10}} {}^1B_{2u}\,, \tag{1}$$

$$^1B_{2u} \xrightarrow{Q} {}^3B_{1u}\,, \tag{2}$$

$$^1B_{2u} \xrightarrow{\sigma_{21}} C_6H_6^+\,. \tag{3}$$

where $^1A_{1g}$ is the electronic ground state, $^1B_{2u}$ is the resonant intermediate state, $^3B_{1u}$ is the non-photoionizing lowest triplet state, and $C_6H_6^+$ is the ionic ground state of benzene; σ_{10} and σ_{21} are the corresponding absorption cross sections, and Q is the effective rate of deactivation of the resonant intermediate state with radiative (fluorescence) and non-radiative (intersystem crossing) components. With the aid of known values for σ_{10} of 3.7×10^{-19} cm^2 and Q of 2.2×10^7 s^{-1}, an ionization cross section of 4.4×10^{-18} cm^2 was found for σ_{21}, together with a small non-resonant two-photon cross section of $< 0.5 \times 10^{-27}$ cm^4/W [7].

The solid line in fig. 4 describes the absolute ionization yields using the above molecular parameters for benzene and our laser beam temporal profile. The low-intensity yields (black symbols in fig. 4) were then fitted to the calculated curve, because the absolute scale for the experimental points is arbitrary. The low-intensity data fit a second-order dependence on laser intensity rather well up to the point where fragmentation begins to become important (5% of total ion current at 2.5×10^6 W/cm^2 is distributed to lower-weight-fragment ions, see table 1). The high-intensity mass integrated ion yields (open symbols in fig. 4) were fitted such that the lowest two intensity data points coincided with the prediction from our rate equation model. The experimental results at intensities exceeding 7.5×10^6 W/cm^2 fall well below the prediction, which suggests either that an additional loss process "turns on" at higher laser power, or that space-charge effects reduce the collection efficiency for all ions at higher ion densities. However, the relative ionization yield for a variation of the benzene backing pressure of as much as a factor of 100 was found to be unchanged, which we take as an indication that space charge effects or recombination kinetics were not responsible for the depression of the MPI yield at higher laser power.

At this point our results lead us to postulate a neutral precursor state that can either undergo autoionization or absorb an additional photon to decay into neutral fragments. The depression of the MPI yield at higher laser intensities cannot be due to saturation effects because they have already been taken into account in the rate equation model. Furthermore, saturation effects are unimportant in the present case because $\sigma_{21} > 10\sigma_{10}$. This state is thought of as a superexcited state of benzene at an energy of twice the photon energy above ground state and is most likely a molecular Rydberg state of benzene. Using this neutral intermediate the resonant MPI scheme is given by

$$M + h\nu \rightarrow M^{*}, \quad (4)$$

$$M^{*} + h\nu \rightarrow M^{+} + e, \quad (5)$$

$$M^{*} + h\nu \rightarrow M^{**}, \quad (6)$$

$$M^{**} + h\nu \rightarrow A + B, \quad (7)$$

$$M^{**} \rightarrow M^{+} + e, \quad (8)$$

where M represents C_6H_6, M^{*} the one-photon resonant intermediate, and M^{**} the superexcited state of benzene.

4. Conclusions

We have reported careful quantitative measurements of the distribution of ions resulting from photoionization of benzene with a KrF laser at 248 nm. The fragmentation is extensive, as reported previously by Reilly and Kompa, but our measurements indicate that it occurs at about one-tenth the laser intensity that they reported. Our results are in reasonable agreement with those of Antonov, Letokhov and Shibanov, although their intensities for comparable fragmentation were even lower than ours. We have also reported absolute MPI yields at high laser powers which led us to postulate a neutral superexcited molecular state of benzene. The presence of this superexcited state is thought to be responsible for the depression of the absolute MPI yield with respect to the predicted yield for laser powers exceeding 7.5×10^{6} W/cm^2.

Acknowledgement

We are grateful to H. Helm for his assembling and testing the TOF mass spectrometer. This work was supported by the Defense Advanced Research Projects Agency through Office of Naval Research Contract N000 14-84-C-0718 and by the Army Research Office through Contract DAAG29-83-K-0113.

References

[1] S. Rockwood, J.P. Reilly, K. Hohla and K.L. Kompa, Opt. Commun. 28 (1979) 175.
[2] J.P. Reilly and K.L. Kompa, J. Chem. Phys. 73 (1980) 5468.
[3] V.S. Antonov, V.S. Letokhov and A.N. Shibanov, Appl. Phys. 22 (1980) 293.
[4] C.T. Rettner and J.H. Brophy, Chem. Phys. 56 (1981) 53.
[5] W.B. Martin and R.M. O'Malley, Intern. J. Mass Spectrom Ion Phys. 59 (1984) 277.
[6] W.E. Martin, G.J. Caporaso, W.M. Fawley, D. Prosnitz and A.G. Cole, Phys. Rev. Letters 54 (1985) 685.
[7] W.K. Bischel, L.E. Jusinski, M.N. Spencer and D.J. Eckstrom, J. Opt. Soc. Am. B2 (1985) 877.
[8] N. Bjerre, R. Kachru and H. Helm, Phys. Rev. A31 (1985) 1206.

APPENDIX C

MULTIPHOTON IONIZATION OF VINYLCHLORIDE, TRIFLUOROETHYLENE, AND BENZENE AT 193 nm

Michel J. Rossi and Hanspeter Helm
Chemical Physics Laboratory
SRI International, Menlo Park, CA 94025

ABSTRACT

The multiphoton ionization-fragmentation pattern of vinylchloride, trifluoroethylene and benzene has been measured at 193 nm using time-of-flight mass spectrometry and gas chromatographic analysis. Relative cross sections for multiphoton ionization and the laser power dependence have been determined for the three species at 193 nm at low laser fluence (<10 mJ/cm^2) and relative cross sections for multiphoton ionization of benzene have been obtained at 193 and 248 nm. The dominant fragmentation and ionization channels in the two substituted ethylenes are discussed.

Submitted to JChemPhys
01/23/87
CK85-40

INTRODUCTION

We have recently observed that mixtures of vinylchloride (C_2H_3Cl) with helium and trifluorethylene (C_2F_3H) with helium, both of which exhibit extremely low attachment rates for thermal energy electrons, can be converted into strongly attaching gases following soft irradiation at 193 nm.[1] We attribute this "photo-induced" attachment behavior to the presence of vibrationally excited photodissociation products that are formed from the substituted ethylenes following laser irradiation. In the course of these measurements, we also observed volume ionization in the samples at higher laser powers. We attributed the volume ionization to multiphoton-ionization of vinylchloride (VCl) and trifluorethylene (TFE). The present paper addresses the multiphoton-ionization properties of the two compounds in some detail and compares the cross sections with that of benzene.

The ionization/fragmentation behavior of polyatomic molecules observed in multiphoton ionization may be classified according to two distinctly different excitation modes. In one mode, called nonladder switching by Gedanken and coworkers,[2] the parent ion appears as soon as the molecule has absorbed a sufficient number of photons to reach the molecular ionic ground state. The molecular ion may subsequently absorb additional photons that cause fragmentation. The other mode, ladder-switching,[3] appears in compounds which first photodissociate into neutral molecular fragments that subsequently ionize upon further photon absorption. The mode under which any particular molecule ionizes obviously depends upon wavelength and upon laser power.

Thus, following single-photon excitation to a dissociative electronic state in the molecule, the degree of fragmentation versus ionization depends on the ratio of the rates of dissociation and photoabsorption of the (single photon) excited state.

In the current paper, we investigate the ionization/fragmentation behavior of three molecules, which fall to a varying degree between the two generic modes discussed above. The mass-analyzed ionization yields of vinylchloride (C_2H_3Cl, VCl), trifluoroethylene (C_2F_3H, TFE), and benzene (C_6H_6) were measured on a relative basis at 193 nm at low power. For benzene, relative ionization yields were determined at 193 nm and 248 nm and used together with the previously known absolute cross section of benzene at 248 nm to determine absolute ionization cross sections for the substituted ethylenes at 193 nm. We also attempt to interpret the observed power dependences and specific fragmentation patterns in terms of known molecular excited-state structures. To support these conclusions, we have performed reference experiments on the neutral photodissociation yield and the ion yield at high laser fluence. We find strong differences in the photoionization and fragmentation pattern between VCl and TFE. Particularly noteworthy is the absence of the parent molecular ion of VCl and TFE under soft, unfocused irradiation conditions, a result which may weaken the generic application of MPI for analytical purposes.[4]

EXPERIMENT

The multiphoton ionization experiments were performed using a time-of-flight mass spectrometer which has been described previously.[5,6] The ions are produced with a collimated laser beam in a free jet formed from a 40 μm-diameter tungsten capillary nozzle. They are extracted coaxially to the free jet using a weak electric field and are then accelerated to 2.9 keV. After a flight distance of 160 cm, they are accelerated to between 5 and 5.5 keV before impinging on a secondary electron multiplier (SEM). In benzene, at higher laser powers at 248 nm, it was found necessary to reduce the nozzle stagnation pressure to avoid space charge effects on the ion time-of-flight distributions. No space charge effects were evident in the other gases investigated. Due to the open geometry of the mass spectrometer and the observed independence of the spectra on the magnitude of the extraction field,[7] we are led to assume that all ions formed are effectively collected on the SEM. An unknown, mass-dependent detection efficiency of the SEM is inherent in the spectra. Over the mass range studied here (12 to 82 amu), the SEM efficiency is expected to vary by less than a factor of three.[8] We used an excimer laser operated with standard stable resonator optics. One of four apertures (1.7, 2.5, 3.6, and 4 mm diameter) cut out a circular uniform beam cross section of the excimer laser which was brought to interact with the free jet at right angles. The distance between the edge of the laser beam and the tip of the tungsten nozzle was about one mm. Particular care was exercised to ensure that no photoelectrons created by

the laser beam at apertures contributed to the observed ionization yield. Back-to-back measurements were performed with respect to both the wavelength (193 nm versus 248 nm) and the molecular species (vinlychloride vs. benzene and trifluorethylene versus benzene, respectively) to check the consistency of our results.

The time-of-flight mass spectra were recorded using a transient digitizer. In general signal-to-noise ratios of better than 100:1 were achieved after 10 to 500 laser shots. The ionic species which we discuss here are those which appear in the time-of-flight spectra at levels exceeding typically 1% of the total ionization observed. We found it difficult to quantitatively detect protons due to interference with the early photo electron signal produced at the SEM by scattered excimer photons, but in no case considered here could an H^+ signal have exceeded 5 to 10% of the total ionization. The temporal behavior of the laser pulse was measured with a fast photodiode by photographically recording the oscilloscope trace. The pulse energy of the collimated beam was measured with an accuracy of 5% using a commercial power meter. The dependence of the ionization signal on the laser power was studied by attenuating the beam with up to 12 Suprasil quartz windows of 1/8" thickness. Benzene (Baker) and TFE (PCR, stabilized with .5% limonene) were used pure, whereas VCl was introduced into the vacuum system as a 2% mixture in He (Matheson Gas Products). GCMS analysis of the TFE sample revealed dipentene ($C_{10}H_{16}$) as the dominant impurity (1%). Two heavier unidentified hydrocarbons were detected in the VCl sample at a level <1% relative to VCl.

EXPERIMENTAL RESULTS

A. Mass Spectra and Pathways at 193 nm

We tested our experimental setup by studying photoionization in benzene. With the unfocused laser, the mass spectrum of benzene at 193 nm consisted exclusively of a weak signal from the parent molecular ion (m/e = 78). If at the same pulse energies (typically 8 mJ/cm^2 corresponding to $1MW/cm^2$) a short focal length lens (25 cm) was used, the signal strength increased dramatically, and significant fragmentation was observed, the dominant fragments appearing at mass 39 and mass 12. This observation is consistent with previous studies which were carried out at 193 nm.[9]

Vinylchloride

When vinylchloride (VCl) was irradiated with the unfocused 193-nm laser beam, no signal from the parent molecular ion (m/e = 62 and 64) was detectable. Ions at m/e = 36 and 38, corresponding to HCl^+, were the only observable ionization products. This result may be compared with the 70 eV electron impact ionization mass spectrum,[10] where HCl^+ constitutes less than 1% of the total ionization and where the parent ion amounts to 40% of the total ion yield. Under focused beam irradiation, increased fragmentation was observed, but again, no mass corresponding to the parent ion appeared. Typical MPI mass spectra for VCl are presented in Figure 1a and 1b. It should be noted that in both the focused and unfocused case, the appearance of $^{37}Cl:^{35}Cl$ is reproducibly different from the natural isotopic abundance

(32:100).[11] This difference appears in both the atomic ion (62±5:100) as well as in the HCl^+ yield (42±5:100).

In order to help interpret the photoionization mass spectra, we studied the nature of one-photon photodissociation of vinylchoride gas[12] at 193 nm in a static VCl sample using gas chromatographic analysis of the neutral products. The sample was typically 1 to 2 Torr of VCl in 500 Torr of helium. It was irradiated at 1 mJ/cm^2 at 193 nm for 10 to 100 laser shots (unfocused) and the photodissociation products, C_2H_2 and C_4H_6, were observed. These neutral products are considered to be formed in the strongly exothermic photodissociation reactions,

$$C_2H_3Cl \xrightarrow[193\ nm]{h\nu} C_2H_2^{\ddagger} + HCl^{\ddagger} + \leq 5.4\ eV \qquad (1)$$

and

$$C_2H_3Cl \xrightarrow[193\ nm]{h\nu} C_2H_3^{\ddagger} + Cl + \leq 3.7\ eV \qquad (2)$$

The C_4H_6 molecules observed by gas chromatography are considered to be recombination products of C_2H_3, which is formed in reaction (2). Our GC analysis showed a branching ratio for reaction (1) and (2) of 86:14. This value can be corrected for the recombination (reverse of reaction 2) to give a value of 67:33, a value that should be representative for the mechanisms active in the free jet. This ratio may be compared with previous measurements for the relative yields for HCl vs Cl elimination of 65:35,[12] 47:53,[13] and 42:58.[14]

As we will discuss in detail later, we attribute the dominant ionization pathway in VCl under unfocused conditions to reaction (1), followed by

two-photon ionization of the vibrationally excited HCl product.

$$HCl^{\ddagger} \xrightarrow[193\ nm]{2h\nu} HCl^{+} + e \qquad (3)$$

In order to investigate the role of internal excitation of HCl in reaction (3), we performed a reference experiment in which a 2% HCl in helium mixture was expanded through the jet and irradiated at 193 nm. No ions were detected in this experiment, even under focused conditions. We therefore conclude that HCl in reaction (1) is formed in vibrationally excited levels, and we will show in the discussion section how vibrational excitation may enhance the two-photon ionization cross section of HCl.

The appearance of atomic chlorine ions under focused conditions is attributed to photodissociation of HCl^{+} ions

$$HCl^{+} \xrightarrow[193\ nm]{h\nu} H + Cl^{+} \qquad (4)$$

Two low abundance species appear in the spectrum under focused conditions which cannot be direct ionization products of VCl. They appear at mass 28 and 29 and are tentatively identified as $C_2H_4^{+}$ and $C_2H_5^{+}$. Their origin may lie with the impurities in the vinylchloride sample stated above.

Trifluoroethylene

Mass spectra observed for C_2F_3H (TFE) upon 193 nm excitation are presented in Figure 2a and 2b. For TFE only two ion species are detectable under unfocused conditions, CHF^{+} and CF^{+}. Likewise, the multiphoton ionization mass spectrum is different from that obtained in 70 eV electron impact ionization,[10] where the parent ion constitutes 26%, CF^{+} 17%, and CHF^{+} 6% of the total ionization.

Also for TFE reference experiments using GCMS analysis of static samples (10 Torr in 500 Torr He) irradiated at typically 1 mJ/cm^2 for 10 to 100 laser shots were performed. The sole reaction products detected in the samples by GC were C_2F_4 and $C_2H_2F_2$. The two species are regarded to be the recombination products of CF_2 and CHF, both of which are formed in the photodissociation step:

$$C_2F_3H \xrightarrow[193\ nm]{h\nu} CHF^{\ddagger} + CF_2^{\ddagger} \qquad (5)$$

On the basis of the findings of Sirkin and Pimentel[15] in 1,2-difluoroethylene, we expect that in addition to reaction (5) the photodissociation process is also active:

$$C_2F_3H \xrightarrow[193\ nm]{h\nu} C_2F_2^{\ddagger} + HF^{\ddagger} \qquad (6)$$

The absence of either the C_2F_2 and HF products in our GC analysis is attributed to the difficulty in sampling these species by gas chromatography.

The ionic products observed under unfocused conditions may then be due to two-photon ionization of the CHF product from reaction (5):

$$CHF^{\ddagger} \xrightarrow[193\ nm]{2h\nu} CHF^{+} + e \qquad (7)$$

and to two-photon ionization of the C_2F_2 product from reaction (6):

$$C_2F_2^{\ddagger} \xrightarrow[193\ nm]{2h\nu} CF^{+} + CF \qquad (8)$$

Additional pathways to CF^+ can arise from photodissociation of CHF^+:

$$CHF^{+} \xrightarrow[193\ nm]{h\nu} CF^{+} + H \qquad (9)$$

and the dissociative ionization of $CHF^{\ddagger}$:

$$CHF^{\ddagger} \xrightarrow[193\ nm]{2h\nu} CF^{+} + H \qquad (10)$$

A striking difference is observed for the formation of CHF^{+} and CF^{+} in the time-of-flight spectra of these ions. Under unfocused conditions, the mass spectra for CHF^{+} reveal significant kinetic energy release as evidenced by the width of the arrival time peak (see Figure 3). By contrast, no such broadening is observed for mass 31 (CF^{+}). Since the broadening of the arrival time peak is near symmetric with respect to the expected arrival time, we conclude that $CHF^{\ddagger}$ is produced with excess kinetic energy in reaction (5). If this ion were the product of a unimolecular decomposition or photodissociation reaction of a larger molecular ion, an asymmetric arrival time profile with a trailing edge should result.

Under focused conditions, the CHF^{+} contribution to the total ionization yield vanishes (less than one percent for the conditions in Figure 2b), and only a minor amount of the CF^{+} signal (<5%) appears with a broadened arrival time spectrum. We must therefore conclude that upon stronger irradiation, the reaction channel to CHF^{+} (reactions 5 and 7) is bypassed in favor of other channels, leaving behind an only small amount of CHF^{+} which may be further fragmented to CF^{+} in reaction (9) following additional photoabsorption.

As in the case of VCl, the rate of decay of the single-photon excited state of the parent molecule must be faster than the rate of optical pumping of this state thus precluding the formation of parent molecular ions under weak irradiation. However, in contrast to VCl, a small amount of the parent molecular ion was observed in TFE under focused conditions. The focussing of the laser for the conditions given in Figure 2b represents roughly a flux

increase by a factor of 200 over that used in Figure 2a (pulse duration ~ 8 ns). An upper limit of the lifetime of the one-photon excited state of TFE may therefore roughly be estimated to lie in the nanosecond range. Under focused conditions, a small amount of C_2HF^+ (m/e = 44), comparable to that of the parent ion appears (see Figure 2b). This ion may originate from the same neutral precursor $C_2HF_3^*$ from which ionization to the parent molecular ion takes place.

B. Formal Intensity Laws

The laser power dependence of the ion signal reveals a lower limit to the number of photons n, required to form that particular ion. Typical experimental results of the laser power dependence of the dominant ion signals for benzene, VCl and TFE obtained by attenuating the unfocused laser beam are displayed in Figure 4. Over the one order-of-magnitude change in laser power, the log-log plots assume a linear form within experimental error. The numbers quoted in Table 1 were derived from a linear least-squares treatment of the logarithmic data. For benzene, a value near n = 2 is observed as has been found at 248 nm when the parent ion at m/e = 78 is monitored.[6]

For both VCl and TFE, n has been found to be 3 within experimental error. As indicated in the previous section, the third-order process can be interpreted in terms of a short-lived one-photon-excited intermediate which dissociates in reactions (1), (2), (5), and (6). The primary photoions then arise from two-photon ionization of the hot photoproducts $HCl^‡$ for VCl, $CHF^‡$ and $C_2F_2^‡$ for TFE.

In our previous drift-tube experiment[1] with VCl, we investigated the power dependence of the volume photoionization yield (total charge) at a pressure of 500 Torr of He. The power range was identical to the present experiments and a formal intensity law of $n = 2.9 \pm 0.1$ was found.

C. Relative Ionization Cross Sections of VCl and TFE

Table 1 also presents our results for the relative ionization cross sections of VCl and TFE when measured against benzene. The relative cross sections were obtained from the relative ionization yields, normalized to the same nozzle stagnation pressure. The pressure was varied over a range of typically a factor of five in each gas, and no systematic pressure dependence was observed. The error bars given represent the absolute range of variation of 28 pairs of measurement. Due to the fact that the formal intensity law in VCl and TFE was different from that of benzene, the cross section ratios $\sigma_{benzene}/\sigma_x$ are given in units of mJ/cm^2, and they are therefore dependent on laser fluence or power density. An interesting fact is that for VCl at 193 nm, the magnitude of the cross section renders 3-photon ionization competitive with the 2-photon ionization of benzene at powers of 5 mJ/cm^2.

D. Absolute Ionization Cross Sections

To obtain absolute MPI cross sections for VCl and TFE at 193 nm, we measured the relative ionization cross sections for benzene at 193 and 248 nm and calibrated the relative cross sections from Table 1 against the absolute MPI cross section for benzene which has been reported at 248 nm.[16] Table 2 presents our results for benzene in terms of the ionization yield

ratio, which is defined as the intensity of the ion signals in benzene (m/e = 78) measured at 248 and 193 nm. This ratio corresponds to a relative efficiency for ionization, and only for the special case of equal temporal laser profiles at both wavelengths may the ratio be identified with a relative cross section.

Table 2 gives the results from two sets of data for which the pulse duration and the pulse shapes at both wavelengths are equal to within the experimental uncertainty in the measurement. The pulse shapes and lengths depend upon the age of the excimer gas filling, fresh samples giving the longest pulse durations. The two data sets, and the associated error bars in Table 2 represent averages obtained at four different pressures and at four different laser beam diameters. It can be noted that the ratio varies with the absolute duration of the laser pulse. The trend is towards higher values of the ratio with increasing pulse width. Bischel et al.[16] have reported that for benzene the ionization cross section at 248 nm is invariant to changes in pulse duration. The observed increase of the ratio may therefore be attributed to a decrease in the cross section of benzene at 193 nm with increasing pulse length at constant fluence.

The relative cross sections given in Table 1 for VCl and TFE were all obtained for pulse lengths of typically 7 to 8 ns. We therefore use the benzene cross section ratio 28 ± 6 (see Table 2) to obtain absolute cross sections for benzene, VCl and TFE at 193 nm. The results are given in Table 3 in terms of the ionization yield coefficient. The coefficient, C, is defined as $N_+/N_o = CF^n$ where N_+ and N_o are the ion density and the neutral gas density, respectively, F is the laser fluence (mJ/cm^2), and n the integer power density exponent observed. It is difficult to quote the absolute

error of these data. Among the error sources not explored explicitly is an uncertainty introduced through the possibly different spatial extent of the free jet diameter in the various gases, and hence the laser beam-molecular beam overlap. Since the relative cross sections were found independent of the laser beam diameter, this error is likely to fall within the error brackets given in Tables 1 and 2. A second error source not considered explicitly is the absolute detection efficiency of the SEM for various ions. Disregarding the uncertainty in the absolute cross section of benzene[16] at 248 nm, we quote in Table 3 the added uncertainties for the benzene cross-section ratio at 193 and 248 nm (Table 2) and the relative cross sections at 193 nm (Table 1).

DISCUSSION

The photoexcitation of chloroethylenes in the UV has been studied extensively in the past. Among the more recent and pertinent studies are the measurements of the kinetic energy release in chloroethylene fragmentation upon 193 nm photolysis by Umemoto et al.,[13] the VUV and UV emission studies of chlorine containing compounds upon 193 nm irradiation by Kenner et al.[17] and the FTIR emission study of VCl excited at 193 nm by Donaldson and Leone.[18] According to Umemoto et al.,[13] the two primary pathways of the photofragmentation at 193 nm are as follows: Cl· atom ejection (reaction 2) occurs by internal conversion to a predissociating $^1(\pi\pi^*)$ state, which releases the Cl· atom with high kinetic energy, whereas the molecular elimination (reaction (1)) occurs by internal conversion through an electronically excited $^1(\pi\pi^*)$ state (lowest singlet state in VCl) and on to high lying vibrational states of the electronic ground state, from which HCl is eliminated. The kinetic energy distribution in the molecular elimination pathway shows a broad maximum at 15 kcal/mol and suggests a similar distribution in the remaining degrees of freedom, namely rotation and vibration of both photofragments. This conclusion[13] is nicely supported by the results of Donaldson and Leone[18] who show a broad distribution of vibrationally excited HCl upon 193 nm photolysis of VCl. They specifically measured the emission from HCl v = 1-4 states, but their vibrational population distribution suggests significant population in higher vibrational levels.

UV and VUV emission spectra of Cl-containing molecules,[17] which were irradiated by unfocused 193-nm laser light indicate the importance of photodissociation and subsequent electronic excitation of the photofragment molecules in a multiphoton excitation process. Kenner et al.[17] could specifically rule out a non-ladder switching mechanism in the case of the 193-nm photolysis of $CHCl_3$ and CH_2Cl_2, which results in 230-nm emission from HCl ($B^1\Sigma^+$) following single-photon absorption from highly vibrationally excited states of the ground potential energy surface of HCl ($X^1\Sigma^+$). This mechanism of HCl excitation is similar to our 3-photon ionization scheme of VCl discussed below.

To our knowledge, no previous measurements on the multiphoton ionization of TFE and VCl have been published. It may be noted from Table 1 that at 193 nm, the multiphoton ionization cross section for TFE, is a factor of 10 lower than that of VCl. This may not be surprising in view of the fact that at 193 nm the single-photon absorption cross section for TFE is a factor of 7 lower than that of VCl. Our experiments show that the parent ion is absent from the mass spectra in both gases under weak irradiation conditions. Since the three-photon ionization cross sections, which we measured for the two gases, follow the magnitude of their single-photon absorption cross sections (factor of ten versus a factor of seven), this implies that the efficiency of two-photon ionization of photodissociation products formed from both gases following single-photon absorption are comparable. Yet, the final ionic products which appear in the two substituted ethylenes are greatly different. In the following, we attempt to interpret the observed differences in the multiphoton ionization process.

Multiphoton Ionization of Vinylchloride

The primary observables in VCl at low laser power are the single-photon photodissociation pathways (1) and (2) and the formation of HCl^+ in a three-photon process. Since the experiments of Umemoto,[13] Donaldson and Leone,[18] and Kenner et al.[17] prove that HCl is formed with considerable internal excitation in 193 nm photolysis. we first consider the role of vibrational excitation of HCl in a multiphoton ionization process.

In Figure 5, we show a potential energy diagram for HCl.[19] The ionization potential of HCl (12.748 eV)[19] is less than the combined energy of two ArF laser photons (12.85 eV). Consequently two-photon ionization of HCl with ArF laser light is energetically allowed. However, we observed also that ground-state HCl does not multiphoton-ionize at 193 nm, even under focused conditions. The explanation may be with the resonantly-excited intermediate HCl $A^1\Pi$ state, which is reached with one ArF photon (see Figure 5) when exciting from the ground-vibrational level of HCl with 193 nm. The repulsive A state as intermediate in the two-photon event will have a lifetime too short (10^{-13} s) to allow efficient absorption of a second photon within the same laser pulse. The situation does however change drastically if HCl is vibrationally excited. In Figure 5 we have drawn a second pair of arrows representing two-photon absorption at 193 nm from a high vibrational level of the HCl ground state ($v'' = 8$ in Figure 5). At large internuclear distances, this absorption step bypasses the dissociative channel and will become near-resonant with either the $C^1\Pi$ or $V^1\Sigma^+$ excited states of HCl as intermediate. In particular, the transition moment to the ionic V state will be very large.[20] We note that vibrational excitation as high as $v = 10$ in reaction (1) requires less than 50% of the excess energy available in this

photodissociation process. We therefore conclude that vibrational excitation of the HCl product of reaction (1) is a most important aspect for the efficient multiphoton ionization of VCl.

The observation of HCl^+ as the dominant ion formed from VCl under unfocused conditions has to be contrasted with the lack of formation of HF^+ from TFE. The very much higher ionization potential of HF (16.04 eV) would require that as much as 3.23 eV of vibrational energy be concentrated in the photodissociation product HF to render two-photon ionization energetically allowed. This value has to be set in relation to the excess energy available in the photodissociation step (6), 3.9 ± 0.65 eV. It appears highly unlikely that almost the full excess energy be concentrated in a single degree of freedom of one of the dissociation products.

Our reference experiment, which showed that ground-state HCl does not multiphoton-ionize easily at 193 nm, may also be used to help explain the ionization/fragmentation pattern in VCl at higher laser fluence. The appearance of Cl^+ ions in VCl under focused conditions could be attributed to reaction (4), or three-photon ionization of atomic chlorine formed in reaction (2). Both steps require four photons altogether, and this is consistent with the appearance of this ion at only higher laser fluence. However, in our reference experiment in pure HCl, where we expect the formation of atomic chlorine following photodissociation via the $A^1\Pi$ state, no ionization pathway to Cl^+ was observed. We therefore rule out a significant contribution from three-photon ionization of atomic chlorine generated by single-photon dissociation of VCl in reaction (2).

The first dissociation limit[19] in HCl^+ lies only 4.65 eV above the vibrational ground state of the molecular ion and leads to $H(^2S) + Cl^+(^3P)$.

Above this limit, no spectroscopic observations have been reported, but predissociation is predicted[21] to occur for bound states above this limit through a repulsive $^4\Pi$ state. The second dissociation limit[19] for HCl^+, H^+ + $Cl(^2P)$ is reached at 5.23 eV above the ground state of the molecular ion. Hence both the Cl^+ and the H^+ limits are within reach of one ArF laser photon from ground-state HCl^+. We therefore conclude that reaction (4) is the dominant channel for the formation of atomic chlorine ions. We note that a predissociation process leading to the formation of Cl^+ may also explain the observed deviation from the natural isotopic abundance. We mention also that a three-photon ionization scheme to Cl^+ is energetically possible if reaction (1) formed $HCl^{\ddagger}$ with vibrational excitation higher than 4.55 eV (the exothermicity of reaction (1) being 5.4 eV). For such high vibrational excitation, two ArF photons can reach above the H + Cl^+ dissociation limit. However, this sequence cannot explain our observation that the Cl^+ formation is enhanced by focusing the laser, and we consider this path as unimportant.

We conclude that the dominant ionization pathway in VCl at 193 nm is single-photon photodissociation into vibrationally excited HCl, followed by near-resonant two-photon ionization to HCl^+, which at higher fluence is further fragmented by photodissociation into H + Cl^+.

Multiphoton Ionization of Trifluoroethylene

A completely different ionization pattern is observed in TFE. We explained above why HF^+ is not expected to be a dominant ion in TFE. Here, we attempt to explain the observed ionization/fragmentation channels. The arrival time spectra of the two ions (see Figure 3) reveal that, owing to the difference in translational energy content of the two species, only a very small amount (< 5%) of CF^+ can be a daughter ion of CHF^+ from reaction (9).

The ionization potential of ground-state CHF is not known, but is likely to be within 0.5 eV of the ionization potential of CF_2 which is 11.8 eV.[22] We therefore expect that two-photon ionization of CHF in reaction (7) is energetically allowed. The excess kinetic energy observed for CHF^+ ions must then be attributed to excess energy imparted to the products of the photodissociation, step (5). The carbon double bond energy in TFE is less than 3.0 eV. Since the excitation energy at 193 nm is 6.4 eV, it is plausible that some excess energy appears in the form of translational motion of the products. This would imply the presence of an exit-channel barrier for reaction (5). Evidence for such a barrier is the kinetic stability of CF_2 with respect to recombination in the gas phase.

If we assume that (5), followed by reaction (7), is a dominant channel leading to CHF^+, we have to explain the absence of CF_2^+ from the mass spectra: the dissociation energy D(FC-F) is 5.2 eV and predissociation has been observed[23] in the $\tilde{A} \leftarrow \tilde{X}$ transition of CF_2 at photon energies above 41680 cm^{-1}. If the dissociative excitation region of the $\tilde{A}$ state (or some other electronic state) extends to 51813 cm^{-1} (193 nm), then predissociation of one-photon-excited CF_2 formed in reaction (5) may dominate over two-photon ionization. This may explain the absence of CF_2^+. Ionization of the photodissociation products of CF_2, CF and F, would require two and three additional ArF photons, respectively. Such an ionization path to CF^+ is therefore less likely than the sequence via reactions (6) and (8), which involves a total of only three ArF photons. The translational energy content for the fragments observed from reaction (5) also rules out reaction (10) as a dominant channel for producing CF^+ for which no translational broadening is observed (see Figure 3). We therefore conclude that reactions (6) and (8)

are responsible for the formation of CF^+ under unfocused conditions, while CHF^+ arises from the reactions (5) and (7).

The reader may at this point wonder why then the acetylene product from VCl in reaction (1) does not follow a similar ionization path as does the C_2F_2 product from reaction (6). A possible explanation is again predissociation: for acetylene, diffuse absorption bands are known[23] in the wavelength region between 155 and 200 nm. These energies are high enough to break the $H-C_2H$ bond, and this process may dominate over the two-photon ionization of C_2H_2 which has an ionization potential of 11.41 eV.[22]

Multiphoton Ionization of Benzene

The multiphoton ionization pattern of benzene at 193 and 248 nm has been discussed in detail by Reilly and Kompa.[9] A new result, which we can add to their conclusions, is the observation that the ionization yield at 193 nm does depend on the pulse length. This is consistent with their estimate of the lifetime of the one-photon excited intermediate at this wavelength of 55 ps. Since this lifetime is short compared to the duration of the laser pulses (7.5 and 12 ns), a linear relationship between ionization efficiency and pulse length should be expected. Indeed, we observe an increase by a factor of 1.5 in ionization efficiency for a decrease in pulse length by a factor of 1.6 (see Table 2). A second result for benzene is that its two-photon ionization cross sections at 193 nm is about a factor of thirty to forty lower than that at 248 nm. In this context, it is interesting to note that Otis, Knee and Johnson[24] reported recently that the ArF laser does not produce any ionization of benzene in a pulsed supersonic molecular beam.

CONCLUSIONS

We have demonstrated that mass-analyzed photoionization yields from a crossed laser-molecular beam experiment can be used to obtain absolute cross sections for multiphoton ionization of vinylchloride and trifluoroethylene by normalizing the results against a standard of known cross section, in the case here against benzene.

We have also made an attempt to identify the observed ionization pathways. The interpretation is based on neutral photodissociation data that were known previously and on data that we obtained by gas chromatography and spectroscopic and thermochemical information known for the species involved.

Our interpretation of the individual photoionization pathways under unfocused conditions rests on the assumption that ionization follows the one-photon photodissociation of the parent molecule. While this picture is consistent with our observations, we have to keep in mind that two-photon excited states of the parent molecule may also contibute to the ionization path, and their relative importance will increase with laser fluence. No information on such states is currently available, and their importance in multiphoton ionization cannot be estimated at present. A hint that two-photon excited states of the parent can play a role is our observation that under increasing laser fluence, the ionization channel to CHF^+, which originates in a one-photon photodissociation process of TFE, is bypassed in favor of other channels with less fragmentation.

ACKNOWLEDGEMENTS:

This research was supported by the U.S. Army Research Office under contract number DAAG 29-83-K-0113.

REFERENCES

1. M. J. Rossi, H. Helm, and D. C. Lorents, Appl. Phys. Lett. 47, 576 (1985).

2. A. Gedanken, M. B. Robin, and N. A. Kuebler, J. Phys. Chem., 86, 4096 (1982).

3. St. W. Stiller and H. V. Johnston, J. Phys. Chem., 89, 2717 (1985).

4. S. H. Liu, Y. Fujimura, H. J. Neusser and E. W. Schlag (eds.), Academic Press, Multiphoton Spectroscopy of Molecules, chapter 7.1, 198 (1984).

5. N. Bjerre, R. Kachru, and H. Helm, Phys. Rev. A 31 1206 (1985), and Proceedings Int. Conf. Lasers '84. (STS Press, McLean, 1985) page 322.

6. M. J. Rossi and D. J. Eckstrom, Chem. Phys. Lett., 120, 118 (1985).

7. K. Stephan, H. Helm, and T. D. Mark, J. Chem. Phys. 73, 3763 (1980).

8. Assuming a linear dependence of the detection efficiency on velocity, (H. Helm, unpublished).

9. J. P. Reilly and K. L. Kompa, J. Chem. Phys., 73, 5468 (1980).

10. 70 eV electon impact spectra from EPA/NIH Mass Spectral Data Base.

11. CRC Handbook of Chemistry and Physics 57th Edition, The Chemical Rubber Company.

12. H. Okabe, Photochemistry of Small Molecules, John Wiley, New York 1978.

12. M. J. Berry, J. Chem. Phys., 61, 3114 (1974).

13. M. Umemoto, K. Seki, H. Shinohara, U. Nagashima, N. Nishi, M. Kinoshita, and R. Shimada, J. Chem. Phys., 83, 1657 (1985).

14. T. Fujimoto, A. M. Rennert, and M.H.J. Wijnen, Ber. Bunsenges. Phys. Chem., 74, 282 (1970).

14. C. E. Otis, J. L. Knee, and P. M. Johnson, J. Chem Phys. 78, 2091 (1983).

15. E. R. Sirkin and G. C. Pimentel, J. Chem. Phys. 75(2), 604 (1981).

16. W. K. Bischel, L. E. Jusinski, M. N. Spencer, and D. J. Eckstrom, J. Opt. Soc. Am., B2, 877 (1985).

17. R. D. Kenner, H. K. Haak, and F. Stuhl, J. Chem. Phys., 85, 1915 (1986).

18. D. J. Donaldson and St. R. Leon, manuscript submitted for publication.

19. K. P. Huber and G. Herzberg, Constants of Diatomic Molecules, Van Nostrand Reinhold, New York (1979).

20. D. L. Huestis, private communication.

21. J. Raftery and W. G. Richards, J. Phys. B. 6, 1301 (1973).

22. H. M. Rosenstock, K. Draxl, B. W. Steiner, and J. T. Herron, J. Phys. Chem. Ref. Data, 6, Supplement Number 1, (1971).

23. G. Herzberg, Electronic Spectra of Polyatomic Molecules, Van Nostrand Reinhold, New York (1966).

Table 1

FORMAL INTENSITY LAW EXPONENTS AND RELATIVE IONIZATION CROSS SECTIONS FOR MULTIPHOTON IONIZATION at 193 nm OBTAINED IN THE UNFOCUSED CASE

Parent Gas	Observed Ion	Exponent	$\sigma_x^3/\sigma_{Benzene}^3$ [a] (mJ^3/cm^2)
Benzene (C_6H_6)	m/e = 78	1.86 ± 0.1	---
Vinylchloride (C_2H_3Cl)	m/e = 36	3.1 ± 0.3	
	m/e = 38	3.0 ± 0.2	4.9 ± 1.0
Trifluoroethylene (C_2F_3H)	m/e = 31	3.1 ± 0.3	490 ± 60

[a] x corresponds to vinylchloride and trifluoroethylene, respectively.

Table 2

RELATIVE TWO-PHOTON IONIZATION CROSS SECTIONS
FOR BENZENE AT 248 AND 193 nm

(The error bars represent absolute nonsystematic variations over energy densities of 4 to 36 mJ/cm^2 at 248 nm and 5 to 10 mJ/cm^2 at 193 nm, and laser beam diameter between 1.7 and 4 mm).

Pulse Length 248 nm (ns)	Pulse Length 193 nm (ns)	Ionization Yield Ratio (248:193 nm)
6.5 ± 1	7.5 ± 1	28 ± 6
12.5 ± 1	12.0 ± 1	43 ± 8

Table 3

ABSOLUTE IONIZATION YIELDS, APPLICABLE FOR AN EXCIMER LASER PULSE LENGTH OF ~ 7 ns AT LOW FLUENCE (< 10 mJ/cm^2)

Parent Gas	Observed Ion	Wavelength (nm)	Ionization Yield
Benzene	n.a.[a]	248	1.1 (-6) cm^4/mJ^2
	$C_6H_6^+$	193	4 ± 1 (-8) cm^4/mJ^2
Vinylchloride	HCl^+	193	8 ± 4 (-9) cm^6/mJ^3
Trifluorethylene	CF^+	193	8 ± 3 (-11) cm^6/mJ^3

[a]Total ionization experiment, Reference 13.

FIGURE CAPTIONS

Figure 1 Bar representation of mass spectra of ions observed for vinylchloride at 9 mJ/cm^2. For the focused case a 36 cm focal length lens was used at the same pulse energy.

Figure 2 Bar representation of mass spectra of ions observed for trifluorethylene at 9 mJ/cm^2. For the focused case, the fluence is 6 mJ/cm^2 before the 36-cm focal length lens.

Figure 3 Arrival time spectra of CF^+ and CHF^+ formed at 193 nm from trifluoroethylene (conditions as in Figure 2).

Figure 4 Power dependence of the ionization yield. (a) benzene at 193 nm (unfocused beam), (b) vinylchloride at 193 nm (unfocused beam, full triangles: mass 38, open squares; mass 36: the signal for mass 36 has been multiplied by a factor of two), (c) trifluoroethylene at 193 nm (unfocused beam; the symbols indicate runs at different pressure. The CF^+ signal has been normalized to the TFE stagnation pressure).

Figure 5 Potential energy diagram for HCl, drawn according to the spectroscopic data given in Reference 19.

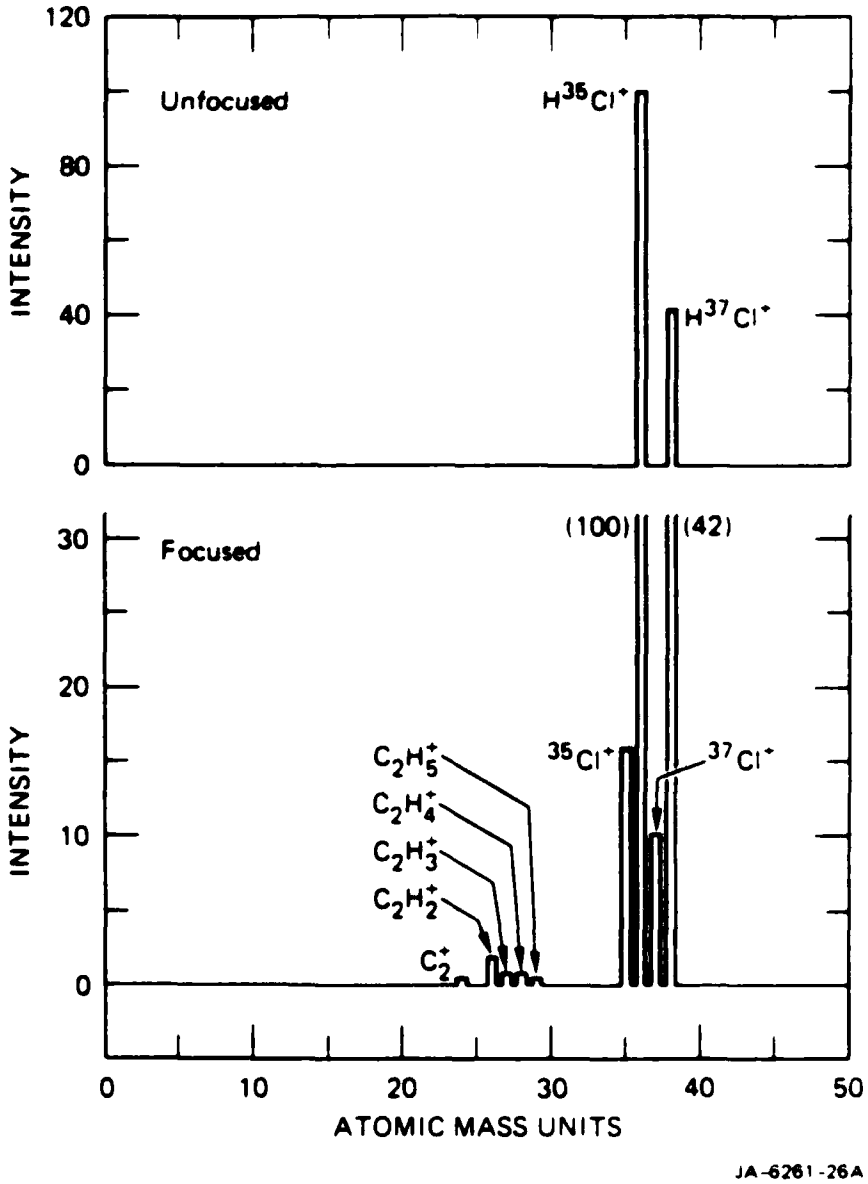
Unfocused
$H^{35}Cl^+$
$H^{37}Cl^+$
INTENSITY
120
80
40
0
Focused
(100)
(42)
$C_2H_5^+$
$C_2H_4^+$
$C_2H_3^+$
$C_2H_2^+$
C_2^+
$^{35}Cl^+$
$^{37}Cl^+$
INTENSITY
30
20
10
0
0
10
20
30
40
50
ATOMIC MASS UNITS
JA-6261-26A

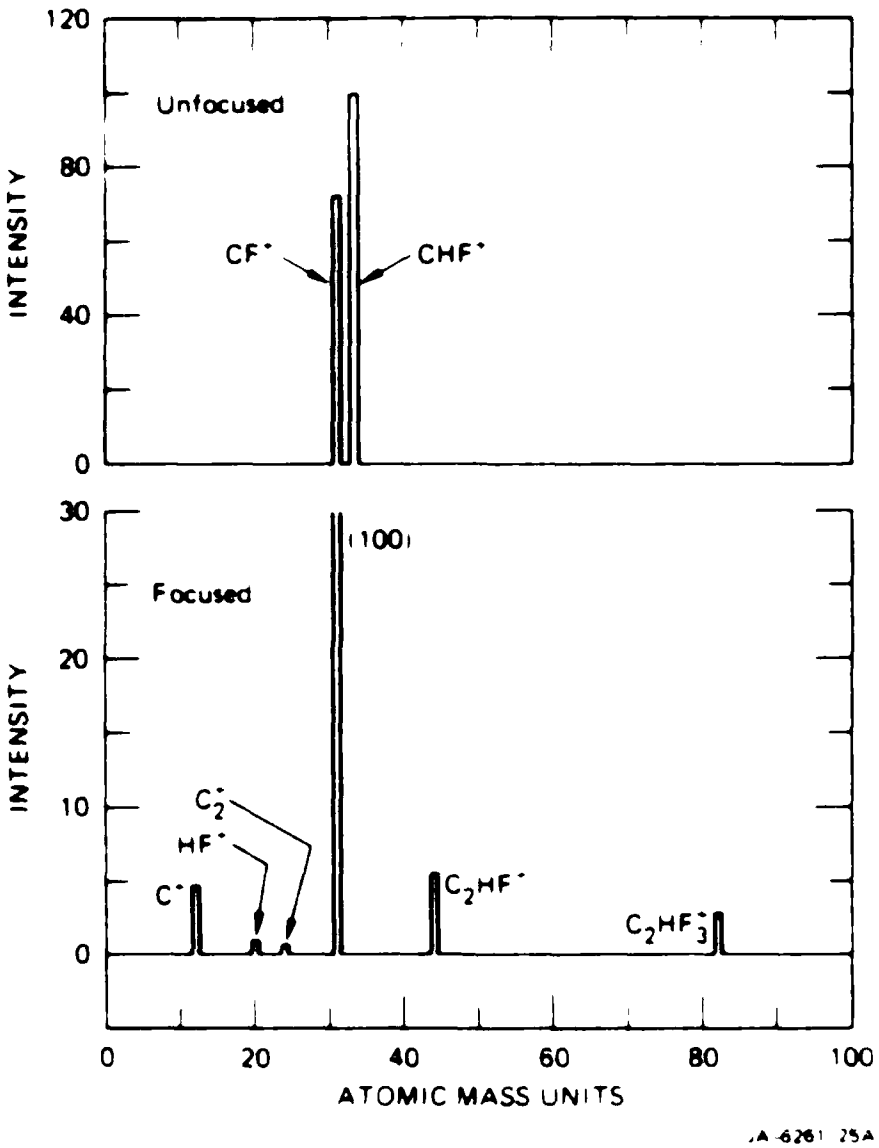
120
80
40
0
INTENSITY
Unfocused
CF⁺
CHF⁺
30
20
10
0
INTENSITY
Focused
(100)
C₂⁺
HF⁺
C⁺
C₂HF⁺
C₂HF₃⁺
0
20
40
60
80
100
ATOMIC MASS UNITS

A-6261 25A

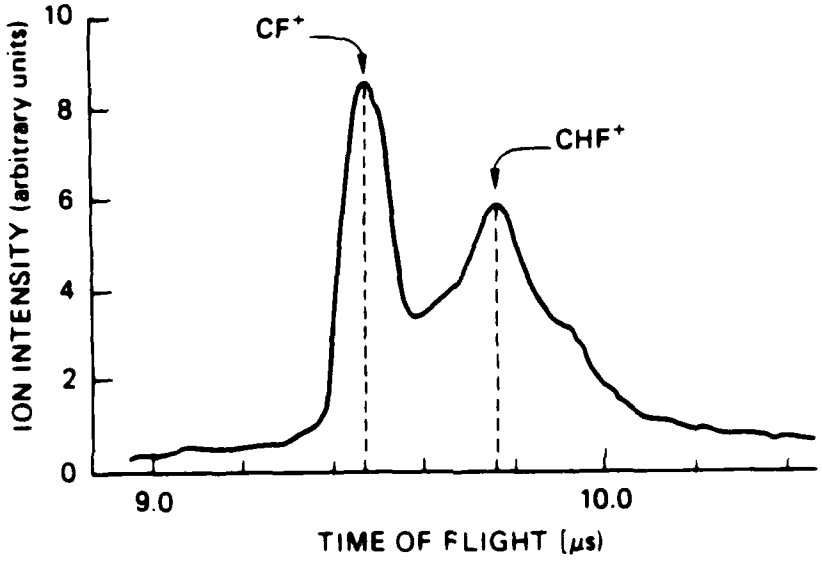
ION INTENSITY (arbitrary units)
10
8
6
4
2
0
CF+
CHF+
9.0
10.0
TIME OF FLIGHT (μs)

JA-6261-30

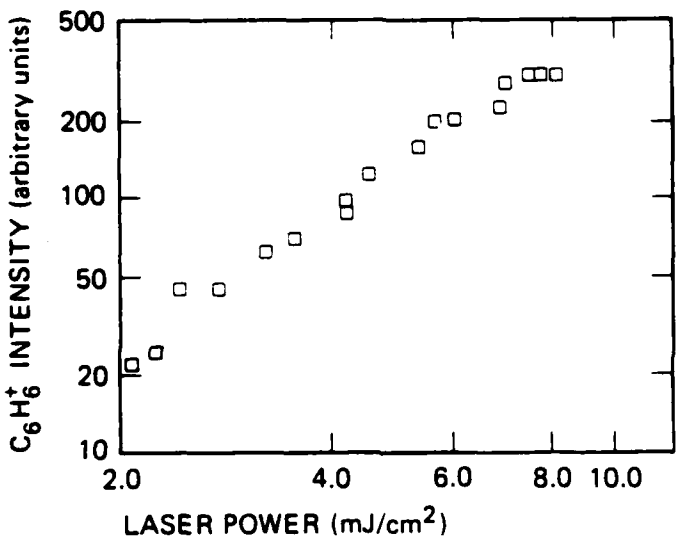
500
200
100
50
20
10
$C_6H_6^+$ INTENSITY (arbitrary units)
2.0
4.0
6.0
8.0
10.0
LASER POWER (mJ/cm^2)

JA-6261-27

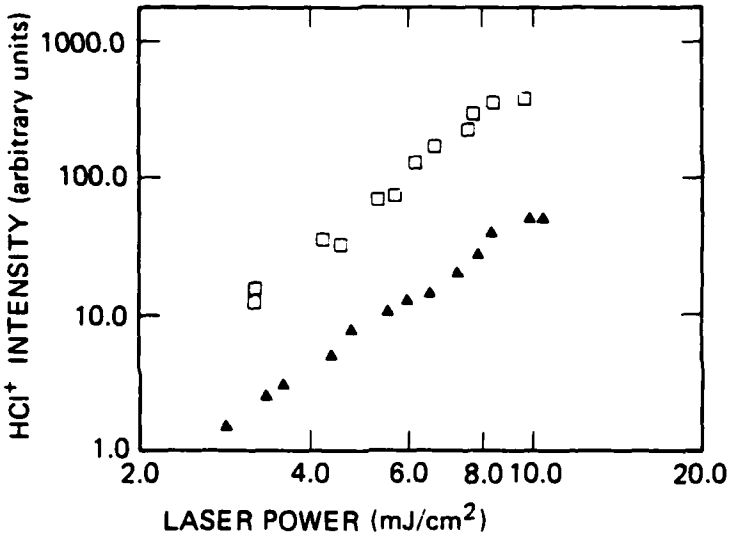
HCl+ INTENSITY (arbitrary units)
1000.0
100.0
10.0
1.0
2.0
4.0
6.0
8.0
10.0
20.0
LASER POWER (mJ/cm2)

JA-6261-28A

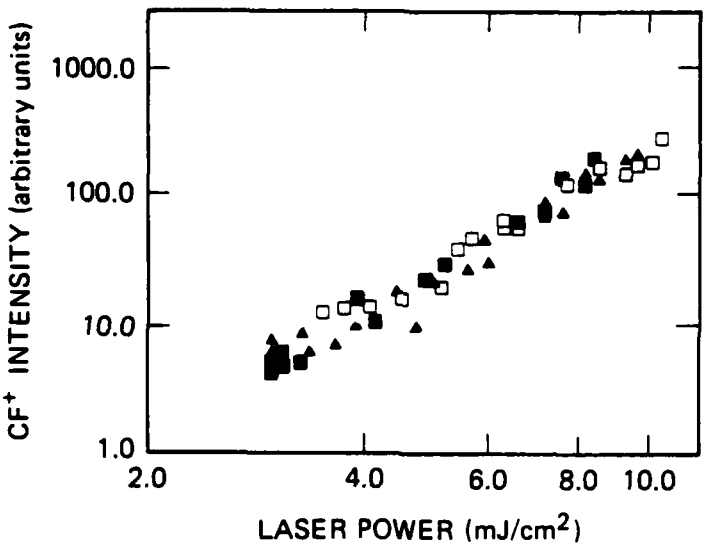
CF+ INTENSITY (arbitrary units)
1000.0
100.0
10.0
1.0
2.0
4.0
6.0
8.0
10.0
LASER POWER (mJ/cm2)

JA-6261-29

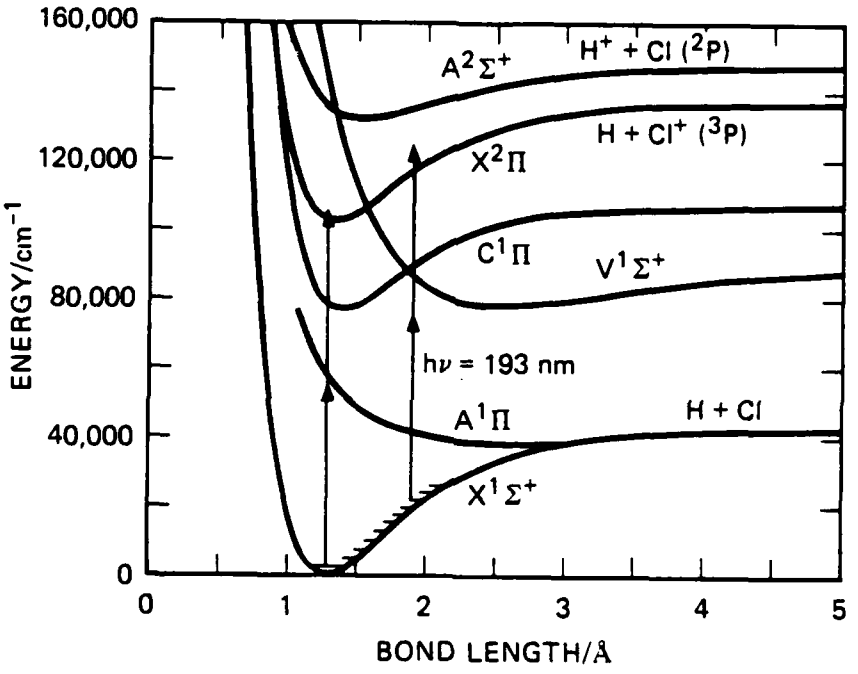
160,000
120,000
80,000
40,000
0
ENERGY/cm^{-1}
$A^2\Sigma^+$
$H^+ + Cl\ (^2P)$
$H + Cl^+\ (^3P)$
$X^2\Pi$
$C^1\Pi$
$V^1\Sigma^+$
$h\nu$ = 193 nm
$A^1\Pi$
$H + Cl$
$X^1\Sigma^+$
0
1
2
3
4
5
BOND LENGTH/Å

RA-2276-1

APPENDIX D

OPTICAL SWITCHING OF A DC DISCHARGE USING AN EXCIMER LASER

Mykola Saporoschenko,† Michel J. Rossi and Hanspeter Helm
Chemical Physics Laboratory
SRI International, Menlo Park CA 94025

ABSTRACT

The effects of unfocused 193- and 248-nm laser radiation of 3-30 mJ/cm^2 on DC discharges of vinychloride in helium are described. Laser-initiated striking and quenching of the DC discharge are described as well as the fact that the phenomenon exists at pulse repetition rates of 10 to 0.001 S^{-1}. The results are described qualitatively and the apparent paradox of the coexistence of strike and quench conditions is discussed.

†Visiting Scientist. Present address: Department of Physics
Southern Illinois University
Carbondale, IL 62901

††This work was supported by ARO under Contract DAAG29-83-K-0113.

CK87-02
1/20/87

INTRODUCTION

We recently observed that the attachment behavior of a vinylchloride (C_2H_3Cl)-helium mixture can be significantly altered as a result of its irradiation by an unfocussed beam of 193 nm laser light. The enhancement of the attachment coefficient η which is a quantitative measure of the attachment rate of the gas mixture, is most pronounced at low reduced electric field strength (0.1 Townsend and lower) and approaches unity at a few Townsends in the region where vinylchloride (VCl) has a dissociative attachment peak. We believe that the increased electron attachment of the gas mixture occurs as a result of the 193-nm photolysis of VCl that generates highly vibrationally excited HCl according to equation (1)

$$C_2H_3Cl \xrightarrow{193nm} C_2H_2^* + HCl^* + \leq 5.4 \text{ eV} \qquad (1)$$

where the asterisk denotes internal excitation.

Our experiments do not directly address the question of the basic mechanism underlying the observed effect in the VCl/He gas mixture. However, all the observables gathered are consistent with the presence of vibrationally excited molecular fragments following 193 nm photolysis of VCl/He, although the identity of the excited attacher has not been assessed.

The present experiments were undertaken to study the influence of the pulsed injection of electron attachers on a DC glow discharge with respect to the transient current/voltage characteristics. In these experiments we investigated the macroscopic change in the discharge impedance following illumination with unfocused soft excimer laser radiation. Of particular interest was the question whether the DC discharge could be quenched with UV laser radiation and, if so on what time scale. This phenomenon was expected based on our experimental results from the drift tube in that the irradiated system (VCl + He) attached low energy electrons very efficiently. The emphasis of this paper is to present the qualitative features of the phenomenon.

EXPERIMENTAL

A variety of discharge tubes were built and tested. A representative design is shown in Figure 1, and all the cathodes of the "successful" discharge tubes were of cylindrical geometry with a diameter varying between 1 and 4 cm with the length of the cathode being observed to be uncritical for the existence of the described phenomenon. Various anode shapes were tried: spherical, wire loop, anode tube, ribbon and pointed wire. All shapes worked although cylindrical geometries appeared most reliable in producing a stable steady-state discharge that could be operated close to threshhold. However, the discharge could not be quenched in a plane-parallel gap (electrodes 2 by 2 cm^2, 4 cm apart).

The parameter space for the existence of the laser-induced turn-off was a flowing gas sample at pressures of 0.2 to 1 Torr, a discharge current of 0.2 to 1.2 mA, and a laser power of 3 to 30 mJ/cm^2 at 193 and 248 nm respectively. The laser power at 193 nm was approximately a factor of 2 lower than at 248 nm for nominally identical conditions. The gas was a 2.05% mixture of VCl in He. A series of experiments with a helium misture was also conducted.

The current transient that resulted from the discharged gas - laser interaction was converted into a transient voltage using a 1-kΩ resistor. The signal was fed into a transient recorder and processed with a microcomputer. The laser was apertured outside the discharge tube to minimize scattered photons inside the tube.

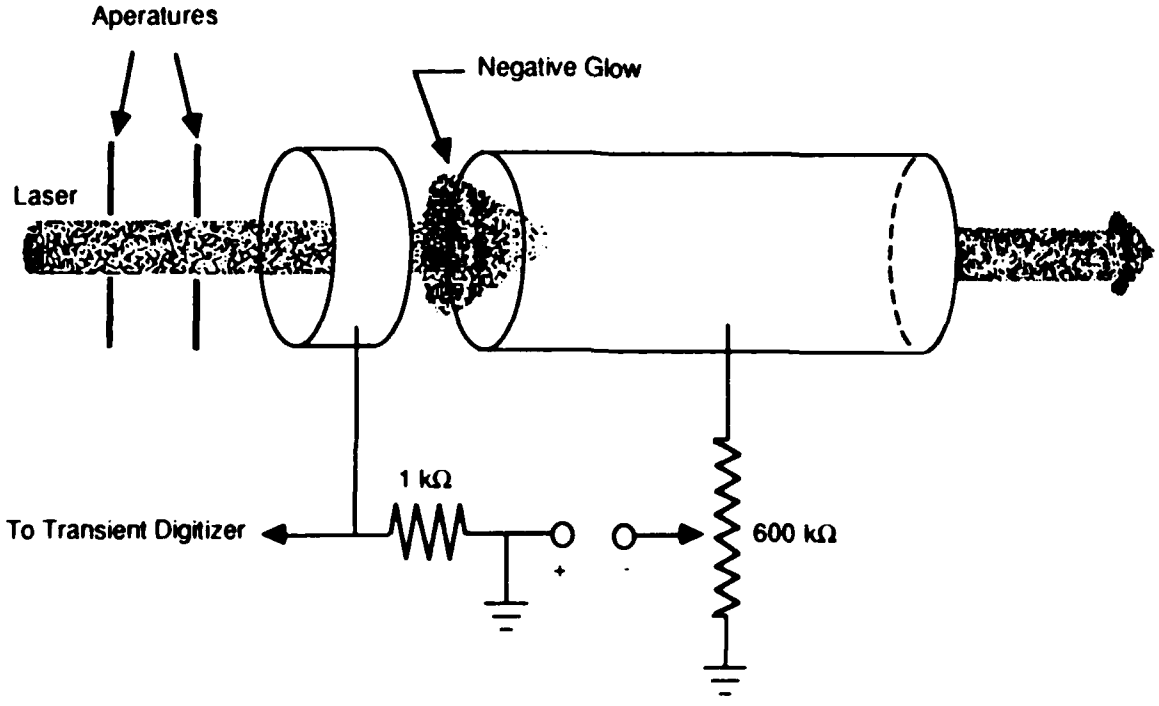

JA-M-6261-40

FIGURE D-1 HOLLOW CATHODE DISCHARGE TUBE FOR LASER-INDUCED SWITCHING EXPERIMENTS IN A SLOWLY FLOWING 2% VINYLCHLORIDE-HELIUM GAS MIXTURE

The laser enters and leaves the discharge tube through quartz windows. The diameter of the cylindrical steel electrodes is 1.5 inch. The shape of the anode is not critical for the occurrence of the phenomenon.

RESULTS AND DISCUSSION

We basically observed three phenomena as we perturbed an active discharge volume with UV laser photons.

- Laser-induced initiation of a discharge
- Laser-induced quenching of the discharge
- The capability to perform multiple strike-quench cycles with repetition rates of 10 Hz down to 0.001 Hz.

These three phenomena are discussed in detail below.

The sequence of events in the experiment were as follows. First, at a given voltage the tube is irradiated by an excimer laser pulse after which the discharge turns on if the chosen conditions are correct. The next laser pulse extinguishes the discharge under a given set of conditions, after which the system returns to the dark, prebreakdown state, ready for another strike-quench cycle. The turn-off phenomenon is observed only in VCl-He gas mixtures. It is not observed when pure argon or helium is used as a discharge gas. On the other hand, laser-induced initiation of the discharge was possible in a variety of gases.

The voltage at which the above events are occurring under unfocussed laser irradiation is below self-breakdown for the VCl-He gas mixture, but high enough to sustain a DC glow discharge after laser initiation. The breakdown curve for the VCl-He mixture is on the average 25% higher than the one for pure He and is depicted in Figure 2. In this mode of operation the discharge develops a negative glow at the anode end of the hollow cathode, which partially penetrates into the cathode. The shape of the anode does not seem to have a significant effect on the observables.

Figure 3 shows the current transient of .6 Torr VCl/He after irradiation by 27 mJ/cm^2 of 193 nm laser light at an applied voltage of 980 V. The oscilloscope trace, originally at 0 (indicating zero discharge current), shows a sharply rising transient at the time the excimer laser fires into the discharge coaxially without directly impacting any electrode surfaces. The peak of the transient is off-scale in Figure 3, but the current drops on a time scale of approximately 10μs and converges slowly to a final steady-state value. In this example the steady-state current is reached after about 1 ms, which is outside the time scale shown in the left side of Figure 3. The

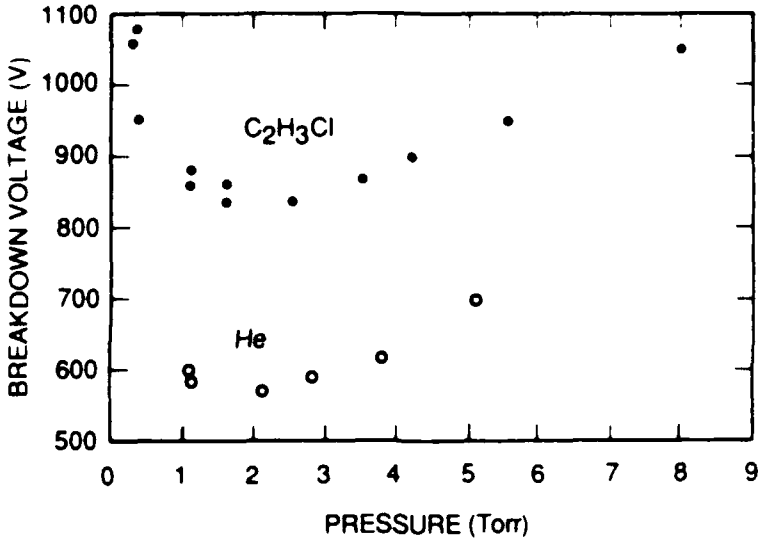

JA-m-6261-38

FIGURE D-2 BREAKDOWN CURVE FOR PURE HELIUM AND A 2% VINYLCHLORIDE-HELIUM MIXTURE IN A HOLLOW CATHODE DISCHARGE TUBE DESCRIBED IN FIGURE D-1

The gas is slowly flowing through the discharge tube

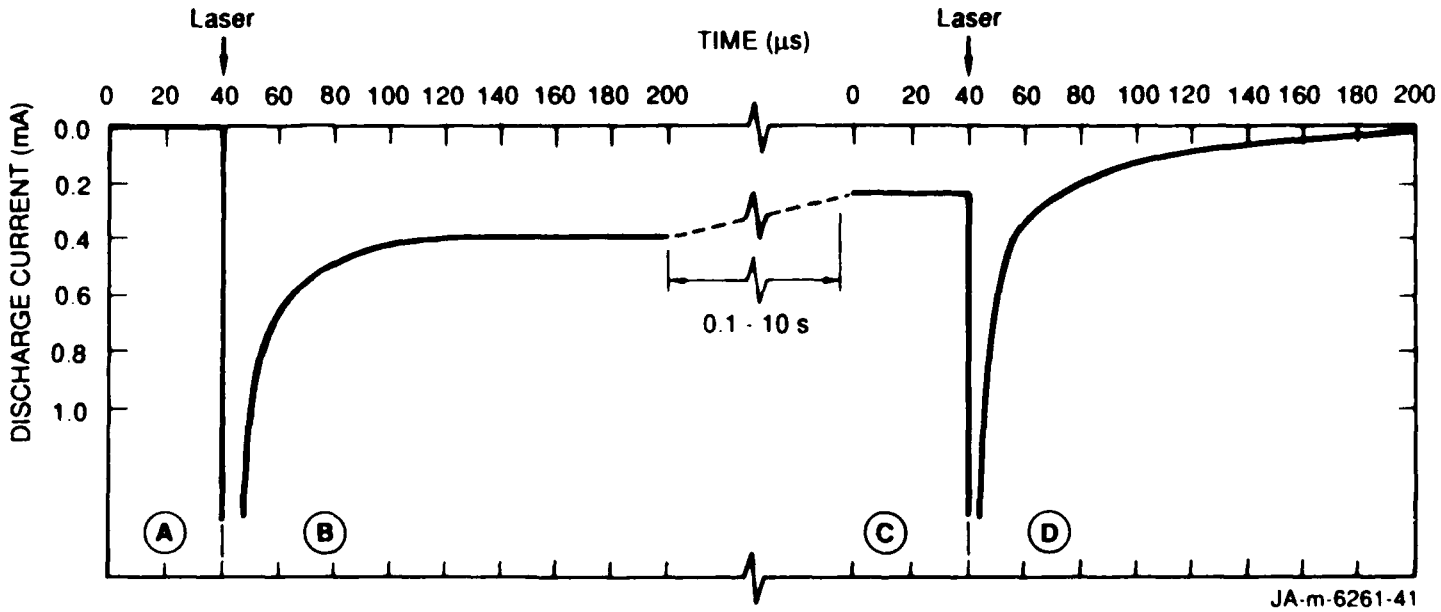

FIGURE D-3 OSCILLOSCOPE TRACE OF TRANSIENT DISCHARGE CURRENT MEASURED ACROSS 1 kΩ IN A 2% VINYLCHLORIDE-HELIUM MIXTURE UNDER 193-nm LASER IRRADIATION IN THE DISCHARGE TUBE SHOWN IN FIGURE D-1

The laser pulse coaxially irradiates the gas mixture at (A) after which the active discharge settles into steady state at (B) toward the self-sustaining regime. The second 193-nm laser pulse induces a strong current transient at (C), which slowly decays at (D) concomitant with the extinction of the discharge. The pressure was 0.6 Torr vinylchloride-He, the current-limiting resistor was 360 kΩ, so the initial voltage of 980 V decreased to 900 V at steady state.

measured voltage under discharge conditions was measured as 900 V, which corresponds to a decrease of about 80 V due to the discharge current of .23 mA flowing through the load resistor of 360 Ω.

The right side of Figure 3 shows the discharge current before and after irradiation of a second laser pulse. Before the laser pulse the current was measured as .25 mA by the 1-kΩ load resistor. At the time indicated a rapidly rising transient discharge current is observed, peaking at values up to 10 times the steady state discharge current. Within 10 μs this transient decays to a value close to the original current value. Following that the discharge current decays with a slower time constant (~ 20 to 40 μs) until the discharge current decreases to zero. The discharge will not restart although the external power source is still on. It is important to realize that the external power source is on during the laser-induced quenching cycle.

Quenching of the discharge occurs only for selected conditions. Outside this parameter space a strong laser-induced perturbation (optogalvanic effect) on greatly varying time scales can be observed which however does not lead to quenching of the discharge. The three main variables for laser-induced quenching of a stationary discharge are discharge current, pressure and laser fluence. It was observed that the laser fluence did not have a large effect on the extinction of the discharge as long as the fluence was between 2.5 to 20 mJ/cm^2. The range of existence for the laser-induced discharge quenching phenomenon is 0.3 to 1 Torr VCl/He with a discharge current of 0.1 to 0.55 mA for a 1-inch-diameter discharge tube with a point anode about 1 inch away from the cylindrical cathode.

When a slowly flowing VCl/He gas mixture was used, sequential pulses from the excimer laser could initiate and extinguish the discharge. We have observed this phenomenon for repetition rates as slow as 1 pulse per 10 minutes to 10 pulses per second. Furthermore, those effects have been observed in a variety of dischaage tubes described in the experimental section.

DISCUSSION

Two effects are thought to be important in laser initiation of glow discharges by an excimer laser: (1) photoemission of secondary electrons from an irradiated cathode surface and (2) gas-phase multiphoton ionization. Because the operating conditions of the discharge are chosen close to self-breakdown, a single electron avalanche may initiate the discharge. That is a few photoelectrons generated at the cathode may be sufficient for turning on ahe discharge. Because about 10^{15} to 10^{16} UV photons are transmitted across the discharge per pulse, some photons are likely to reach the geometrically shielded cathode surface following scattering at the windows of Raleigh scattering in the gas-phase.

We observed that the shape and the amplitude of the transient which occurs in the switch-on phase depends on the laser beam diameter. Figure 4 shows that when the laser beam diameter is reduced the transient decreases in height. At the smallest diameter used (1.5 mm) the sharp spike at the leading edge of the transient diappeared altogether although a fast rising component still persists. This picture also shows the slower rising and decaying transient which we attribute to volumetric gas-phase ionization, whereas the fast component of the transient is related to the photoelectric effect brought about by scattered photons from the laser.

To assess the importance of volumetric ionization processes by excimer laser irradiation we measured the multiphoton ionization cross section of VCl using a time-of-flight mass spectrometer in a separate experiment. At 193 nm the ionization yield of VCl is $(8 \pm 4)(-9)$ cm^6 mJ^{-3} for an unfocussed laser beam at low fluence ($\leq$10 mJ/cm^2). The only ionic product in this case is HCl^+, which is formed by two-photon ionization of vibrationally highly excited HCl ($v \geq 8$) generated by single-photon photodissociation of VCl. Therefore, under typical operating conditions of our discharge experiment the excimer laser (5 mJ/cm^2) forms 10^8 ion-electron pairs per irradiated cubic centimeter. This density is apparently sufficient to initiate the discharge for a small-diameter laser beam (see Figure 4), whereas the density of photoelectrons from the surface process can be higher for a large-diameter laser beam. However, even the approxiamte density of surface photoelectrons is difficult to estimate under a given set of conditions. The laser

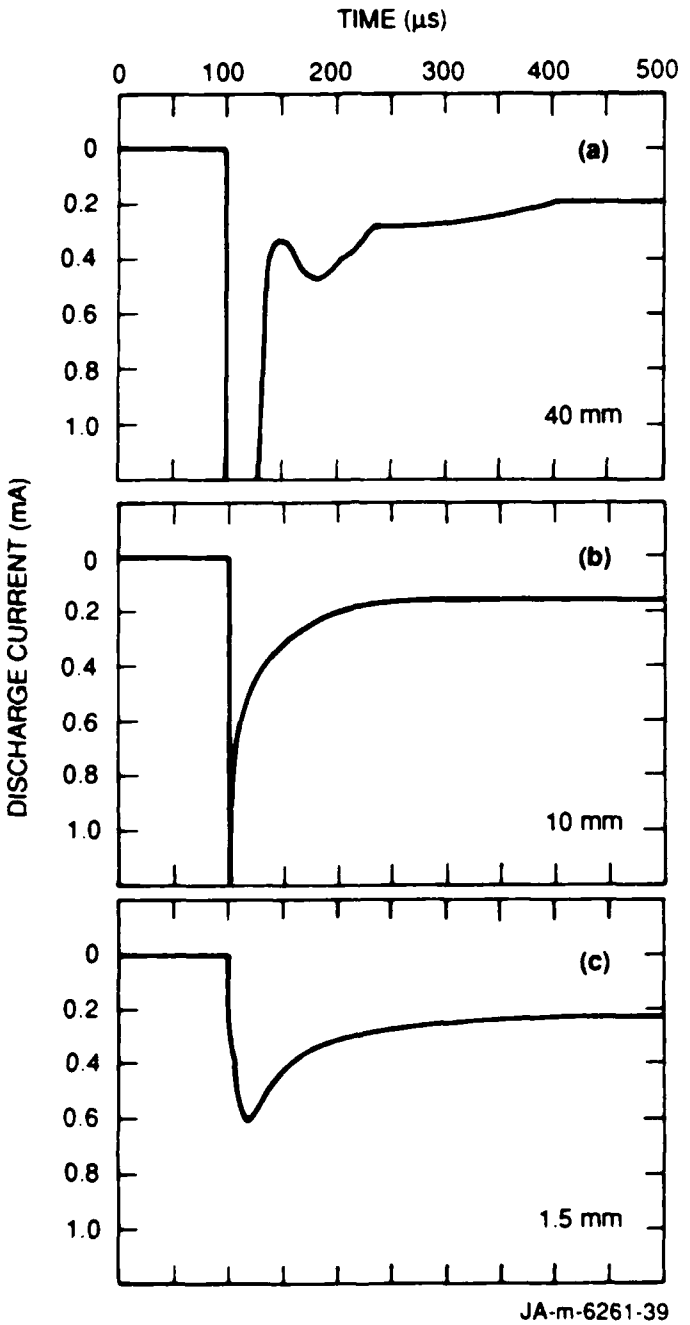

FIGURE D-4 THE EFFECT OF THE 193-nm LASER-BEAM DIAMETER ON THE TRANSIENT CURRENT MEASURED ACROSS 1 kΩ

The conditions are identical to those of Figure D-3.

initiation of pure and mixed gases (pure Ar and He versus VCl/He mixture) worked at both 193 and 248 nm. The latter wavelength is not absorbed by either of these gases, so we conclude that the discharge initiation is enabled by the photoelectric effect due to scattered photons in this case.

Whereas generation of charged species determines the initiation of the discharge attachment of low energy electrons is likely to be responsible for the quenching of the running discharge. The photodissociation cross section for VCl to form HCl is 1.7×10^{-17} cm^2. Under typical conditions the excimer laser (5 mJ/cm^2) forms about 10^{12} excited HCl molecules per irradiated cubic centimeter of the discharge. We believe that the enhanced attachment properties of the laser excited gas, even under discharge conditions lead to the quenching of the discharge. According to the results from our drift tube studies, the laser affects primarily low energy electrons, as they exist in the negative glow and anode region of the active discharge. Consistent with this hypothesis is the fact that no quenching was observed in a parallel-plate glow discharge where the negative glow region was confined to a region near the cathode.

It is surprising that both effects, initiation and quenching, coexist upon firing the laser into the gas discharge. Both laser pulses, the first irradiation the cold discharge and the second irradiating the hot discharge, generate the same species. However, the effect of those species on the discharge may be very different. In the initiation phase the role of generating a certain density of charge carriers is emphasized because of the applied high voltage. It will be the high energy electrons, whose attachment behavior will be most likely similar for laser excited and unexcited gas, that will initiate an avalanche and so strike the discharge. The low energy electrons, which are most affected by the presence of the excited attachers, do not play a dominant role in this phase. A second order effect that may support the discharge initiation may be the fact that the vibrationally excited attachers are efficiently deactivated in collisions or dissociated/ionized by high energy electron impact during the swith-on phase, which is charaacterized by an increasing electrical field.

Our results indicate that the same order of magnitude electron and ion densities are created at the beginning of the turn-off phase. However, the role of the high energy electrons is deemphasized because of the lower

voltages due to the discharge current on one hand, and on the other hand the missing supply of low energy electrons due to dissociative attachment to the laser generated excited attachers. With the "hole" in the distribution of the low energy electrons the supply of high energy electrons, which are essentially responsible for sustaining the discharge, is diminished.

The quenching also occurs under 248-nm laser radiation, where ground state VCl does not absorb. However, the DC glow discharge may form species absorbing at 248 nm and may generate attachers through the 248-nm photodissociation. Consistent with this idea is the observation of absorbing species at 254 and 313 nm, but not at 365 nm.

END

7-87

DTIC